



# Høgskulen på Vestlandet

## MMO5017 Master thesis

MMO5017-MOPPG-1-2022-VÅR-FLOWassign

### Predefinert informasjon

**Startdato:** 22-04-2022 14:11  
**Sluttdato:** 03-06-2022 14:00  
**Eksamensform:** Master thesis  
**Flowkode:** 203 MMO5017 1 MOPPG-1 2022 VÅR  
**Intern sensor:** (Anonymisert)

**Termin:** 2022 VÅR  
**Vurderingsform:** Norsk 6-trinns skala (A-F)

### Deltaker

<b>Naun:</b>	Preben Aarland Aga
<b>Kandidatnr.:</b>	418
<b>HVL-id:</b>	180325@hvl.no

### Informasjon fra deltaker

**Antall ord \*:** 20318

Sett hake dersom Ja  
besvarelsen kan brukes  
som eksempel i  
undervisning?:

Jeg bekrefter at jeg har Ja  
registrert  
oppgavetittelen på  
norsk og engelsk i  
StudentWeb og vet at  
denne vil stå på  
vitnemålet mitt \*:

**Egenerklæring \*:** Ja  
**Inneholder besvarelsen Nei**  
**konfidensielt**  
**materiale?:**

### Gruppe

**Gruppenaun:** Enmannsgruppe  
**Gruppenummer:** 7  
**Andre medlemmer i gruppen:** Deltakeren har innlevert i en enkeltmannsgruppe

Jeg godkjenner autalen om publisering av masteroppgaven min \*

Ja

**Er masteroppgaven skrevet som del av et større forskningsprosjekt ved HVL? \***

Nei

**Er masteroppgaven skrevet ved bedrift/virksomhet i næringsliv eller offentlig sektor? \***

Ja, Offshore Kinetics



Høgskulen  
på Vestlandet

# MASTER'S THESIS

Numerical Assessments of a Hybrid  
Offshore Wind Turbine Concept

**Preben Aarland Aga**

Maritime Operations

Department of Maritime Studies, HVL

Supervisor: Zhenhui Liu

03.06.2022

I confirm that the work is self-prepared and that references/source references to all sources used in the work are provided, cf. Regulation relating to academic studies and examinations at the Western Norway University of Applied Sciences (HVL), § 12-1.



## Acknowledgement

I am grateful for all support I have had during the process of writing this thesis. I would like to thank Tommy Beinset and Håkon Ola Velund from Offshore Kinetics for presenting their concept for me, and providing relevant information and documentation related to their concept.

I would also like to thank my colleges at Semar for the support through the writing process.

Last, but not least, I wish to sincerely thank my internal supervisor from HVL, Zhenhui Liu, for extraordinary guidance throughout the whole semester. I am grateful for all conversations and discussions we have had, which have contributed to constantly improving the research. I would highly recommend Zhenhui as internal supervisor to all future candidates.

## Abstract

This thesis contains a numerical assessment of Offshore Kinetics' hybrid wind turbine support structure concept with the aim to find the values and the eventual causes of torque applied to the structure's universal joint. The turbine's efficiency in various sea states and at different yaw misalignments, in addition to the structure's stability properties are also considered.

From the given information of the concept, all relevant calculations of the structure have been performed. The structure has then been modelled in Inventor to validate some of the calculations, before a determination on the structure's stability properties was executed. A model was then created in Orcaflex with the calculated inputs for the structure, and the sea state input was calculated by using statistics from historical data. From here, a yaw controller was improvised using external function by modifying a Python script and implementing the function using a constraint in Orcaflex. Simulations were performed for different sea states and yaw rates, before the results were analysed.

It is concluded in the research that an increase in yaw rate influences the torque applied to the universal joint significantly more than an increase in significant wave height, and that it is the deacceleration of the yawing of the turbine which creates the high torque values.

It is also concluded that the turbine's efficiency is reduced when the structure is put into motion due to waves, but a further increase in wave height does not impact the generator efficiency in great measures because the inclination of the structure is not much increased by an increase in wave height.

The stability of the structure was sufficient for the simulated scenarios with a max inclination of approximately 2.7 degrees in the roughest wave conditions.

It is found that a yaw misalignment of 4 and 8 degrees does not impact the turbine efficiency significantly in the short-term but will result in a greater loss over a long-term period. A yaw misalignment error of 20 degrees reduces the turbine efficiency in a short-term period, and over time the turbine can be seen as inefficient with such large yaw misalignments.

## Sammendrag

I denne masteroppgaven blir det gjort numeriske vurderinger av Offshore Kinetics hybrid offshore vindturbin konsept, med mål om å finne verdier av dreiemomentet som oppstår i universalleddet I operasjoner hvor turbinen snur seg etter vinden og i forskjellige sjøtilstander. En vurdering av konseptes stabilitet og turbinens effektivitet i ulike sjøtilstander og ved 'yaw misalignments' er også inkludert.

Alle nødvendige beregninger er gjort manuelt før noen av disse er sjekket ved hjelp av modellering i programmet Inventor. Inventor beregner verdier automatisk etter design og valg av materiale. En vurdering av stabiliteten til strukturen ble også utført både med og uten hensyn til ballast.

På bakgrunn av disse beregningene ble konseptet modellert i Orcaflex og bestemmelser av hvilke sjøtilstander som skulle være inkludert ble gjort ved bruk av statistikk-beregninger av historiske data. I Orcaflex ble det også laget en improvisert "yaw controller" ved bruk av eksterne funksjoner i Python som ble implementert i en "constraint" i Orcaflex.

Simuleringer ble basert på ulike sjøtilstander og "girhastighet" (vinkelhastigheten som turbine snur seg etter vinden med).

Det ble konkludert med at økende vinkelhastighet bidrar betydelig mer til økende dreiemoment på universalleddet enn økende bølgehøyde, og at det er deakselerasjonen til turbinen som er hovedårsaken til økende dreiemoment.

Den generelle stabiliteten til strukturen ble funnet til å være god, med en maks 2.7 grader helning i den verste sjøtilstanden. Effektiviteten til turbinen reduseres når den blir satt i bevegelse på grunn av bølger, men en videre økning i bølgehøyde bidrar ikke til økt reduksjon i effektivitet.

Det ble også konkludert med at yaw misalignments (feilvinkling av turbin mot vind) ikke reduserte effektiviteten til turbine betydelig i forsøk ved 4 og 8 grader feil. En feilvinkling på 20 grader gjorde derimot et mer betydelig utslag i redusert effektivitet.

## Preface

This is a 30-credit point master thesis in Maritime Operations at Western Norway University of Applied Sciences, 2022. The degree specializes in Offshore and Subsea operations, and the campus site is located in Haugesund, Norway. Due to the pandemic, the participation and all work have been performed from home using digital tools.

The general research is based on an offshore wind turbine support structure concept which has been developed by Offshore Kinetics. Tommy Beinset and Håkon Ola Velund have been the contact persons from the company.

The research topic and scope have been developed by me in cooperation with my internal supervisor, Zhenhui Liu, after approval from Offshore Kinetics representatives.

The thesis includes numerical assessments of the Offshore Kinetics' offshore wind turbine support structure, which can be considered as a hybrid offshore wind turbine concept. The structure is based on an articulated tower support structure, and the properties and forces on the structure have been assessed using numerical tools.

The workload has been significant, and at times overwhelming but has also been very rewarding and challenging. I have learned a lot through the process of this research and will use this knowledge going into the future.



## Contents

Acknowledgement.....	iii
Abstract .....	iv
Sammendrag.....	v
Preface.....	vi
Figures.....	ix
Tables .....	0
<b>1. INTRODUCTION.....</b>	<b>1</b>
1.1 Background .....	1
1.2 Research objective and state of the art .....	8
<b>2. RELEVANT THEORIES.....</b>	<b>11</b>
2.1 Environmental Forces.....	11
2.2 Environmental inputs .....	16
2.3 Classical mechanics.....	23
2.4 Hydrostatics.....	26
2.5 Turbine yawing theory .....	30
<b>3. NUMERICAL ASSESSMENTS .....</b>	<b>34</b>
3.1 Current design of Hybrid Wind Turbine .....	34
3.2 Numerical tools and calculations.....	36
3.3 10 MW wind turbine .....	44
3.4 Initial Stability.....	47
3.5 Environmental inputs .....	49
3.6 Simulation setup.....	53
<b>4. RESULTS AND DISCUSSIONS.....</b>	<b>55</b>
4.1 Applied torque on universal joint.....	56
4.2 Applied torque summary .....	62
4.3 Turbine efficiency .....	65
4.4 Turbine efficiency summary.....	71

5.	<b>CONCLUSION</b> .....	73
6.	<b>FURTHER WORK</b> .....	75
7.	<b>REFERENCES</b> .....	76
	Appendix 1 – Torque results $H_s = 1.5$ .....	80
	Yaw rate = 0.1.....	80
	Yaw rate = 0.3.....	81
	Yaw rate = 0.5.....	83
	Appendix 2 – Torque results $H_s = 3.5$ .....	86
	Yaw rate = 0.1.....	86
	Yaw rate = 0.3.....	88
	Yaw rate = 0.5.....	90
	Appendix 3 – Torque results $H_s = 6.5$ .....	92
	Yaw rate = 0.1.....	92
	Yaw rate = 0.3.....	93
	Yaw rate = 0.5.....	95
	Appendix 4 – Calculation of Moment of inertia, $I_z$ , for tower section .....	98
	Appendix 5 – Excel calculation sheet .....	102
	Appendix 6 – Excel Solver.....	104
	Appendix 7 – Building the model in Orcaflex .....	106

## Figures

Figure 1: Offshore Kinetics' offshore wind turbine concept[4].....	2
Figure 2: Trend of installed capacity of OWT[8].....	3
Figure 3: Trend of annual offshore wind farm size[8] .....	3
Figure 4: Typical designs of wind turbine structures[9].....	4
Figure 5: Installed substructures in Europe (2020) [8].....	4
Figure 6: Nacelle Cross-section [11].....	5
Figure 7: Articulated tower principle [19].....	7
Figure 8: Waves on slender cylinder .....	12
Figure 9: Drag and Inertia force .....	13
Figure 10: Maximum drag force.....	14
Figure 11: Maximum Inertia force .....	14
Figure 12: Lift force on foil.....	16
Figure 13: Wave contour at time t.....	17
Figure 14: surface elevation at position x,.....	17
Figure 15: isobaric contours across depth .....	18
Figure 16: Energy spectrum[35].....	19
Figure 17: Pierson-Moskowitz spectrum[36].....	20
Figure 18: Wind turbine Degrees of Freedom[46] .....	27
Figure 19: Vessel stability[35] .....	28
Figure 20: Metacenter .....	29
Figure 21: Rightening moment[47].....	30
Figure 22: Yaw system configuration[26].....	31
Figure 23: Non-yawing torque[26].....	33
Figure 24: Yawing torque[26] .....	33
Figure 25: Hybrid Wind Turbine overview[22] .....	34
Figure 26: Hybrid Wind Turbine Submerged Section[22].....	35
Figure 27: Hybrid Wind Turbine top section[22].....	35

Figure 28: Orcaflex 6D-buoy parameters[38] .....	37
Figure 29: Modelled wind turbine concept in Orcaflex[38].....	37
Figure 30: Orcaflex COB visualization.....	38
Figure 31: Modelled substructure in Inventor[55] .....	40
Figure 32: Constraint options in Orcaflex[38] .....	46
Figure 33: Turbine before and after yawing[38] .....	55
Figure 34: Structure inclination over time.....	56
Figure 35: Structure inclination excluding wind force.....	56
Figure 36: Torque on universal joint at yaw rate 0.1.....	57
Figure 37: Turbine yawing behaviour .....	58
Figure 38: Turbine behavior after deacceleration .....	58
Figure 39: Torque on universal joint, only wind, Yaw rate = 0.1 .....	62
Figure 40: Torque on universal joint, only wind, Yaw rate = 0.3 .....	62
Figure 41: Torque on universal joint, only wind, Yaw rate = 0.5 .....	63
Figure 42: Angular deacceleration at Yaw rate 0.1 and 0.5 .....	63
Figure 43: Average torque from increasing yaw rate .....	64
Figure 44: Max torque from increasing yaw rate .....	64
Figure 45: Increase in torque from increasing Hs .....	65
Figure 46: Highest torque simulation.....	65
Figure 47: Turbine efficiency over time.....	66
Figure 48: Turbine efficiency, Hs = 1.5 m.....	66
Figure 49: Turbine efficiency during heeling trend.....	67
Figure 50: Turbine efficiency, Hs = 3.5 m.....	67
Figure 51: Turbine efficiency during heeling trend.....	68
Figure 52: Turbine efficiency, Hs = 6.5 m.....	68
Figure 53: Turbine efficiency during heeling trend.....	69
Figure 54: Generator power influence by turbine yawing.....	69
Figure 55: Turbine efficiency, yaw misalignment = 4 degrees .....	70

Figure 56: Turbine efficiency, yaw misalignment = 8 degrees .....	70
Figure 57: Turbine efficiency, yaw misalignment = 20 degrees .....	71
Figure 58: Turbine efficiency trend.....	71
Figure 59: Turbine efficiency at yaw misalignments .....	72
Figure 60: Generator efficiency trend by increasing yaw misalignment.....	72
Figure 61: $T_z = 5.5$ .....	80
Figure 62: $T_z = 6.5$ .....	80
Figure 63: $T_z = 7.5$ .....	80
Figure 64: $T_z = 8.5$ .....	81
Figure 65: $T_z = 9.5$ .....	81
Figure 66: $T_z = 10.5$ .....	81
Figure 67: $T_z = 5.5$ .....	82
Figure 68: $T_z = 6.5$ .....	82
Figure 69: $T_z = 7.5$ .....	82
Figure 70: $T_z = 8.5$ .....	83
Figure 71: $T_z = 9.5$ .....	83
Figure 72: $T_z = 10.5$ .....	83
Figure 73: $T_z = 5.5$ .....	84
Figure 74: $T_z = 6.5$ .....	84
Figure 75: $T_z = 7.5$ .....	84
Figure 76: $T_z = 8.5$ .....	85
Figure 77: $T_z = 9.5$ .....	85
Figure 78: $T_z = 10.5$ .....	85
Figure 79: $T_z = 6.5$ .....	86
Figure 80: $T_z = 7.5$ .....	86
Figure 81: $T_z = 8.5$ .....	86
Figure 82: $T_z = 9.5$ .....	87
Figure 83: $T_z = 10.5$ .....	87

Figure 84: $T_z = 11.5$ .....	87
Figure 85: $T_z = 6.5$ .....	88
Figure 86: $T_z = 7.5$ .....	88
Figure 87: $T_z = 8.5$ .....	88
Figure 88: $T_z = 9.5$ .....	89
Figure 89: $T_z = 10.5$ .....	89
Figure 90: $T_z = 11.5$ .....	89
Figure 91: $T_z = 6.5$ .....	90
Figure 92: $T_z = 7.5$ .....	90
Figure 93: $T_z = 8.5$ .....	90
Figure 94: $T_z = 9.5$ .....	91
Figure 95: $T_z = 10.5$ .....	91
Figure 96: $T_z = 11.5$ .....	91
Figure 97: $T_z = 7.5$ .....	92
Figure 98: $T_z = 8.5$ .....	92
Figure 99: $T_z = 9.5$ .....	92
Figure 100: $T_z = 10.5$ .....	93
Figure 101: $T_z = 11.5$ .....	93
Figure 102: $T_z = 12.5$ .....	93
Figure 103: $T_z = 7.5$ .....	94
Figure 104: $T_z = 8.5$ .....	94
Figure 105: $T_z = 9.5$ .....	94
Figure 106: $T_z = 10.5$ .....	95
Figure 107: $T_z = 11.5$ .....	95
Figure 108: $T_z = 12.5$ .....	95
Figure 109: $T_z = 7.5$ .....	96
Figure 110: $T_z = 8.5$ .....	96
Figure 111: $T_z = 9.5$ .....	96

Figure 112: $T_z = 10.5$ .....	97
Figure 113: $T_z = 11.5$ .....	97
Figure 114: $T_z = 12.5$ .....	97

# Tables

- Table 1: Hand calculation comparison with inventor..... 40
- Table 2: Properties..... 41
- Table 3: Verifying hand-calculations ..... 43
- Table 4: 10 MW turbine properties[50]..... 45
- Table 5: Yaw control functions in DLL-file..... 46
- Table 6: Environmental inputs in Excel ..... 48
- Table 7: List of simulations ..... 53
- Table 8: Torque values when only wind is applied..... 57
- Table 9: Hs=1.5, Average torque on universal joint ..... 59
- Table 10: Hs=1.5, Max torque on universal joint..... 59
- Table 11: Hs=3.5, Average torque on universal joint ..... 60
- Table 12: Hs=3.5, Max torque on universal joint..... 60
- Table 13: Hs=6.5, Average torque on universal joint ..... 61
- Table 14: Hs=6.5 Max torque on universal joint..... 61



# 1. Introduction

This research aims to numerically assess a hybrid wind turbine structure developed by Offshore Kinetics in regard to basic functionality in terms of stability and power efficiency as well as occurrence of torque force on the universal joint related to turbine yaw motions.

This chapter introduces the research based on the background of the offshore wind industry today and the general concept considered.

## 1.1 Background

On the 11<sup>th</sup> of May 2022, the Norwegian government presented a major initiative to promote power from offshore wind with an aim to use offshore wind power to generate new electricity on par with the total amount currently produced in Norway today[1]. The prime minister, Jonas Gahr Støre, says in the press release that the current government have worked since day one to develop Norway as an offshore wind nation, and that the large seas, world-class technology expertise, and a well-established cooperation between the government administration and the business sector are factors that puts Norway in a good position to succeed.

The government aims to open up areas for offshore wind power production to generate 30 000 MW of power in Norway by 2040, and in 20 years Norway will have around 1500 offshore wind turbines[1].

The operation to install Equinor's Hywind Tampen project has started in 2022, with the aim to start production in the third quarter of 2022 [2] The project involves a wind turbine park on the Tampen field in the North Sea, where the park is to produce electric energy to supply five oil platforms and cover 1/3<sup>rd</sup> of their demanded power supply. The wind park consists of 11 floating wind turbines of the spar buoy type, in which each has a production capacity of 8 megawatts[3].

One of the companies which has widely studied the maritime evolution of the wind turbine industry are Offshore Kinetics. Offshore Kinetics is a Norwegian private limited company which was established in 2009 to develop and commercialize their offshore wind turbine support structure. The founders have worked in senior positions within the offshore industry for 40 years, and the company specializes many various aspects such as engineering, design, fabrication, testing, assembly, installation, marine and subsea operations, maintenance, project execution and contract management[4].

Offshore Kinetics[4] have developed a concept based on an articulated tower substructure using a universal joint at the bottom, a ballast tank, and a stabilization tank which can also be used for production/containment of Hydrogen.

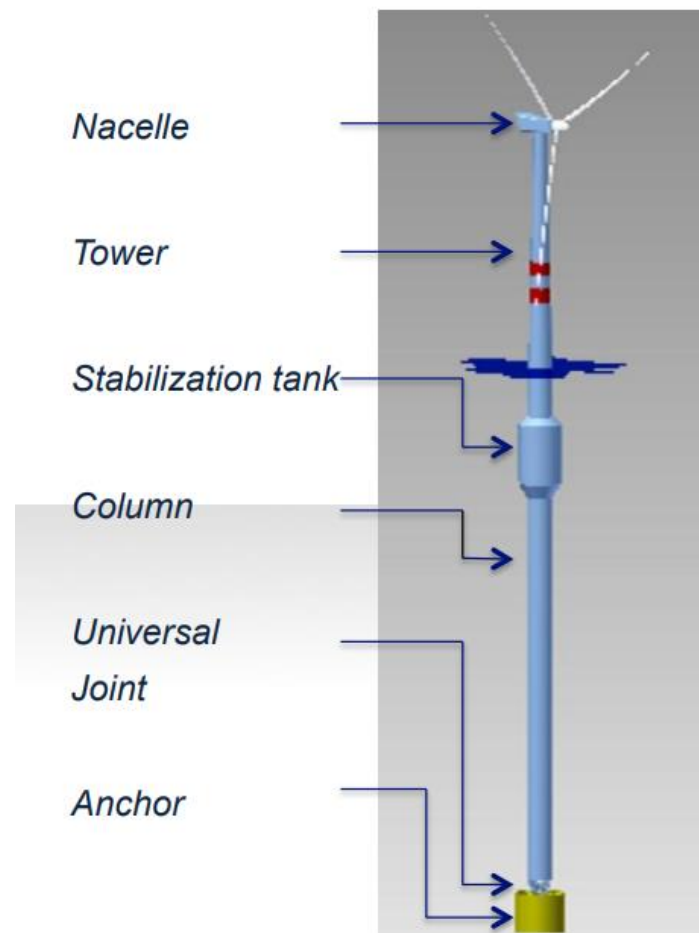


Figure 1: Offshore Kinetics' offshore wind turbine concept[4]

As the wind direction is not constant and might not always act in the same direction as waves, the wind turbine must adjust for the change of wind direction and then yaw the turbine so that it is facing the wind and maximizing the transformation of energy [5]. This adjustment is done by a yaw controller which rotates the nacelle towards the wind direction at a certain angular velocity, called the yaw rate[6].

The universal joint near seabed represents a single hinged mooring which allows rotation about the X and Y-axis, but do not allow rotation about the z-axis (yaw). It is suspected that this universal joint could be exposed to large torque from yawing operations, wind and wave forces, and the combination of yawing operations in different sea states.

### 1.1.1 Trends of Offshore wind today

Offshore wind is the industry involving generation of energy from wind turbines installed offshore. The environmental conditions offshore make the generation of energy more efficient than onshore, but the industry has been met with some resistance concerning damages to marine life and pollution[7]. However, the trends shows that the offshore wind industry is increasing in Europe. As the technologies advances the turbine rated capacity also increases for newly installed offshore wind turbines. For 2020

the average wind turbine capacity for new installations was over 8 MW. The trend can be seen in the figure below[8].

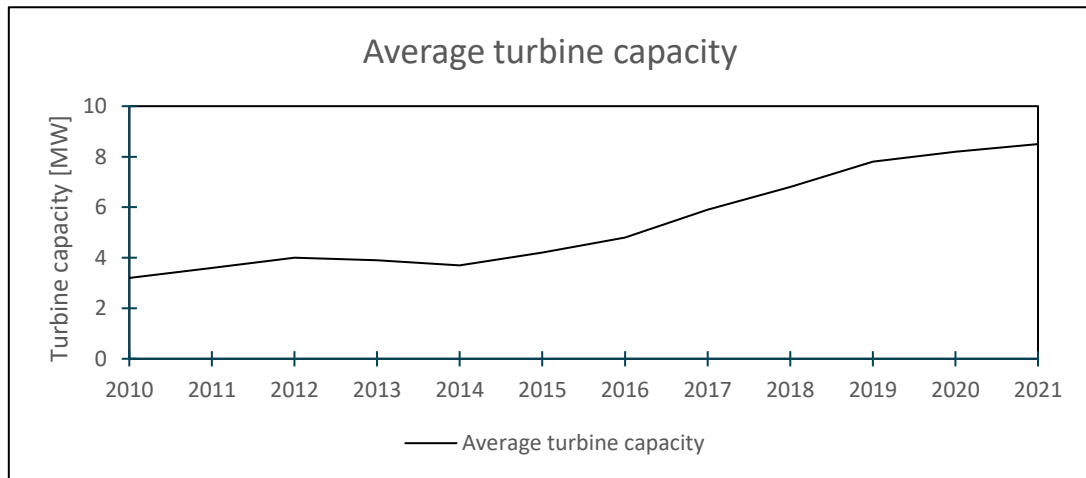


Figure 2: Trend of installed capacity of OWT[8]

This increasing trend can also be seen when considering annual total wind farm capacities/sizes in projects as seen in the figure below.

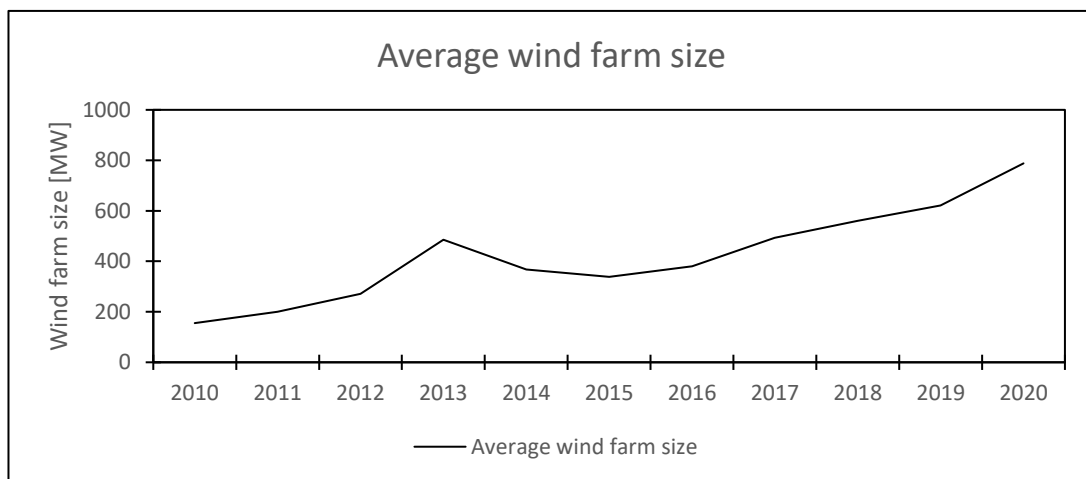


Figure 3: Trend of annual offshore wind farm size[8]

Included in this trend are several different types of wind turbine substructure designs which varies on environmental factors such as weather, water depth, seabed soil, and coastal distance.

### 1.1.2 Design of offshore wind turbines

Several different designs for wind turbines have been developed over the years and the design is dependent on environmental conditions. Below is a figure which shows some of the designs in the industry today[9].

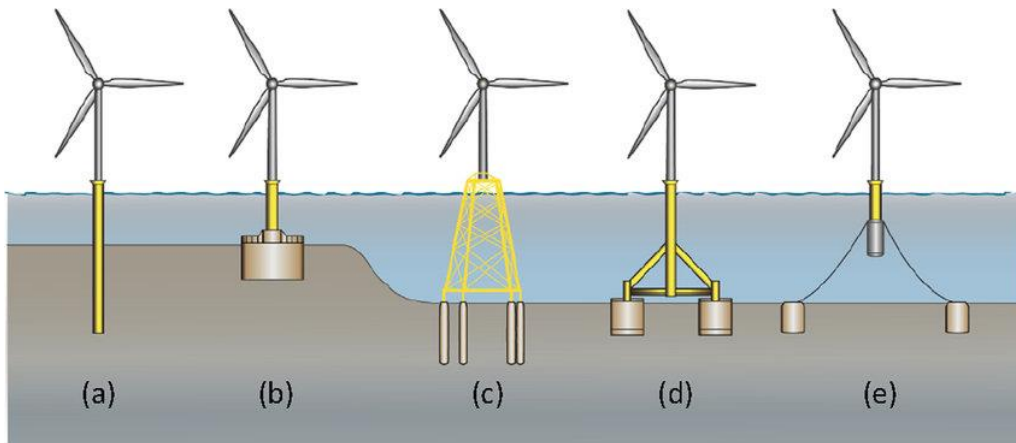


Figure 4: Typical designs of wind turbine structures[9]

- a) Monopile
- b) Monopod with typically suction anchor
- c) Jacket structure
- d) Tripod
- e) Floating turbine (often spar buoy with anchors)

The most common OWT substructure in Europe is the monopile structure with 81.2% in 2020 [8]. The monopile structure is relatively cheap to produce and is less complex but does have limitations on water depth applicability. Below is an overview of the total installed substructures in 2020.

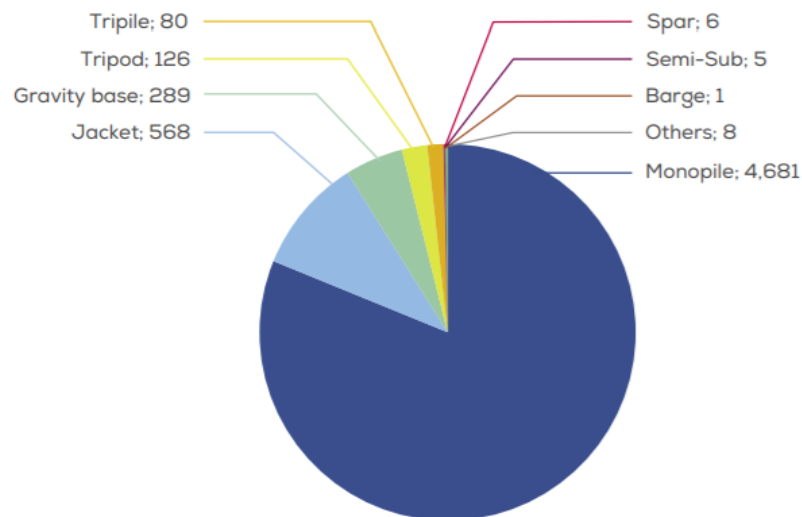


Figure 5: Installed substructures in Europe (2020) [8]

As the offshore wind technology advances, floating wind turbines are likely to increase due to deep water conditions.

### 1.1.3 Typical offshore wind turbine components

The components of offshore wind turbines will vary for its intended location and is dependent on environmental conditions. The common components for most offshore wind turbines are the nacelle, rotor blades, tower, and the support structure[10].

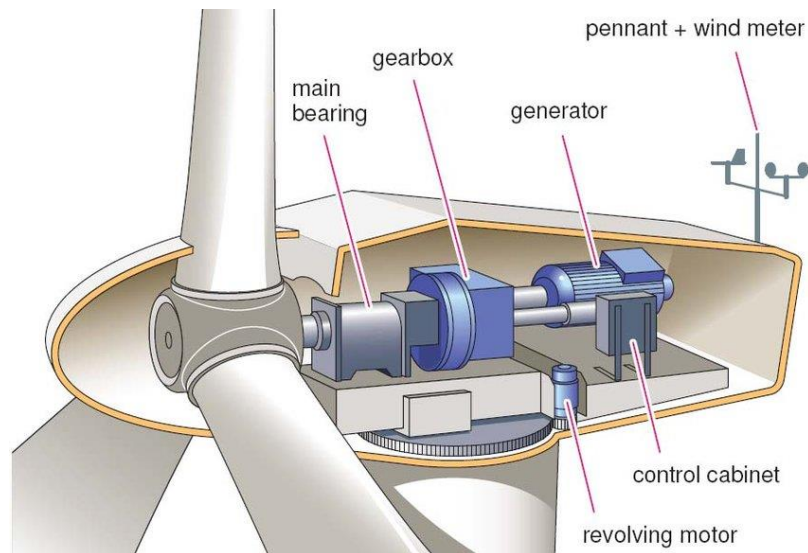


Figure 6: Nacelle Cross-section [11]

The nacelle is the housing of components such as the generator, gearbox, control cabinet, main bearing and the revolving motor[11]. The gearbox is used to increase the rotational speed from a low-speed shaft to a high-speed shaft. Generator converts the mechanical energy to electrical energy, while the yaw system helps turning the turbine against the wind from signals of wind direction collected by the wind meter[12].

### **Rotor blades**

The rotor blade's job is to activate the generator by rotation. This rotation is forced by the wind lift force which is generated by the differential air pressure when the wind flows across the blades. As the lift force is greater than the drag force because of the geometry of the blades, the blades start to rotate. There are usually three blades in a typical wind turbine configuration[13].

### **Tower**

The tower is the upper part of the support structure and are often assembled in three parts. The tower must be designed to withstand the static and dynamic forces from the generator and rotor blades in addition to drag forces from the wind[14]. Wind speeds increases with height so the generator is more efficient at higher altitudes[15], meaning that the tower heights often increases with the increase in

turbine production. The tower section is normally coned, meaning that the diameter reduces with height.

### **Support structure**

The support structure is the lower support structure of offshore wind turbines and can have many different designs as shown in figure 4[9]. The submerged part of the structure is exposed to the hydrodynamic forces as well as static and dynamic forces from the nacelle, blades (with and without rotation) and the mass of the tower.

### **Mooring**

As there are many varieties of support structure concepts, the mooring of these will also differ. The monopile structure is driven into the seabed using a hydraulic hammer[16]. The friction between the soil and the structure keeps the monopile structure in place.

The jacket and tripod concepts often use suction anchors or anchor piles with the substructure foundation directly connected to the anchors[16].

For floating wind turbines a combination of mooring lines and anchors are used[16]. Floating wind turbines are more often used at larger water depths and to reduce the amount of material, lengths of chain is connected between the floating substructure and suction anchors on seafloor.

The suction anchors are large, but thin, hollow structures with ventilation lids. When placed at the seafloor, it self-penetrates some meters due to its weight. Then, a pump is connected to the ventilation lids, and pumps the water out of the anchor. This then creates an under pressure inside the anchor such that the anchor penetrates through the soil[17].

#### *1.1.4 Articulated Tower*

The articulated tower design for offshore wind structures is less common in offshore wind but the structure was introduced to the oil and gas industry in the 1970s[18]. In the spring of 1974, the drilling rig “Deepsea Driller” found a gas reservoir 18 kilometers north-east of the Frigg field in block 25/1 on the Norwegian Continental Shelf. The field became the first Frigg satellite to be brought on stream with the aid of subsea technology, with wellheads installed on the seabed and with an unmanned control column. The design chosen for the concept was a tower attached by a universal joint to a concrete foundation. This arrangement allowed the tower to move with the waves and currents. The design concept is called ‘Articulated tower’ and this is a single point mooring tower which includes shaft, buoyancy chamber, ballast chamber, universal joint, connector, and the base, as seen in the figure below[19].

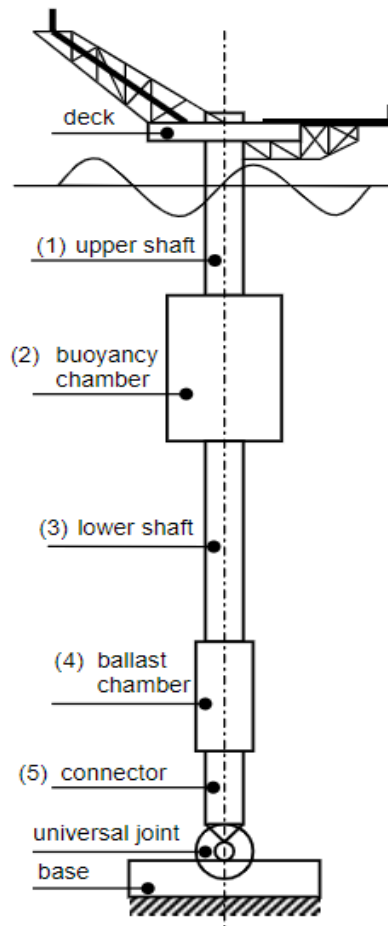


Figure 7: Articulated tower principle [19]

This type of substructure excludes the need of mooring lines but is exposed to both horizontal and vertical loads. The horizontal loads make the structure tilt about the universal joint and is retrieved to static state by buoyancy from the displaced volume in addition to the properties of the buoyancy chamber. The ballast in the lower chamber keeps the center of gravity of the substructure low, increasing the overall stability.

As the articulated tower design is single hinged using a universal joint, they often seem to fail because of large fatigue due to imposed, extensive rotation on the universal joint[20].

However, the articulated tower design has influenced the wind turbine substructure developed by Offshore Kinetics.

#### 1.1.5 Offshore Kinetics Offshore wind turbine

Articulated tower design principle has been adopted to the offshore wind turbine industry, and Offshore Kinetics have developed an offshore wind turbine support structure concept with an articulated tower as substructure[21]. The concept is also referred to as a Hybrid Wind Turbine structure. The design is similar to the articulated tower but uses an internal ballast chamber which is to be loaded with high density ballast. The buoyancy/stabilization chamber is to be filled with Hydrogen for containment and

production but is also suspected to give a significant lift force. The Offshore Kinetics design concept[22] consists of:

- Nacelle: Housing for generator, gearbox, drive train and brake assembly
- Tower: Coned, hollow cylinder
- Stabilization tank: The buoyancy chamber containing hydrogen
- Column: Hollow cylinder
- Universal joint: The point where the substructure tilts about its X and Y-axis.
- Anchor: Suction anchor

## **1.2 Research objective and state of the art**

The objective of the research is to perform numerical assessments of the Offshore Kinetics wind turbine support structure, with the main aim of identifying the torque applied to the structures universal joint, and to conclude on the contributing factors for the torque. The structure's stability is also to be assessed in initial condition and in different sea states. Finally, the concept's feasibility of supporting a wind turbine is to be assessed by looking at the turbine efficiency in various sea states and at different yaw alignment errors.

Many papers on relevant topics such as articulated towers and forces from wind turbine yawing have been published through time, and of the basis of the construction of the Northeast Frigg articulated tower[18], there was presented a design report in which proposed a maximum torque value on the universal joint to  $600 \text{ T}\cdot\text{m}$ , which is approximately  $5886 \text{ kN}\cdot\text{m}$ . The Northeast Frigg was designed to have a helicopter deck on top, but otherwise no external motions were to be applied to the top of the tower as for a wind turbine using the same substructure concept.

Bar Avi and Benaroya(1997)[23] studied the stochastic response of a two degree of freedom articulated tower, which was an extension of their previous paper where they considered an articulated tower with only one degree of freedom. In the study from 1997 the tower was modelled as a spherical pendulum which was subjected to wave, current, and vortex shredding loads. It was found from the analysis that the standard deviation of the rotation angle was larger than for the deflection angle, and that the average equilibrium position depended on the drag coefficient, current velocity, and the current direction. It was also concluded that the sway-motion of the tower oscillated about the equilibrium position. The wind forces on the platform structure above sea level was not considered in this study.

Zaheer and Islam(2017)[24] researched dynamic response of articulated towers under correlated wind and waves, in which included a double hinged tower design. In addition to the regular universal joint, it was also implemented an intermediate hinge placed in a vertical distance from the bottom (universal joint) hinge. The sea states considered was low sea state, moderate sea state, and high sea state, in which



included the parameters wind velocity, significant wave height, and the average zero-crossing period. It was concluded in the paper that the contribution of wind forces on the articulated tower response was governed by the size of the wind driven waves, and that for higher wind speeds producing larger waves, the contribution of wind forces on the dynamic response was small. On the other side, for the lower wind speeds producing small waves, the contribution of wind forces on the dynamic response became significant.

In Energies(2020)[25], studied the dynamic response of an articulated tower offshore wind turbine at different water depths. The turbine included in the study was an NREL 5 MW wind turbine, and was tested in water depths of 50, 70, and 75 meters. A hydrostatic analysis was performed in which the restoring moments was found to be almost linear up to 30 degrees. In the hydrodynamic analysis responses of natural frequencies, pitch, and wave moments was presented. The tension on the hinged joint was also researched and results showed that the max tension on the hinged joint occurred at water depth of 50 meters.

Murtedjo et.al (2005) [19], studied the influence on the dynamic behavior of an Articulated Tower in which the parameters of the buoyancy tank in the articulated tower configuration was adjusted for different trials to obtain an understanding of how the natural frequency and general response of the structure changed due to change in buoyancy tank parameters. The study is based on a general articulated tower concept, not including wind turbine, and the results showed that a 20% change in the diameter of the buoyancy tank affected the natural frequency of the structure up to +/- 27.3%, depending on 20% increase or decrease of diameter. The length of the buoyancy was also adjusted, but it was concluded that the change in diameter gave the largest increase/decrease in both natural frequency and exciting moment.

Kim and Dalhoff (2014)[26], presented moments and torques generated from non-yawing and yawing operations. The torque's contribution was suggested to occur from aerodynamic loads, braking torque from yaw brakes, and driving torque from yaw brakes.

Zhang et al.[27] investigated the feasibility of an offshore wind turbine at 75 meters depth, focusing primarily on a sensitivity check on hydrostatic performance by adjusting the support structure's diameter. The occurrence of tension on the hinged joint was also investigated in this work, and it was concluded that the concept was in general feasible at a 75 m water depth as the hydrostatic performance of the structure met the requirements regarding stability and economy.

A hydrodynamic analysis performed by Noraziah Nor[28] showed that the articulated tower was a good option to use in the oil & gas industry. The reason for this conclusion was that the articulated tower was less complex, cheaper to build, easier to maintain and the hydrodynamic properties. The analysis proved the articulated tower to be very stable and showed a maximum 30 feet displacement under 100-year

hurricane conditions.

Sadeghi and Bichi[29] studied several offshore tower platforms regarding design, analysis, construction and installation. Amongst these offshore tower platforms were fixed (jacket, tension leg, gravity, etc.), moveable (jack-up, semi-sub), floating production system (FPSO), and compliant structures which includes the Guyed Tower and Articulated tower. For the articulated tower structure, some of the advantages and disadvantages were:

*Advantages:*

- Low cost
- Large restoring force due to high center of buoyancy
- Natural period greater than wave period
- Lower dynamic amplification factor (DAF) than fixed structures
- Simple design, installation, and decommissioning
- No base moment due to hinged joint

*Disadvantages:*

- Applicable for relatively shallow waters only
- Structure oscillations increase with water depth
- Fatigue on universal joint
- Limited to small field

## 2. Relevant theories

This chapter contains relevant theories for researching the critical aspects of the Hybrid Wind Turbine, including environmental forces and theories, statistics, yaw mechanism and components, initial stability, and classical mechanics.

### 2.1 Environmental Forces

The environmental forces must be considered for feasibility studies of offshore structures, and these include the forces from waves, winds and currents. The forces from waves and currents are often referred to as hydrodynamic forces[30].

#### 2.1.1 Wave forces

Wave forces are vital to consider for all marine structures, and the structures are often classified to large-volume or small-volume constructions[31]. The classification can be done through using known analytical results for a cylinder in regular, sinus waves. Small-volume construction can be divided into drag-dominant and inertia-dominant structures, and while there might be one which is dominant, both will most often contribute and need to be included[31]. Drag and inertia forces are referred to as Morison forces and can be calculated using Morison's equation of wave forces on cylindrical geometries[31].

#### Morison force

Morison's equation is used to calculate wave forces on constructions or construction parts of circular geometries as shown in the figure below.

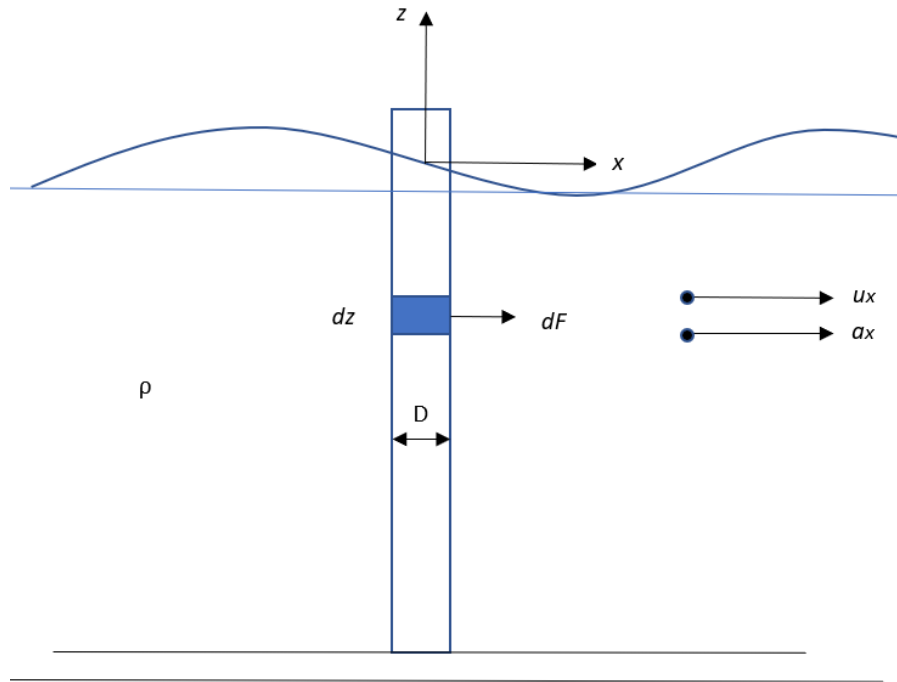


Figure 8: Waves on slender cylinder

Morison's equation says that the horizontal force on a strip of a length can be written as:

$$dF = \rho \frac{\pi D^2}{4} c_M a_x dz + \frac{1}{2} \rho C_D D u |u| dz \quad (2.1)$$

Where

$\rho$  = Water density  $\left[\frac{kg}{m^3}\right]$

$D$  = Diameter of cylinder [m]

$c_M$  = Mass coefficient [-]

$C_D$  = Drag coefficient [-]

$a_x$  = Horizontal water particle acceleration  $\left[\frac{m}{s^2}\right]$

$u$  = Horizontal water particle velocity  $\left[\frac{m}{s}\right]$

The force distribution of drag and inertia forces depends on the relationship between wave height, wavelength and the diameter of the structure exposed to the wave[31]. In principle, the dominance of either drag forces or inertia forces can be comprehended using the figure below.

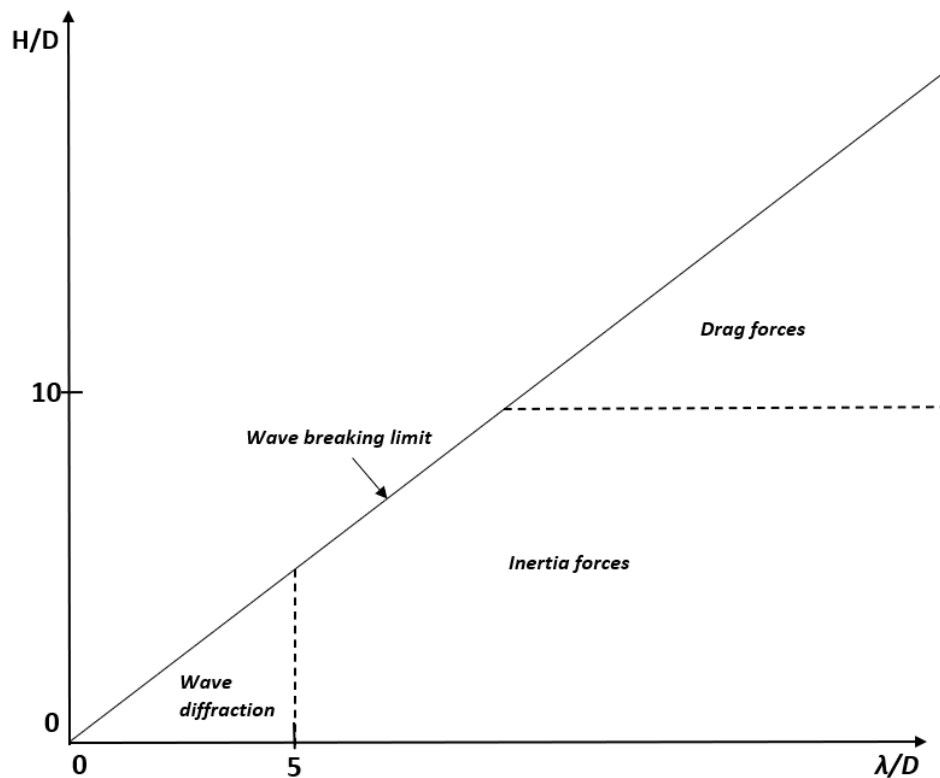


Figure 9: Drag and Inertia force

Drag force is the force acting opposite the relative motion between a construction and the surrounding fluid. It is sometimes called fluid friction which describes the physical action of the force. This force is proportional to the squared of the velocity for high-speed flows and is dependent on the density of the surrounding fluid, particle velocity, cross section area and the drag coefficient[31]. The drag coefficient is a dimensionless number which depends on the structure's shape and on Reynolds number[31]. To reduce the drag force for moving vessels an optimization on the shape of the hull is often performed to decrease the drag coefficient.

Maximum drag force in regular sine waves occurs when the wave peak is on  $X=0$  in the local axis of a structure as seen in the figure below.

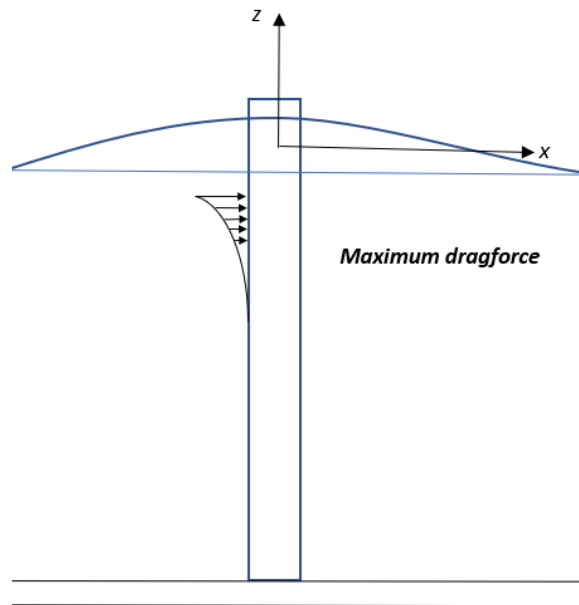


Figure 10: Maximum drag force

The fluid inertia force is the fluid's resistance force to change in velocity and is dependent on the fluid density, volume of the structure, inertia coefficient, and the horizontal water particle acceleration[31]. The maximum inertia force occurs when the wave node is in  $X=0$  in the structure's local axis as seen in the figure below.

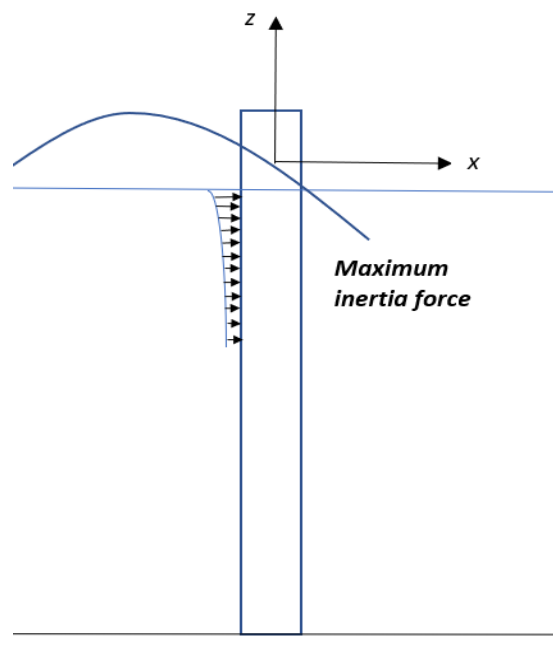


Figure 11: Maximum Inertia force

The flow velocity of fluids decreases with the water depth, and since the drag and inertia force is

dependent on the wave particle's velocity and acceleration respectively, the overall force will also decrease with the depth.

### 2.1.2 Wind loads

As for the submerged section of the wind turbine structure, the top side is also exposed to loads, but here in terms of wind. For the tower it is the wind drag which is most relevant while it is a lift force which primarily acts on the turbine blades.

### Wind drag force

The wind drag force acts in the same way as for the wave drag, but the density of air is much less than for sea water and therefore the air drag contribution will be less than the wave drag. It is however not at all negligible since the air drag acts on a much higher altitude than the wave and thereby create a significant momentum about the bottom part of the wind turbine structure. In addition, since the drag force increases with the square of the speed, and the reference wind speed at high altitudes could be significant. The air drag formula is given as

$$F_D = \frac{1}{2} \rho C_D U^2 A \quad (2.2)$$

Where,

$$\rho = \text{Air density} \left[ \frac{\text{kg}}{\text{m}^3} \right]$$

$$C_D = \text{Drag coefficient} [-]$$

$$U = \text{Wind velocity at reference point}$$

$$A = \text{Reference cross section area}$$

For most wind turbine top sides, the tower part is coned for aerodynamic purposes, as well as for reducing material costs[32]. This change in the diameter, and thus the reference cross section area, must be considered when calculating the air drag force. The change in area due to change in diameter can be written as:

$$A = A(z) = D(z) \cdot dz \quad (2.3)$$

then drag force for a coned cylinder becomes

$$F_D = \frac{1}{2} \rho C_D U^2 \int_0^z D(z) \cdot dz \quad (2.4)$$

assuming constant wind speed at the whole structure.

The reference height of wind action should in general be equal to the maximum height above sea surface of the section being considered[33].

### Lift force

Considering the basic concept of an air foil, the lift force should be greater than the drag force in order to achieve lift of an airplane foil or for making wind turbine blades rotate. Fluid mechanics have proven that the pressure increases at lower velocities meaning that the pressure underneath the foil is larger than above, creating a lift force[34].

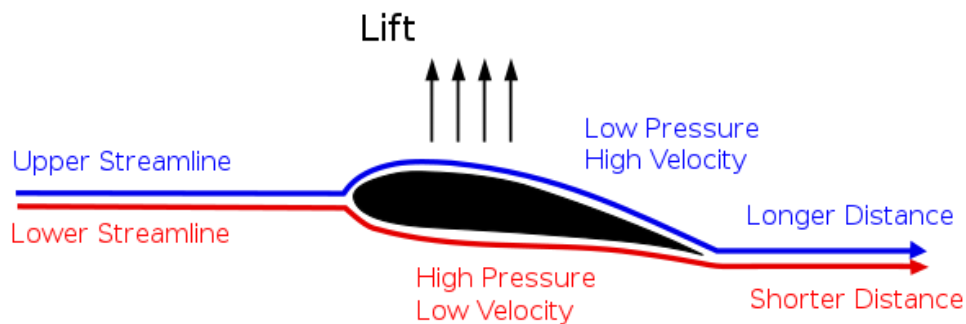


Figure 12: Lift force on foil[34]

The lift force acts perpendicular to the flow direction, while drag force acts opposite of the flow direction[34]. To achieve sufficient lift and thus rotation of the wind turbine blades, the lift force must be greater than the drag force.

The lift force can be expressed as

$$F_L = \frac{1}{2} \rho v^2 s \cdot C_L \quad (2.5)$$

where  $s$  is the projected wind area and  $C_L$  is the lift coefficient at the desired angle of attack, Mach and Reynold's number. The angle of attack will impact the Lift-to-Drag ratio so that by changing this angle can make the blades turn faster or slow them down if the speed is too high. Changing this angle of attack will then decrease the lift and increase the drag to slow the rotation down.

## 2.2 Environmental inputs

To find the forces and moments from environmental loads, knowledge on the most probable



environmental conditions must be obtained. The forces from wind and waves depends on their properties and these weather conditions differ from day-to-day, seasonally and annually. From historical data and statistics, it is however possible to gain a sense of the most probable weather conditions on locations.

### 2.2.1 Irregular sea states

An irregular wave sea state is a random process which includes a combination of different regular waves. Each of these regular waves has their own particular frequency, phase angles, wave period, amplitude and direction[35]. The sum of these waves creates the irregular sea state that is observable at sea. A part of a simple time history of an irregular wave can be seen in the figure below.

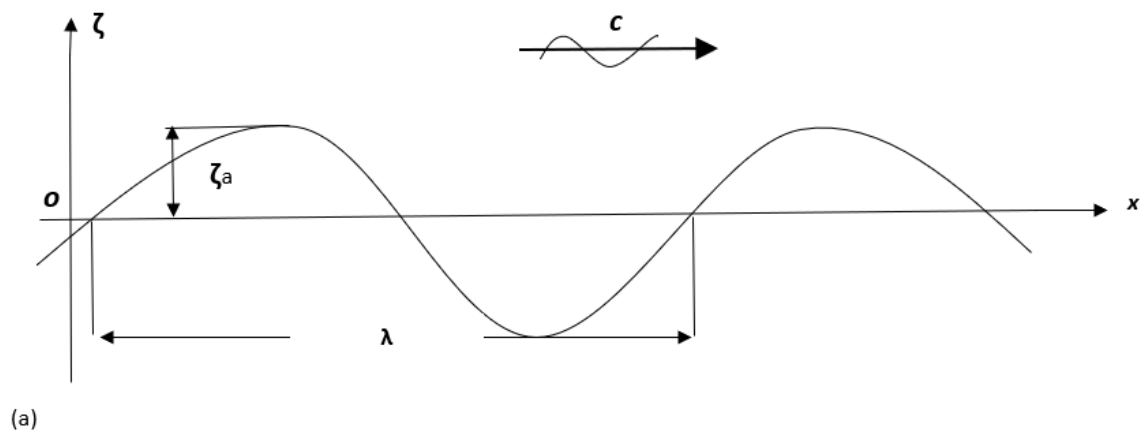


Figure 13: Wave contour at time  $t$

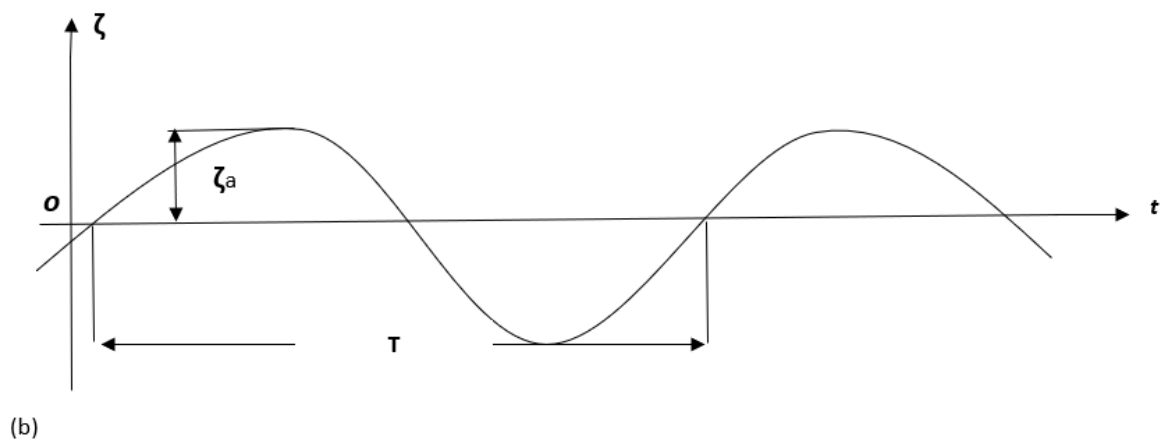


Figure 14: surface elevation at position  $x$ ,

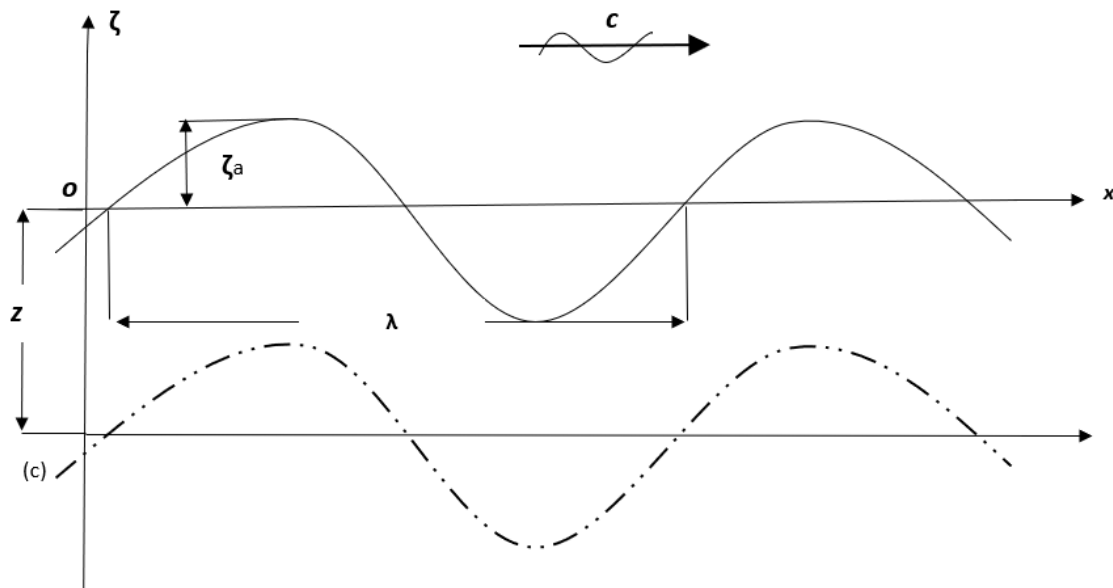


Figure 15: isobaric contours across depth

The average period,  $T$  is obtained from the average zero-crossing period or from the average period of wave crests or troughs[35].

The significant wave height,  $H_s$  or  $H_{1/3}$ , is the average wave height of the largest third of the waves in an observed series. Significant wave height is often used in applications of wave statistics because there is often a fair correlation between this significant wave height and the visually estimated wave height[35]. As the significant wave height is the average height of the highest third of the waves, it implies that encountering the significant wave is not too frequent. On the other hand, it is statistically possible to encounter waves of up to almost twice the height of the significant wave height.

The statistical information can be obtained from a probability density function,  $f(x)$ , and the probability of the wave height  $H_\omega$  exceeds a certain value,  $\alpha$ , in terms of height can be expressed by

$$P[H_\omega > \alpha] = \int_{\alpha}^{\infty} f(x) \cdot dx \quad (2.6)$$

Under short-term statistically stationary conditions, ocean waves can be described mathematically as random or stochastic process with statically steady characteristic appearance. This means that wave characteristics can be analyzed and described by implementing the theory of probability and statistics[35].

### 2.2.2 Energy spectrum

The energy in a series of waves consists of kinetic energy linked to the orbital motion of water particles and potential energy due to change in water level in hollows and crests. In a wavelength  $\lambda$ , the kinetic and potential energy can be expressed as,

$$E_k = \frac{1}{4} \rho g \zeta_a^2 \lambda, \quad E_p = \frac{1}{4} \rho g \zeta_a^2 \lambda \quad (2.7)$$

And the total energy,

$$E_k + E_p = \frac{1}{2} \rho g \zeta_a^2 \lambda \quad (2.8)$$

Ocean waves can be regarded as the linear superposition of simple, harmonic wave components and therefore the energy can be obtained by summarizing the energies in each component. This total average energy per unit area of free surface for wave components of frequencies  $(\omega_i, \omega_i + \Delta\omega)$  is given by

$$E = \sum_{\omega_i}^{\omega_i + \Delta\omega_i} \left( \frac{1}{2} \rho g \delta_{ai}^2 \right) = \frac{1}{2} \rho g \sum_{\omega_i}^{\omega_i + \Delta\omega_i} \delta_{ai}^2 \quad (2.9)$$

And the energy spectrum,  $s_\delta$  as a function of the frequency  $\omega_i$ , is given by

$$s_\delta(\omega_i) = \frac{\frac{1}{2} \sum_{\omega_i}^{\omega_i + \Delta\omega_i} \delta_{ai}^2}{\Delta\omega_i} \quad (2.10)$$

where  $s_\delta(\omega_i)$  denotes the wave energy density at frequencies  $\omega_i$ , and  $s_\delta$  shows distribution of energy of the irregular waves among the different regular components with their unique frequencies[35]. The energy spectrum is often presented as a graph as seen in the figure below.

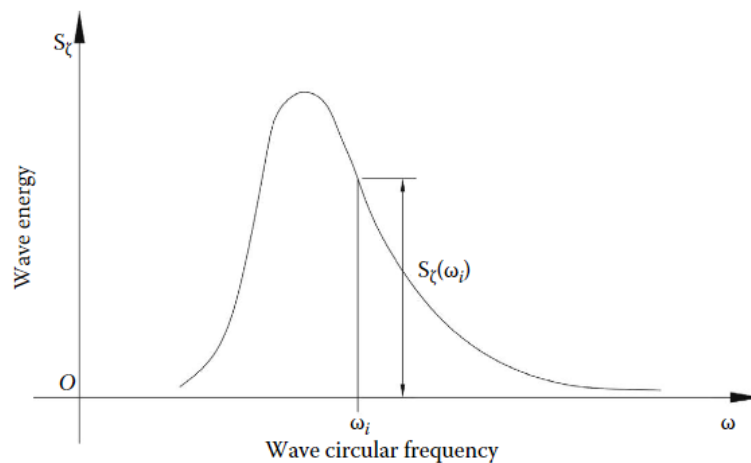


Figure 16: Energy spectrum[35]

### 2.2.3 JONSWAP spectrum

A project called the “Joint North Sea Wave Observation Project”(JONSWAP), found that the wave spectrum is never fully developed [36]. Using a Pierson-Moskowitz spectrum, they added a peak

enhancement factor  $\gamma$  to improve the fit to their measurements, meaning that the JONSWAP spectrum is similar to a Pierson-Moskowitz spectrum, but multiplied by the peak enhancement factor  $\gamma$  [36]. The JONSWAP spectra is expressed as

$$S_j(\omega) = \frac{\alpha g^2}{\omega^5} \exp\left[-\frac{5}{4}\left(\frac{\omega_p}{\omega}\right)^4\right] \gamma^r \quad (2.11)$$

and can be seen graphically together with the Pierson-Moskowitz spectrum in the figure below.

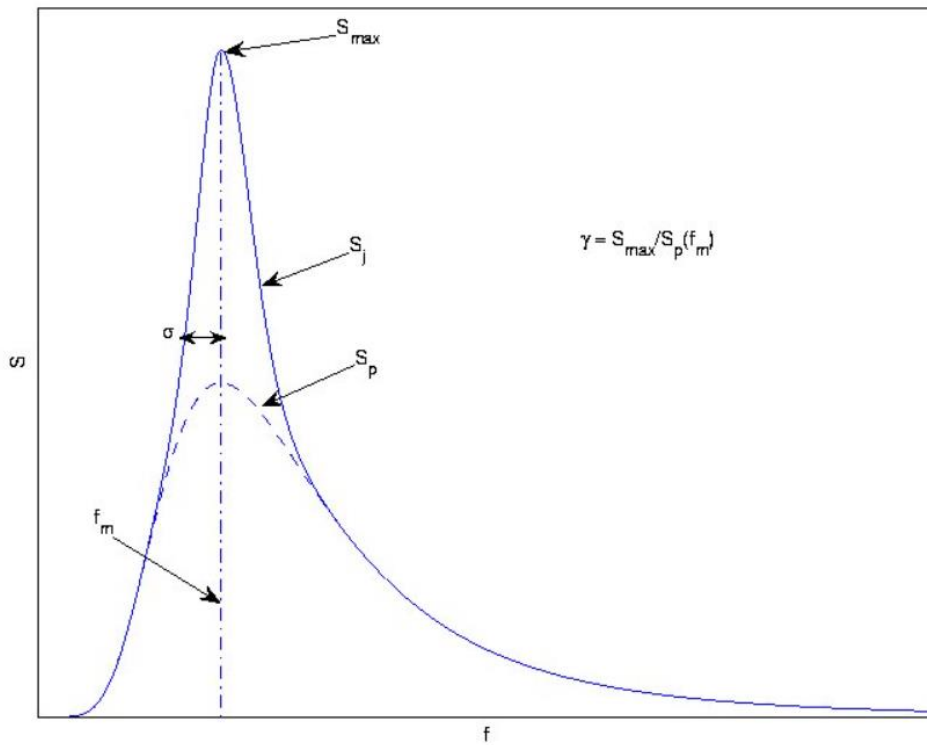


Figure 17: Pierson-Moskowitz spectrum[36]

The parameters are calculated as

$$\alpha = 0.076 \left(\frac{U_{10}^2}{Fg}\right)^{0.22} \quad (2.12)$$

$$\omega_p = 22 \left(\frac{g^2}{U_{10}F}\right)^{\frac{1}{3}} \quad (2.13)$$

$$\gamma = 3.3 \quad (2.14)$$

$$\sigma = \begin{cases} 0.07 & \omega \leq \omega_p \\ 0.09 & \omega > \omega_p \end{cases}, \quad (2.15)$$

And  $F$  is the fetch distance, which is the distance the wind blows with a constant velocity[36].

#### 2.2.4 Short-term statistics

Short-term statistics are used to estimate the statistical response applied from a stationary sea state defined in a wave spectrum. Through time there has been used several methods for gathering information regarding wind, wave height, and wavelength. These methods include data collection from ships, buoys, and sailing vessels. Through these observations and measurements, it was discovered that a sea state can be described in terms of a wave spectrum, in which the probability of a certain wave height can be described as a Rayleigh-distribution[37],

$$f(x) = \frac{x}{m_0} e^{-\frac{x^2}{2m_0}} \quad (2.16)$$

in terms of the wave amplitude, or

$$f(H) = \frac{H}{4m_0} e^{-\frac{H^2}{8m_0}} \quad (2.17)$$

in terms of the wave height.

The significant wave height can then be estimated as follows:

$$H_{1/3} = 4 \cdot \sqrt{m_0} \quad (2.18)$$

When the significant wave height, the zero up-crossing period and the duration of the sea state is known, the probability of a wave height higher than the estimated maximum wave height can be calculated,

$$P(H_{Extreme} > H_{max}) = 1 - G(H_{max}), \quad (2.19)$$

in which

$$G(H_{max}) = 1 - e^{-2\left(\frac{H_{max}}{H_s}\right)^2 N} \quad (2.20)$$

From these equations we find that the correlation between the maximum wave height,  $H_{max}$  and the significant wave height,  $H_s$  is:

$$H_{max} = H_s \cdot \sqrt{0.5 \ln(N)} \quad (2.21)$$

where  $N$  is the number of waves in the time series, and can be calculated from

$$N = \frac{\text{Duration of sea state}}{\text{Zero-crossing period}} = \frac{t}{T_z} \quad (2.22)$$

### 2.2.5 Wind theories

There are several types of wind theories which has been developed through time and spectrums are used to describe short-term stationary wind conditions. Spectrums, meaning the power spectral density of the wind speed, can be site-specific whereas the speed process can be determined from historically measured wind data. The spectrums presented in this section are the theories relevant for the Orcaflex[38] inputs.

“The spectral density,  $s_U(f)$ , shall asymptotically approach the following form as the frequency  $f$  in the high frequency range increases”[39].

$$s_U(f) = 0.14 \cdot \sigma_u^2 \left( \frac{L_u}{U_{10}} \right)^{-\frac{2}{3}} \cdot f^{-\frac{5}{3}} \quad (2.23)$$

Where  $U_{10}$  is the 10-minute mean wind speed at a height of 10 meters,  $\sigma_u$  is the corresponding standard deviation, while  $L_u$  is the integral length of scale of the wind speed process[39].

#### 2.2.5.1 NPD Spectrum

The NPD spectrum is intended for describing gusts at mean wind speeds above 10 m/s and has been developed in the recent years as a new spectrum type. This spectrum is based on wind measurements from off the coast of mid-Norway. It is called NPD spectrum because it was found in a publication from 1992 by the Norwegian Petroleum Directorate (NPD) [40]. The spectrum is expressed as:

$$s_{NPD}(f) = \frac{320 \cdot \left( \frac{u}{10} \right)^2}{(1 + \bar{f}^n)^{5/3n}} \quad (2.24)$$

Where

$$\bar{f} = 172f \cdot \left( \frac{u}{10} \right)^{-3/4} \quad (2.25)$$

And  $n = 0.468$ .

### 2.2.5.2 API Spectrum

The API spectrum[41] assumes the wind speed is horizontally uniform but varies with height above the sea surface according to a power law profile. The spectrum at elevation above sea level,  $z$ , is defined as

$$S(f, z) = U_z^2 I_z^2 f_p^{-1} \left[ 1 + 1.5 * \left( \frac{f}{f_p} \right) \right]^{-5/3} \quad (2.26)$$

Where

$$f_p = 0.025 \cdot \frac{U_z}{z} \quad (2.27)$$

The associated 1-hour mean wind speed is

$$U_z(z) = U_{ref} \cdot \left( \frac{z}{10} \right)^{0.125} \quad (2.28)$$

And the turbulence intensity is given by[41]

$$I_z(z) = \begin{cases} 0.15 \left( \frac{z}{20} \right)^{-0.125} & \text{if } z \leq 20 \text{ m} \\ 0.15 \left( \frac{z}{20} \right)^{-0.275} & \text{otherwise} \end{cases} \quad (2.29)$$

### 2.2.5.3 ESDU Spectrum

The ESDU Spectrum[41] at an elevation above the mean water line is defined as

$$S(f, z) = 4I_z^2 U_z L_u \left[ 1 + 70.8 * \left( \frac{f L_u}{L_u} \right)^2 \right]^{-5/6} \quad (2.30)$$

The associated 1-hour wind speed,  $U_z$ , is here dependent on a friction velocity and a boundary layer scaling parameter which includes a drag coefficient[41].

The turbulence intensity for the ESDU Spectrum,  $I_z$ , is dependent on a Coriolis parameter which includes the Earth's rotational speed in rad/s[41].

## 2.3 Classical mechanics

### 2.3.1 Mass

Mass and its center are an important input for all hydrostatic and hydrodynamic analysis'. For the wind turbine substructure, the calculation of the mass can be found using the equation

$$m = \rho \cdot v \quad (2.31)$$

Where  $\rho$  is the density of the material in  $\frac{kg}{m^3}$  and  $v$  is the volume in which is calculated for hollow cylinders as

$$v = \frac{\pi}{4} \cdot (D^2 - d^2) \cdot h \quad (2.32)$$

or

$$V = \pi(R^2 - r^2)h \quad (2.33)$$

The tower parts of wind turbines are often coned for aerodynamic purposes, and the mass of a coned, hollow cylinder per strip  $dx$  is

$$dm = \rho dv = \rho\pi(R^2(x) - r^2(x)) dx \quad (2.34)$$

which gives

$$m = \rho\pi \int_0^x (R^2(x) - r^2(x)) dx \quad (2.35)$$

### 2.3.2 Mass moment of inertia

Moment of inertia is a quantity which determines the torque needed for a desired angular acceleration about a rotational axis[42]. This is primarily dependent on the object's mass and geometry. For a wind turbine substructure, the mass moment of inertia varies from the different sections because of volume and thereby mass, and geometry.

For a cylinder the mass moment of inertia is[43]:

$$I = \frac{1}{2}Mr^2 \quad (2.36)$$

where  $M$  is the mass of the body and  $r$  is the radius. For hollow cylinders the distance to both the inner and outer body needs to be considered, and the equation then becomes

$$\frac{1}{2}M(a^2 + b^2) \quad (2.37)$$

For the tower part of a wind turbine substructure, this section is both hollow and coned, affecting both the mass and the radius. These parameters then change per slice of a length in which could be called  $dx$ .



Since the radius changes, the volume also changes and must be considered.

Knowing that

$$v = \pi r^2 h \quad (2.38)$$

Calling each slice of the height  $dx$ , then

$$dV = \pi r^2 dx \quad (2.39)$$

and since

$$m = \rho v \quad (2.40)$$

then

$$dm = \rho dv = \rho \pi r^2 dx \quad (2.41)$$

Equation 3.30 becomes

$$dI = \frac{1}{2} dMr^2 = \frac{1}{2} \rho \pi r^2 dx \cdot r^2 \quad (2.42)$$

and

$$I = \int dI = \frac{1}{2} \rho \pi \int_0^x (r(x))^4 dx \quad (2.43)$$

Given that the section is also hollow:

$$I = \frac{1}{2} \rho \pi \int_0^x (R(x) - r(x))^4 dx \quad (2.44)$$

Meaning that a function of the radius in terms of  $x$  must be calculated. The relevant calculations of mass moment of inertia for this thesis are shown in 3.2.5 and in Appendix 4 – Calculation of Moment of inertia,  $I_z$ , for tower section.

### 2.3.3 Torque

Torque is a measure of the force needed to cause an object to rotate about an axis[44]. Torque means as the tendency of a force to rotate an object about an axis. For this thesis the force is the environmental forces in terms of wind and waves, in addition to angular acceleration/deacceleration in yawing operations, while the object is the wind turbine, and the axis is in this case the vertical Z-axis. A rotation

about this axis is called yaw[45], which will be explained further in the next chapter

The net torque of a body determines the rate of change in a body's angular momentum,

$$\tau = \frac{dL}{dt} \quad (2.45)$$

where  $L$  is the angular momentum and  $t$  is the time. The angular momentum for a single point particle is given by

$$\mathbf{L} = \mathbf{r} \times \mathbf{p} \quad (2.46)$$

where  $\mathbf{r}$  is the position vector from the origin and  $\mathbf{p}$  is the particle's linear momentum.  $\frac{dL}{dt}$  is then

$$\frac{d\mathbf{L}}{dt} = \mathbf{r} \times \frac{d\mathbf{p}}{dt} + \frac{d\mathbf{r}}{dt} \times \mathbf{p} \quad (2.47)$$

The time derivative of a position is velocity, which means

$$\frac{d\mathbf{r}}{dt} = \mathbf{v} \quad (2.48)$$

and the net force is equal to the time derivative of the linear momentum, meaning

$$\frac{d\mathbf{p}}{dt} = \mathbf{F} \quad (2.49)$$

thus,

$$\frac{d\mathbf{L}}{dt} = \mathbf{r} \times \mathbf{F} + \mathbf{v} \times \mathbf{p} \quad (2.50)$$

The linear momentum  $\mathbf{p}$  and the velocity  $\mathbf{v}$  are parallel meaning that the cross product of these equal zero from vector theory. The torque can then be expressed as

$$\tau = \frac{dL}{dt} = \mathbf{r} \times \mathbf{F} \quad (2.51)$$

giving the unit [ $N \cdot m$ ].

## 2.4 Hydrostatics

Hydrostatic properties are dependent on the mass, volume and geometry of a structure at sea which could be a vessel, an oil rig, a buoy or, as in this research, an offshore wind turbine. The main goal of a structure's hydrostatic properties is to have a good stability and avoid capsizing. Structures at sea are

influenced by environmental loads which forces movement of the structures. These movements can be divided into three translations and three rotations which combined are referred to as the degrees of freedom, (DOF)[35].

#### 2.4.1 Degrees of freedom

The degrees of freedom include the translations in the three dimensions (X, Y, Z) and the rotations about these[35]. These degrees of freedom have different names as shown in the figure below[46].

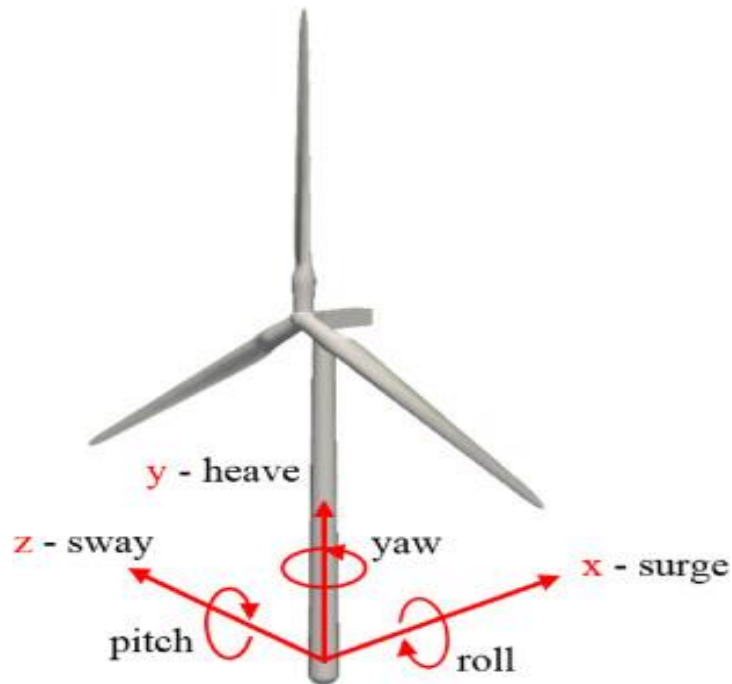


Figure 18: Wind turbine Degrees of Freedom[46]

#### Translations

- Surge is the movement along the X-axis
- Sway is the movement along the Y-axis
- Heave is the upwards movement along the Z-axis

#### Rotations

- Roll is the rotation about the X-axis
- Pitch is the rotation about the Y-axis
- Yaw is the rotation about the Z-axis

#### 2.4.2 Definitions and application of stability terms

The stability of marine structures is dependent of the value of the distance between center of gravity and the metacenter,  $\overline{GM}$ , which is dependent on the distances KG, KB, BM[35]. The distance GM is a value that says something about the vessel's stability and is dependent on the gravitational center and the

center of buoyancy.  $\overline{GM}$  can be written as:

$$\overline{GM} = \overline{KB} + \overline{BM} - \overline{KG} \quad (2.52)$$

and  $\overline{GM}$  should initially be at least 0.15 meters for seagoing vessels[35]. For a vessel these geometrical distances can be configured as seen in the figure below.

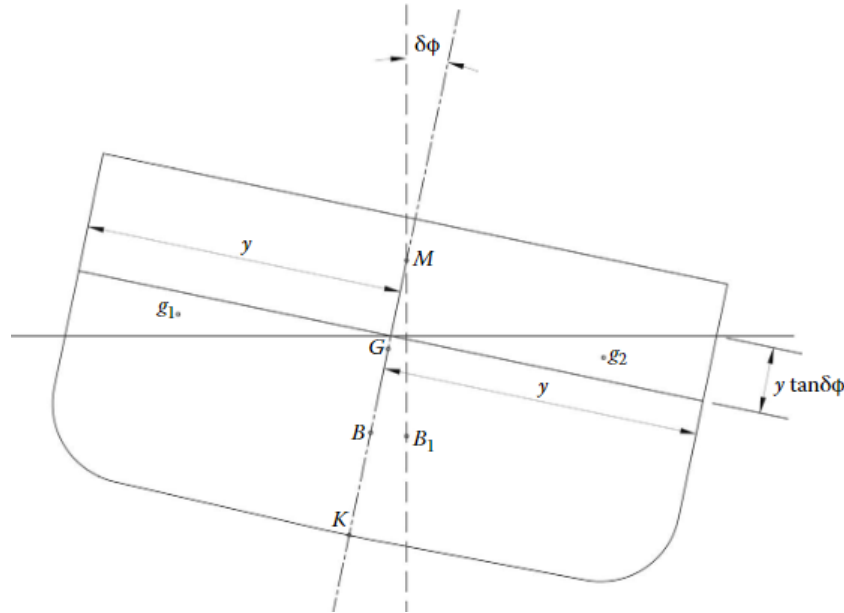


Figure 19: Vessel stability[35]

#### 2.4.2.1 Center of buoyancy

The distance  $\overline{KB}$  is the distance from a vessel's keel to its center of buoyancy. The center of buoyancy is the center of the displaced volume by the vessel and will shift horizontally as the vessel inclines, as shown in figure 19. The initial value of the buoyancy center can be found using the relationship

$$\overline{KB} = z_B = \frac{\int_0^T A_w dz}{\int_0^T A_w dz} = \frac{\sum_{i=1}^n v_j z_i}{\sum_{i=1}^n v_j} \quad (2.53)$$

Where  $A_w$  is the waterline area in  $m^2$ .

#### 2.4.2.2 Center of gravity

The center of gravity of a vessel can be found using a similar method,

$$z_G = \frac{\sum_{i=1}^n m_i z_i}{\sum_{i=1}^n m_i} \quad (2.54)$$

Where  $m$  is the mass, and  $z$  is the vertical distance to the center of the mass.

### 2.4.2.3 Metacenter

The metacenter is an imaginary point in a ship's center plane through which the buoyancy force acts when the ship inclines in still water. To obtain a stable equilibrium the distance from the center of gravity to the metacenter must be positive.

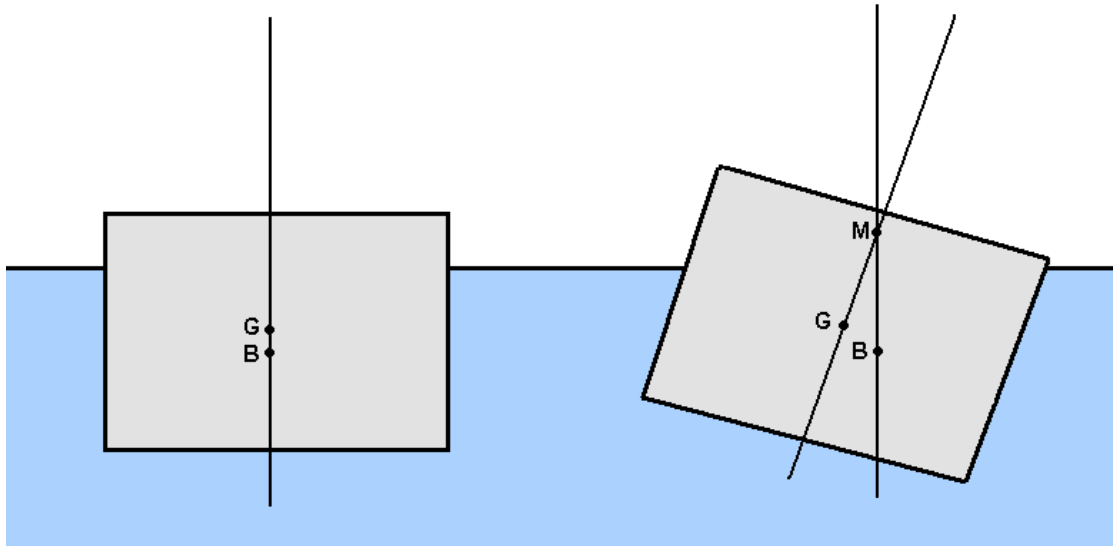


Figure 20: Metacenter

This distance from center of gravity to the metacenter is called GM and should in general for vessels be at least 0.15m to provide sufficient stability[35]. As seen in equation 2.52, this distance is also dependent on the distance from buoyancy center to metacenter, called initial metacenter radius, which can be calculated by

$$\overline{BM} = \frac{I}{\nabla} \quad (2.55)$$

Where  $I$  is the second moment of area for the waterline area [ $m^4$ ], and  $\nabla$  is the total displaced volume [ $m^3$ ].

### 2.4.3 Righting moment

The righting moment is a good indication on a vessels stability property as it describes a ship's tendency to return to equilibrium or static state after heeling[35]. This moment is equal to the ship's righting arm multiplied by the displacement, which will change when the ship inclines.

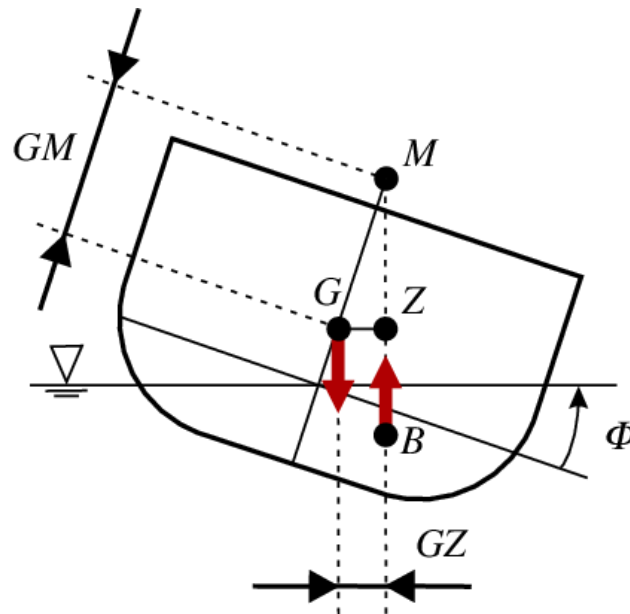


Figure 21: Rightening moment[47]

As the ship inclines, the center of buoyancy shifts horizontally to the point B on the figure above. Drawing a vertical line from this point, the righting arm will be the horizontal distance from the center of gravity to this line. The righting moment can then be written as

$$MR = \Delta * GZ \quad (2.56)$$

where  $\Delta$  is the ship's mass displacement. This moment is vital to prevent capsizing and therefore also the properties of center of gravity, center of buoyancy and the mass is important.

## 2.5 Turbine yawing theory

The yawing mechanism is one of the most important functions of the wind turbine system as the turbine needs to be aligned to the wind direction in order to produce electrical power efficiently[48]. The yawing system of the wind turbine provides this possibility of yawing to the wind direction and captures signals of offset wind before the yaw drive starts and the yawing operation begins. The yawing operations could however also be a factor of significant loads on the tower and substructure.

### 2.5.1 Yaw controller

The yaw controller is one of the most important controllers when designing a wind turbine. Wind turbines work most efficient when facing the wind directly allowing full advantage of the swept area of the blades. Since the wind direction is not constant over time, a system is needed to rotate the nacelle about its vertical axis to the direction of the wind. For most conventional wind turbines, this is done by using a yaw controller. In addition, the yaw controller can avoid forces related to yaw misalignments[49].

### 2.5.2 Yaw controller configuration

A typical yaw system configuration can consist of yaw drives, yaw brakes and bearing, in addition to the gear and electric motor[26]. A such configuration can be seen in the figure below.

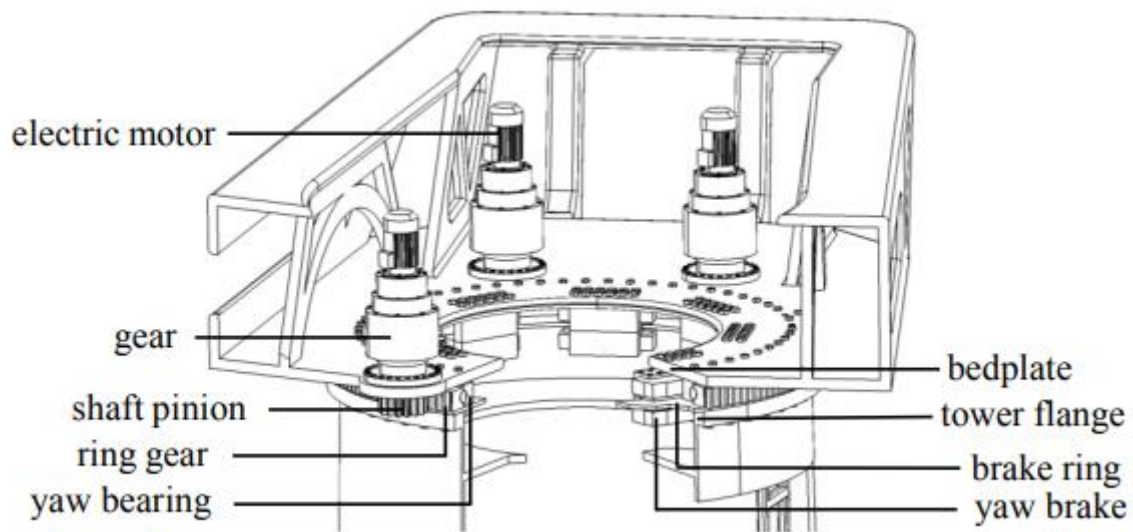


Figure 22: Yaw system configuration[26]

### 2.5.3 Yaw drive

The yaw drive can be provided by an electrical motor as seen in the figure but there is also used hydraulic actuators. The yaw drive can decide the rotational speed of the nacelle, which is often referred to as the yaw rate and has the dimension degrees per second or radians per second. The most conventional yaw rate used today is 0.5 degrees per second. A problem with electro-mechanical vs hydraulic drives are high peak loads and backlash problems which usually occur during start and stop operations of the yawing because of rapid starts and stops[26].

### 2.5.4 Yaw bearing

The bearing is a vital part of the arrangement for avoiding twist of the tower structure and the substructure. If the nacelle rotates about its vertical axis without a bearing system, severe twist and torque could be applied to the lower sections[50].

Yaw bearings for wind turbine often consists of four-point bearings. The configuration of double-row four-point bearing is more expensive but has the advantage of better stress distribution, and thus a longer lifetime. The bearings have breaking and damping properties such that additional yaw brakes could be unnecessary but is dependent on environment[26].

### 2.5.5 Yaw brakes

To avoid movements due to slightly change of wind or low wind speeds, a brake system is present in the yaw system. This means that a certain amount of force from the wind is needed to activate the system to release the breaks. During non-yawing operations the maximum brake force is applied. These forces

are often hydraulically regulated and are released during yawing operations but not entirely to reduce the alternating loads on the gears of the yaw drive[51].

#### 2.5.6 *Yaw rate*

The yaw rate is the speed in which the nacelle rotates about its vertical axis when turning against the wind. The yaw rate is given in degrees per second or radians per second. A typical yaw rate is about 0.5 degrees per second[26], but this varies from site to site. In Equinor's Hywind Tampen project there are to be installed 11 wind turbines with capacity of 8 MW each[3]. The turbines are provided by Siemens Gamesa, and they have informed during conversation that the yaw rate of their Hywind Tampen turbines have been set at default to 0.3 degrees per second, but it is possible to adjust this parameter in the range of 0 to 1 degrees per second[52]. At yaw rates above 1 degree per second it might be applied too much torque from the braking sequence when the turbine is approaching alignment with the wind direction. This force comes from deceleration of significant mass and could be damaging for the yawing bearings and create twist and torque on tower, substructure, and the universal joint.

#### 2.5.7 *Yaw misalignment error*

The yaw misalignment error is a typical error of wind turbines. As the most optimal position of the turbine in terms of producing electrical energy is zero degrees relative angle to the wind direction, the sensors are not precise enough to detect minimal misalignments. A yaw misalignment of 10 degrees could potentially result in a 3.02% annual loss of energy production[53]. A study from 2016[54] measured the misalignments on over 300 wind turbines. The findings were that over 50% of the wind turbines were misaligned to the wind, with most of the turbines having a maximum misalignment of up to 4 degrees, while some had misalignment up to 20 degrees before the yaw drive was activated and the turbine began to yaw to align with the wind.

#### 3.5.8 *Forces from yawing operations*

The forces from the yawing operations are a central topic in this research. The universal joint at the lower part of the substructure has been identified as a possible critical point as it allows rotation about its X and Y-axis but not the Z-axis. The forces from yawing could be translated to this universal joint and therefore be exposed to significant forces and moments from the yawing operation on top.

To reduce the risk of significant forces and moments on the universal joint, an optimal yaw control system is necessary and therefore a look at what creates these forces and moments from the yaw system must be considered.

### **Non-yawing operations**

For non-yawing operations the torque from aerodynamic or environmental loads is dominant, which is illustrated in the figure below[26]



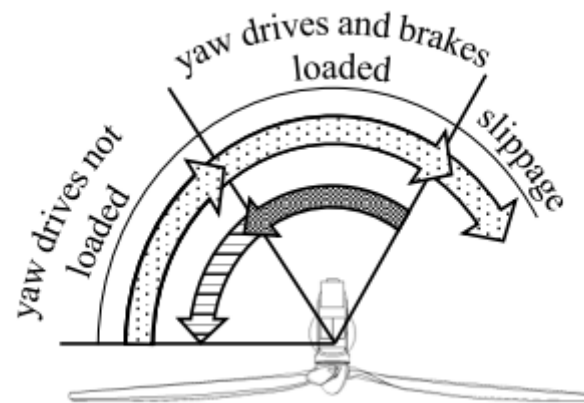


Figure 23: Non-yawing torque[26]

White arrows with dots represent the torque applied from environmental loads, white arrows with black lines represent the braking torque from the yaw brakes, while the black arrow shows the driving/braking torque from yaw drives.

### Yawing operations

During yaw operations, the torque is mainly applied because of the yaw drives which rotates the nacelle towards the wind with the brakes acting opposite way, in addition to the environmental forces which also contributes. Below is a figure showing the torque contributions during accelerated and decelerated yawing[26].

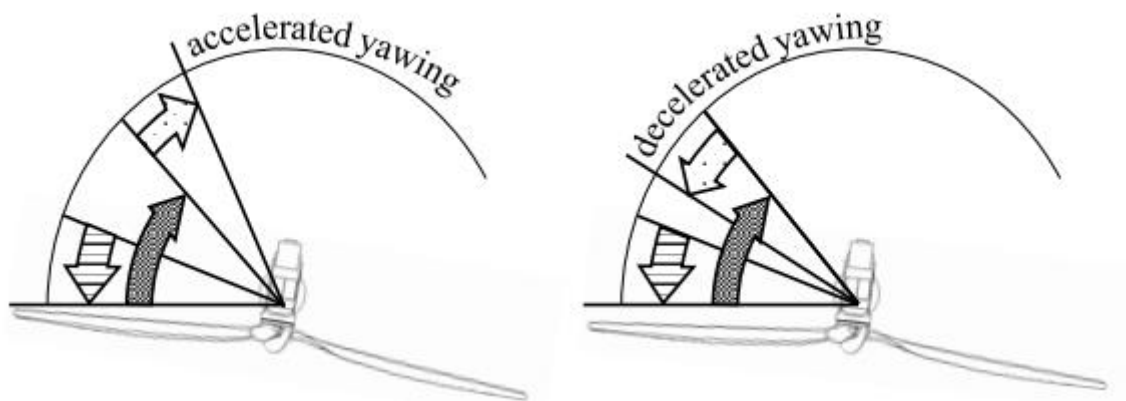


Figure 24: Yawing torque[26]

### 3. Numerical assessments

To find the torque applied to the universal joint and to model a yaw control system for the Hybrid Wind Tower concept, programs such as Inventor[55] and Orcaflex[38] are used in combination with the analytical tool Excel[56].

This chapter explains the process of the research's main part, which consists of:

- Study of current design concept of wind turbine structure
- Calculation of geometrical and hydrostatic properties of current structure for input to Orcaflex
- Adjusting design parameters if necessary.
- Implement a suitable yaw controller.
- Determination of simulation scenarios.
- Running simulation

#### 3.1 Current design of Hybrid Wind Turbine

Offshore Kinetics have come up with a principal design configuration for an 8-9 MW wind turbine which can be seen in the figure below.

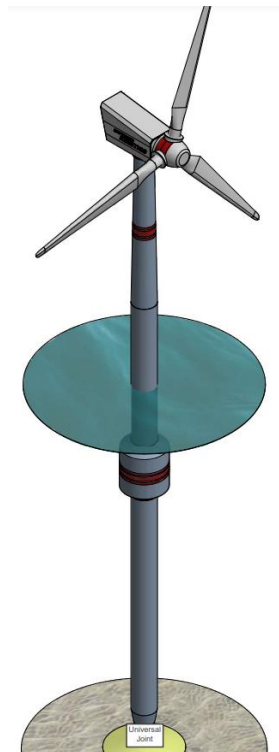


Figure 25: Hybrid Wind Turbine overview[22]

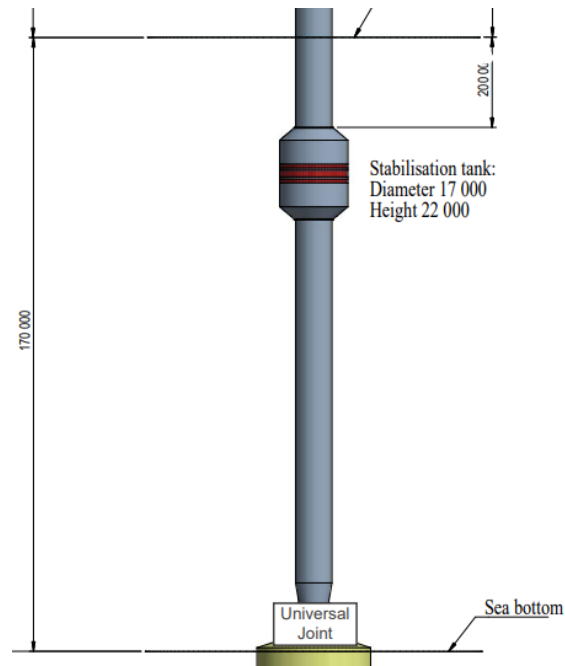


Figure 26: Hybrid Wind Turbine Submerged Section[22]

The depth for this concept is 170 meters. The submerged section then consists of a total of 170 meters where 22 of those are for the buoyancy tank with a diameter of 17 meters. The diameter is 8 m for the remaining submerged sections.

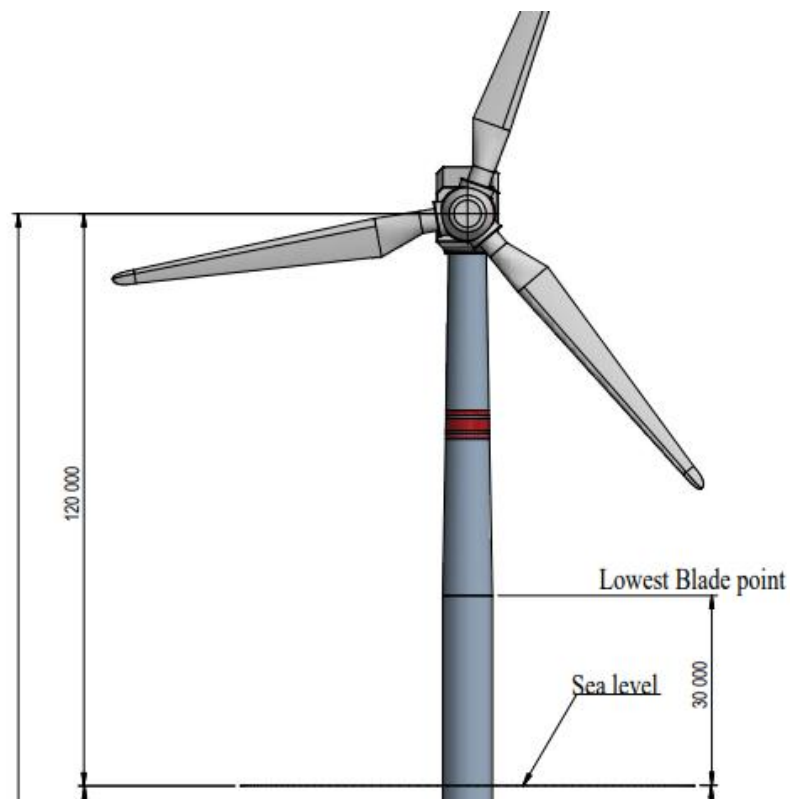


Figure 27: Hybrid Wind Turbine top section[22]

From sea level to the hub, it is 120 meters. The tower section starts at 30 meters above sea level and is

a coned section for aerodynamic purposes. The change in diameter is not stated so it is assumed to start at 8 m diameter at  $z=30$  and a diameter of 4.5 m at  $z = 115$  (120-5, assuming radius of hub to be 5 m).

The thickness of the pipes is also not stated for this concept, so it is assumed to be 40 mm. The blades are 85 meters long and the sweep diameter is 180 meters in total, including the hub.

The concept is innovative in adapting the articulated tower structure to the offshore wind industry. The buoyancy tank is used to contain Hydrogen for production and containment availability. The lift force from submerged Hydrogen is thought to be severe (writer's assumption).

The universal joint allows the structure to rotate about its own X and Y-axis. It does not allow any rotation about the Z (vertical)- axis. This means that the universal joint must be designed to withstand significant torque created by environmental forces. The only rotation about the Z-axis in the wind turbine configuration is done by the yaw controller which calibrates in terms of wind direction and faces the turbine against the wind to increase lift force and reduce drag force on the turbine blades.

### **3.2 Numerical tools and calculations**

Three software programs have been chosen in this research. These consists of Orcaflex[38], inventor[55] and Excel[56]. Orcaflex[38] is the software used for simulations and output of results. The necessary inputs are first calculated manually in Excel[56], before validating the calculations by modelling the structure in Inventor. Inventor can automatically calculate properties of the modelled structure, and this is used to compare to the manual calculations.

#### *3.2.1 Modelling and simulating using Orcaflex*

Orcaflex[38] is a dynamic analysis software for research within several fields such as oil & gas, aquaculture oceanographic, seismic operations and wet renewables. In this thesis Orcaflex[38] is used to model the Offshore Kinetics' offshore wind turbine concept with the relevant parameters. Several environmental inputs can be used as the program supports different wave and wind theories. Given the inputs, the software is used to simulate the behavior of the system in the chosen environment and numerous output results can be displayed.

### **Substructure**

The substructure is the core of this concept as there are not any offshore wind turbines with a substructure of this configuration of universal joint, internal ballast system, and a large buoyancy tank which includes Hydrogen.

In Orcaflex[38] this substructure is modelled using a 6D buoy in which the parameters can be adjusted as shown in the figure below.

Name: 6D buoy2			Type: Spar buoy			Disturbance vessel: (none)						
Connection: Constraint1						Wave calculation method: Specified by environment						
Initial position and attitude:						Inertia:						
x (m)	y (m)	z (m)	Rotation 1 (deg)	Rotation 2 (deg)	Rotation 3 (deg)	Mass (te)	Mass moments of inertia (te.m <sup>2</sup> )			Centre of mass (m)		
						x	y	z	x	y	z	
0.0	0.0	0.0	0.0	0.0	0.0	16.8e3	6.561e6	6.561e6	27.17e3	0.0	0.0	8.48

Figure 28: Orcaflex 6D-buoy parameters[38]

The 6D buoy is a rigid body having three translational degrees of freedom (X, Y, Z) and three rotational (Rx, Ry, Rz). This means that a 6D buoy is allowed to move in all of these degrees of freedom. The modeled structure can be seen in the figure below.



Figure 29: Modelled wind turbine concept in Orcaflex[38]

As the universal joint only allows two degrees of freedom; Rx and Ry, and this restriction must be implemented. This is done by connecting the 6D buoy to a constraint. The constraint gives the option to which of the DOF's to be free and which to be fixed. The 6D buoy is then connected to a constraint below which only allows rotation about the X and Y axis.

As seen in figure 26, the inertia properties inputs include the mass, center of gravity, and mass moments of inertia of the X, Y, and Z axis. These properties must be calculated, and this is shown later in the chapter.

Orcaflex[38] automatically calculates the buoyancy force from the displaced volume given the

geometrical inputs. It also calculates and displays the center of buoyancy as seen in the figure below marked with a green cross.

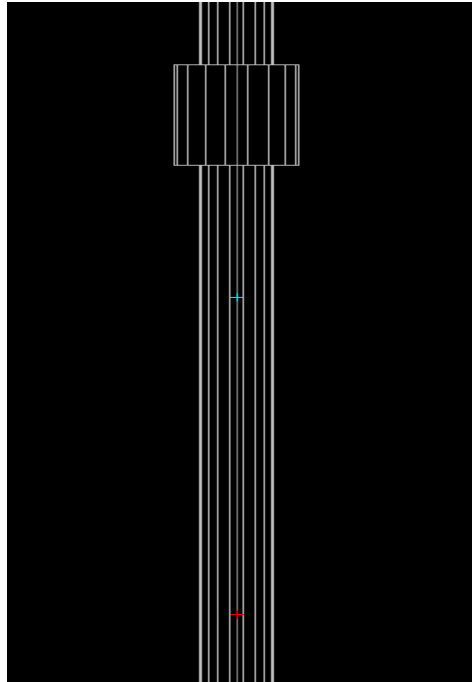


*Figure 30: Orcaflex COB visualization*

The substructure including the buoyancy tank is modelled using cylinders with given outside and inside diameters. Hydrogen is not possible to apply to the 6D buoy directly, so this is done by applying the contributing uplift force in kN at the height of where the force acts.

### **Topside section**

The tower, nacelle, hub, and turbine in this thesis is based on an Orcaflex example[57] which includes a system created for a 10 MW wind turbine. More details on this are shown in 3.3

### **Yaw control system**

Orcaflex[38] does not have a built-in yaw control system meaning that the turbine does not yaw when the wind changes direction. When the turbine does not face the wind, it is not efficient, and the system would therefore not be profitable to build. In real life however, most wind turbines have a yaw control system so that the turbine is always facing the wind to generate the optimized power from the system. Some of the parameters to a yaw control are the yaw rate in deg/s which is the rate in which the turbine rotates towards the wind, and the yaw misalignment which is described in chapter 2.5.6 and 2.5.7

Even though a built-in yaw control system is not present in the program, it is possible to model an improvised yaw control system. As Orcaflex[38] is compatible with Python[58] and allows external functions, a function can be written using python. A yaw control system has been created and published

as open source and using a python script it is possible to adjust the yaw parameters in a separate DLL-file in which the script calls.

This external function is applied to a constraint which has been connected to the top of the tower section, with the rotor-nacelle assembly is connected to the constraint. This will give a somewhat realistic yaw system.

### 3.2.2 *Calculations using Excel*

Excel[56] is used to calculate the necessary and relevant inputs to Orcaflex[38] and the calculations are done based on the given information of the concept design of Offshore Kinetics[22]. Properties which are not given are assumed based on background information of other known structures. As it is the substructure (primarily from seabed to sea surface) which is the new concept, it is also here the most information is given. Most of the properties calculated in Excel[56] are the properties which is necessary to apply to the model, but other relevant properties are also calculated. Some of the calculated properties in Excel include:

- Mass and center of mass
- Volume of steel of structure (substructure + tower)
- Displaced volume
- Center of buoyancy
- Mass moments of inertia
- Buoyancy force from displaced volume
- Buoyancy force from hydrogen
- Ballast mass

These calculations can be seen as “hand calculations” and therefore a validation of some of these properties are checked in Inventor[55].

### 3.2.3 *Validation using Inventor*

Modelling the same substructure as in Orcaflex[38] in Inventor[55], this software can automatically calculate properties such as steel volume, center of mass, and mass moments of inertia in X, Y, and Z. Inventor[55] is just used to validate these properties so that the inputs are correct. The modeled structure in Inventor can be seen in the figure below.

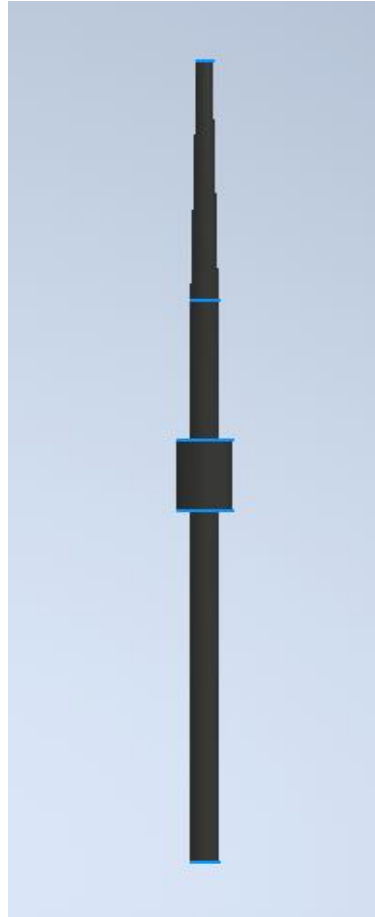


Figure 31: Modelled substructure in Inventor[55]

The calculated properties of the modeled structure in Excel and Inventor are compared in the table below.

Table 1: Hand calculation comparison with inventor

<b>Structure properties comparison</b>			
<b>Properties</b>	<b>Excel calculation value</b>	<b>Inventor value</b>	<b>Accuracy</b>
<i>Total steel volume</i>	<i>145.99</i>	<i>146.1</i>	<i>99.9%</i>
<i>Total mass</i>	<i>1146.07</i>	<i>1146.53</i>	<i>99.9%</i>
<i>Inertia X,Y</i>	<i>6560792.62</i>	<i>6559801.16.</i>	<i>99.9%</i>
<i>Inertia Z</i>	<i>27169.01</i>	<i>26206.10</i>	<i>96.45%</i>
<i>Center of gravity</i>	<i>132.9</i>	<i>134.7</i>	<i>98.61%</i>

The manually calculated properties from Excel seem to be very accurate when comparing to the results in Inventor.

### 3.2.4 Mass and volume

The volume and masses were of the sections were calculated in the Excel spreadsheet and then verified



from the corresponding model in Inventor. Mass and volumes for the different section of the substructure are summarized in the table below:

Table 2: Properties

Properties overview							
Section	Length [m]	OD [m]	ID [m]	Material Density [T/m <sup>3</sup> ]	Volume [m <sup>3</sup> ]	$\nabla$ [m <sup>3</sup> ]	Mass [T]
Bottom cylinder	128	8	7.96	7.85	64.18	6434	503.80
Buoyancy tank	22	17	16.96	7.85	23.47	4994	184.25
Buoyancy tank to surface	20	8	7.96	7.85	10.03	1005	78.72
Topside const.diameter	30	8	7.96	7.85	15.04		118.08
Tower section	85	2*(0.020588x+4)	2*(0.020588x+3.98)	7.85	33.28		261.22

The most complex calculations are related to the tower section, as this section is coned and consists of an outer and inner diameter and radius.

The function of the topside tower diameter was calculated from the assumption that the outer diameter at Z = 115 m was 4.5. Since the volume of a strip can be expressed as in equation 3.36:

$$dv = \pi r^2(x) dx$$

The volume of the coned, hollow structure could be calculated as:

$$v = \pi \int_0^{85} (-0.020588x + 4)^2 \cdot dx - \pi \int_0^{85} (-0.020588x + 3.98)^2 \cdot dx$$

$$= 33.27593 \text{ m}^3$$

Where the first term is the function of the outer radius over the length x and the second term is the function of the inner radius over the length x.

The mass is then

$$m = \rho v = 7.85 \frac{T}{m^3} * 33.28 \text{ m}^3 = 261.22 T$$

The section is modelled in Inventor where the properties are automatically calculated based on material chosen. The inventor values for the tower can be seen in Appendix 4 – Calculation of Moment of inertia, I<sub>z</sub>, for tower section.

### 3.2.5 Mass moment of inertia

The mass moment of inertia is an important input for the simulations. The mass moment of inertia can be described as a quantity of torque needed to rotate an object about an axis and is dependent on the object's mass and geometry. The equation for an object's mass moment of inertia therefore varies by its geometry. For solid cylinders the equation for mass moment of inertia about its central axis (Z-axis) is described in equation 2.36 as:

$$\frac{1}{2}MR^2$$

Where M is the object's mass and R is the radius.

For the parts of the turbine's substructure the calculations are straight forward, as the radius is constant and since it is hollow it gives the equation

$$\frac{1}{2}M(R^2 + r^2)$$

Where  $r$  is the inner radius of the cylinder. The tower part of the substructure is coned, meaning that the radius changes over a distance  $x$ . This must be concerned when calculating the moment of inertia of this part. Obtaining equation 3.41, knowing the height of the tower, and the function of the change in radius has been calculated, the values can be put into the equation,

$$I = \frac{\pi}{2}\rho \int_0^{85} (-0.020588x + 4)^4 dx$$

This equation can be solved using the formula

$$(a + b)^n = \sum_{i=0}^n \binom{n}{i} a^{n-i} * b^i \quad (3.1)$$

Where  $a = -0.020588x$  and  $b = 4$ . This gives

$$\sum_{i=0}^4 \binom{4}{i} (-0.020588x)^{4-i} * 4^i$$

The same procedure is executed using the function of the inner radius which is 3.98 m. 3.98 then replaces the 4 in the equation. After calculating the inertia of the inner radius, this is then subtracted from the calculated value for the outer. The whole calculation can be found in Appendix 4 – Calculation of Moment of inertia,  $I_z$ , for tower section.

The coned tower's total mass moment of inertia was calculated to be 2735.1 Te\*m<sup>2</sup>.

Table 3: Verifying hand-calculations

<i>Tower Inertia (Z) comparison</i>		
Hand-calculation value	Inventor value	Accuracy
2735.1	2734.6	99.9%

### 3.2.6 Substructure GM calculation

The initial substructure's stability properties are calculated in this subchapter without regarding the turbine section or adding ballast to the structure. Center of gravity is calculated using the equation 3.50 presented in the theory-section,

$$Z_G = \frac{\sum_{i=1}^n m_i z_i}{\sum_{i=1}^n m_i} = \frac{\text{Sum of (all masses*vertical distance to center of each mass)}}{\text{Sum of all masses}},$$

Which gives

$$\frac{(503.80 \text{ Te} * \frac{128m}{2}) + (184.25 \text{ Te} * 128m + \frac{22m}{2}) + (78.72 \text{ Te} * (128m + 22m + \frac{20m}{2})) + (118.08 \text{ Te} * (170m + \frac{30m}{2})) + 261.22 \text{ Te} * (200m + \frac{1}{3} * 85m)}{(503.8 + 184.25 + 78.72 + 118.08 + 261.22) \text{ Te}} = 133 \text{ m}$$

Center of buoyancy is calculated as

$$\overline{KB} = Z_B = \frac{\int_0^T A_w dz}{\int_0^T A_w dz} = \frac{\sum_{i=1}^n v_j z_i}{\sum_{i=1}^n v_j}$$

$$= \frac{6434 \text{ m}^3 * \frac{128m}{2} + 4994 \text{ m}^3 * (128m + \frac{22m}{2}) + 1005 \text{ m}^3 * 160m}{(6434 + 4994 + 1005) \text{ m}^3}$$

=96.77 m. The initial metacenter radius is calculated using equation 2.55.

$$\overline{BM} = \frac{I}{V}$$

where the second moment of area is for a cylinder is

$$I_x = \frac{\pi}{4} (r_2^4 - r_1^4) = \frac{\pi}{4} (8^4 - 7,96^4) \quad 3.2$$

Which gives a second moment of area of 63.85 m<sup>4</sup>.

From table 1, the total displaced volume is  $(6434+4994+1005) \text{ [m}^3\text{]} = 12433 \text{ m}^3$ .

$$\overline{BM} = \frac{63.85\text{m}^4}{12433\text{m}^3} = 0.005 \text{ m}$$

Meaning that the metacenter is approximately at the same vertical height as the center of buoyancy. Using equation 3.48, the distance from center of gravity to metacenter, GM, is approximately -33 meters, excluding the turbine section and ballast, which are implemented in the coming subchapters.

### 3.2.7 Buoyancy force from hydrogen tank

The buoyancy tank is filled with hydrogen. This is thought to compensate partly for the significant weight of the upper part of the turbine structure. In addition to buoyancy force from displaced volume, the hydrogen is much lighter than water and will create additional buoyancy force, acting as a lifting gas as often familiarized with air balloons for example. This force is calculated using the formula,

$$F_B = \rho_{sw} - \rho_H \cdot g \cdot v \quad (3.3)$$

Where

$F_B = \text{Buoyancy force}$

$\rho_{sw} = \text{Density seawater}$

$\rho_H = \text{Density Hydrogen}$

$v = \text{Volume of lift gas}$

The volume of the lift gas equals the inside volume of the buoyancy tank and is calculated to be 4970 cubic meters. The buoyancy force from hydrogen in tank below sea surface is then

$$F_B = \frac{(1.025-0.00008375)\text{Te}}{\text{m}^3} \cdot 9.81 \frac{\text{m}}{\text{s}^2} \cdot 4970\text{m}^3 = 49949 \text{ kN.}$$

## 3.3 10 MW wind turbine

Offshore Kinetics' original concept was based on a turbine with a capacity in the range of 8-9 MW. For research and simplicity purposes a 10 MW turbine is implemented from an Orcina example. This turbine is then used while the substructure is modelled according to the Offshore Kinetics' concept design. The properties of the 10 MW turbine can be seen below[59].

Table 4: 10 MW turbine properties[59]

Parameter	Value
<i>Rotor Orientation</i>	Clockwise rotation - Upwind
<i>Cut-in wind speed</i>	4 m/s
<i>Cut-out wind speed</i>	25 m/s
<i>Rated wind speed</i>	11 m/s (Optimized)
<i>Rated electrical power</i>	10 MW
<i>Number of blades</i>	3
<i>Rotor Diameter</i>	198 m
<i>Hub Diameter</i>	4.6 m
<i>Hub height</i>	115 m
<i>Blade mass</i>	47.7 t
<i>Nacelle mass</i>	542.6 t

Some of these parameters have been adjusted to fit the Hybrid Wind Turbine substructure, meaning that the hub height in the table above is to be 115 m from sea surface, and 295 from seabed. The properties of this turbine need to be included in stability calculations.

### 3.3.1 Yaw controller implementation

As Orcaflex[38] does not have an implemented yaw control system in their current versions, the yaw control system must be improvised using external functions and modified to suit the purpose of the thesis.

Using a ‘Constraint’ in Orcaflex[38], it is possible to choose two types of constraint types: Calculated degrees of freedom or externally calculated imposed motion.

Name: Constraint2

Initial position and attitude:

Connect to object	x (m)	y (m)
Tower	0.0	0.0

Constraint type:  Calculated DOFs  Imposed motion

Model type:  Time history  Externally calculated

Externally calculated motion: Drawing Tags

Externally calculated motion: Yaw Control

Initial value:

x (m)	y (m)	z (m)	Rx (deg)	Ry (deg)	Rz (deg)
0.0	0.0	0.0	0.0	0.0	0.0

Figure 32: Constraint options in Orcaflex[38]

The ‘Externally calculated motion’ option which is called ‘Yaw Control’ is the python[58] file in which has been modified and called ‘Yaw Control’.

The externally calculated imposed motion enables the motion of the constraint’s out-frame, relative to the in-frame, to be calculated programmatically by an external function. The external function data sources allow data to be specified by a user defined function in an external DLL or a Python script.

Using Orcina’s python script for their 10 MW example[57], it is possible to extend the script to implement the yaw control function.

The Orcaflex Python wrapper script supports Bladed-style DLL’s. NREL Reference Open-Source Controller (ROSCO) have created a DLL for yaw controller, and by downloading this file, adjustments on yaw control properties can be made as seen in the table below.

Table 5: Yaw control functions in DLL-file

YAW CONTROL	
$Y\_ErrThresh$	Yaw error threshold. Turbine begins to yaw when it passes this. [ $rad^2 * s$ ]
$Y\_IPC\_IntSat$	Integrator saturation (maximum signal amplitude contribution to pitch from yaw-by-IPC), [ $rad$ ]
$Y\_IPC\_n$	Number of controller gains (yaw-by-IPC)
$Y\_IPC\_KP$	Yaw-by-IPC proportional controller gain $K_p$
$Y\_IPC\_KI$	Yaw-by-IPC integral controller gain $K_i$

$Y\_IPC\_omegaLP$	Low-pass filter corner frequency for the Yaw-by-IPC controller to filtering the yaw alignment error, $[\frac{rad}{s}]$
$Y\_IPC\_zetaLP$	Low-pass filter damping factor for the Yaw-by-IPC controller to filtering the yaw alignment error, [-].
$Y\_MErrSet$	Yaw alignment error, set point [rad]
$Y\_omegaLPFast$	Corner frequency fast low pass filter, 1.0 $[\frac{rad}{s}]$
$Y\_omegaLPSlow$	Corner frequency slow low pass filter, 1/60 $[\frac{rad}{s}]$
$Y\_Rate$	Yaw rate $[\frac{rad}{s}]$

The Python script is then modified to call the DLL, so that the inputs are imported to the Orcaflex[60] constraint through Python[58].

### 3.4 Initial Stability

As mentioned in chapter 2.4.2, the distance from keel to the metacenter should in general be at least 0.15 meters to ensure sufficient stability. By implementing the 10 MW turbine example[57] from Orcina[38], this has to be included to the stability calculations. Also further updated information from company representatives on ballast must be included.

#### 3.4.1 Ballast

A specific ballast value has not been specified for the concept, but updated information has implied that there should be enough ballast to ensure a positive downwards net force on the universal joint. This means that the ballast must have a mass which together with the other masses in the structure, is higher than the buoyancy force from displaced volume and the lift force from Hydrogen in the buoyancy tank.

To calculate the needed ballast for a net force equal to zero, the Excel solver function is used based on the initially calculated parameters as shown in the tables below.

Table 6: Environmental inputs in Excel

<b>Environmental inputs</b>			
<b>Description</b>	<b>Symbol</b>	<b>Value</b>	<b>Unit</b>
<i>Wave height</i>	<i>H</i>	<i>TBD</i>	<i>m</i>
<i>Wave period</i>	<i>Tp</i>	<i>TBD</i>	<i>s</i>
<i>Wind speed</i>	<i>Vwind</i>	<i>TBD</i>	$\frac{m}{s}$
<i>Water depth</i>	<i>h</i>	<i>170</i>	<i>m</i>
<i>Density water</i>	<i>Rhow</i>	<i>1.025</i>	$\frac{t}{m^3}$
<i>Density air</i>	<i>Rhoa</i>	<i>0.001225</i>	$\frac{t}{m^3}$
<i>Density hydrogen</i>	<i>Rhoh</i>	<i>0.00008375</i>	$\frac{t}{m^3}$
<i>Gravitational acceleration</i>	<i>g</i>	<i>9.80565</i>	$\frac{m}{s^2}$

Table 7: Substructure properties

<b>Substructure properties</b>			
<b>Description</b>	<b>Symbol</b>	<b>Value</b>	<b>Unit</b>
<i>Total steel volume</i>	<i>Vsteel</i>	<i>146</i>	<i>m<sup>3</sup></i>
<i>Total mass</i>	<i>mtot</i>	<i>1,146</i>	<i>t</i>
<i>Total inertia (X)</i>	<i>Ix_tot</i>	<i>6.46E+06</i>	<i>t * m<sup>2</sup></i>
<i>Total inertia (Y)</i>	<i>Iy_tot</i>	<i>6.46E+06</i>	<i>t * m<sup>2</sup></i>
<i>Total inertia (Z)</i>	<i>Iz:_tot</i>	<i>2.72E+04</i>	<i>t * m<sup>2</sup></i>
<i>Center of gravity</i>	<i>COG</i>	<i>130</i>	<i>m</i>
<i>Center of buoyancy</i>	<i>COB</i>	<i>97</i>	<i>m</i>
<i>Gravitational force</i>	<i>Fg</i>	<i>11238</i>	<i>kN</i>
<i>Lift force Hydrogen</i>	<i>F<sub>lH</sub></i>	<i>49949</i>	<i>kN</i>
<i>Buoyancy force from displaced volume</i>	<i>FB</i>	<i>114855</i>	<i>kN</i>
<i>Total buoyancy force</i>	<i>FB<sub>Tot</sub></i>	<i>164805</i>	<i>kN</i>



<i>Net force</i>	<i>F<sub>net</sub></i>	-135567	<i>kN</i>
------------------	------------------------	---------	-----------

The net force is given by the difference of total buoyancy force and the total gravitational force. The total gravitational force is given by all masses of the substructure + tower and the currently empty cell which is called ‘Mass ballast’. The Excel solver is then adjusted to give the net force a value of zero by changing the variable cell ‘Mass ballast’. The ballast mass needed to give a net force of zero was calculated to be 15661 tonnes. Additional figures that show the procedure can be found in Appendix 6 – Excel Solver.

#### 3.4.2 New COG and GM

By adding the masses of the nacelle, hub, and blades in addition to the mass of the ballast, the new center of gravity is calculated using equation (3.49) and is found to be approximately 33 meters, assuming that the ballast’s center of gravity is 15 meters from the bottom. Replacing the old KG value with 33 meters gives a GM distance of 66.7 meters, which is significantly larger than the lower limit of 0.15 meters.

### 3.5 Environmental inputs

Environmental properties are applied in Orcaflex[38]. The variables listed are Seabed conditions, current, wind, and waves.

#### 3.5.1 Seabed conditions

Orcaflex[38] allows the user to choose seabed conditions regarding seabed shape and properties. The shape of the seabed can be chosen to be flat, 2D profiled, or 3D seabed. The 2D and 3D seabed allows the user to specify the geometry of the seabed. The properties which can be adjusted for the seabed conditions are the origin in terms of X, Y, and Z, and the depth. Stiffness and damping can also be adjusted to present the most realistic seabed conditions for the user’s purpose[60].

As the Hybrid Wind Turbine structure’s depth is 170 m, this is the only parameter adjusted for seabed conditions in this research.

#### 3.5.2 Waves

For wave inputs, several theories and spectrums can be applied for irregular waves, while a choice of regular deep stream waves could also be implemented. Using a JONSWAP-spectrum, the needed inputs to Orcaflex[38] are the significant wave height,  $H_s$ , and the zero-crossing period,  $T_z$ , in addition to the direction of the waves.

The significant wave height and the zero-crossing period is chosen based on historical observations of sea states with occurrences of these. In DNVGL-CG-0130-Wave loads[61], a scatter diagram of

occurrences of Hs and Tz is listed based on 100 000 observations, which can be seen in the table below.

Table 8: Scatter diagram[61]

Tz(s)	3.5	4.5	5.5	6.5	7.5	8.5	9.5	10.5	11.5	12.5	13.5	14.5	15.5	16.5	17.5	18.5	Sum
Hs (m)																	
0.5	1.3	133.7	865.6	1186.0	634.2	186.3	36.9	5.6	0.7	0.1	0.0	0	0.0	0.0	0.0	0.0	3050
1.5	0.0	29.3	986.0	4976.0	7738.2	5569.7	2375.7	703.5	160.7	30.5	5.1	0.8	0.1	0.0	0.0	0.0	22575
2.5	0.0	2.2	197.5	2158.8	6230.0	7449.5	4860.4	2066.0	644.5	160.2	33.7	6.3	1.1	0.2	0.0	0.0	23810
3.5	0.0	0.0	34.9	695.5	3226.5	5675.0	5099.1	2838.0	1114.1	337.7	84.3	18.2	3.5	0.6	0.1	0.0	19128
4.5	0.0	0.0	6.0	196.1	1354.3	3288.5	3857.5	2685.5	1275.2	455.1	130.9	31.9	6.9	1.3	0.2	0.0	13289
5.5	0.0	0.0	1.0	51.0	498.4	1602.9	2372.7	2008.3	1126.0	463.6	150.9	41.0	9.7	2.1	0.4	0.1	8328
6.5	0.0	0.0	0.2	12.6	167.0	690.3	1257.9	1269.6	825.9	386.8	140.8	42.2	10.9	2.5	0.5	0.1	4806
7.5	0.0	0.0	0	3.0	52.1	270.1	594.4	703.2	524.9	276.7	111.7	36.7	10.2	2.5	0.6	0.1	2586
8.5	0.0	0.0	0	0.7	15.4	97.9	255.9	350.6	296.9	174.6	77.6	27.7	8.4	2.2	0.5	0.1	1309
9.5	0.0	0.0	0	0.2	4.3	33.2	101.9	159.9	152.2	99.2	48.3	18.7	6.1	1.7	0.4	0.1	626
10.5	0.0	0.0	0	0.0	1.2	10.7	37.9	67.5	71.7	51.5	27.3	11.4	4.0	1.2	0.3	0.1	285
11.5	0.0	0.0	0	0.0	0.3	3.3	13.3	26.6	31.4	24.7	14.2	6.4	2.4	0.7	0.2	0.1	124
12.5	0.0	0.0	0	0.0	0.1	1.0	4.4	9.9	12.8	11.0	6.8	3.3	1.3	0.4	0.1	0.0	51
13.5	0.0	0.0	0	0.0	0	0.3	1.4	3.5	5.0	4.6	3.1	1.6	0.7	0.2	0.1	0.0	21
14.5	0.0	0.0	0	0.0	0	0.1	0.4	1.2	1.8	1.6	1.3	0.7	0.3	0.1	0.0	0.0	8
15.5	0.0	0.0	0	0.0	0	0	0.1	0.4	0.6	0.7	0.5	0.3	0.1	0.1	0.0	0.0	3
16.5	0.0	0.0	0	0.0	0	0	0	0.1	0.2	0.2	0.2	0.1	0.1	0.0	0.0	0.0	1
Sum	1	165	2091	9280	19922	24879	29870	12898	6245	2479	837	247	66	16	3	1	10 <sup>5</sup>

### Probability of a sea state with Hs in the range from 0.5 to 6.5 meters

The probability of a Hs in the interval of 1 m to 5 meters is:

$$(P(H_s=1.5) + P(H_s=2.5) + P(H_s=3.5) + P(H_s=4.5) + P(H_s=5.5)) / 100\ 000 =$$

$$(3050 + 22575 + 23810 + 19128 + 13289 + 8328 + 4806) / 100\ 000 = 0.949 \sim 95\%$$

This means that 95% of the 100 000 measured waves have had a significant wave in the interval of Hs=0.5 m to Hs=6.5 m.

In this research the significant wave height chosen is then 1.5 m, 3.5m, and 6.5 m

To determine the Tz-values for these respective significant wave heights, probability calculation must be performed.

Calculating the probability of a Hs of 1 meter and a Tz interval from 5.5 to 7.5 seconds:

- **Event A:** Hs = 1.5 m
- **Event B:**  $5.5 \leq Tz \leq 10.5$

And the probability of event B, given that event A has occurred is

$$P(B|A) = \frac{P(A \cap B)}{P(A)}$$

where

- $A \cap B$  is the number of observations of a sea state with event A and B at the same time. Looking at the observations of Hs=1.5 m with Tz in the range of 5.5 to 10.5, the observations are:  
 $968 + 4976 + 7738.2 + 5569.7 + 2375.7 + 703.5 = 22331.1$  observations.
- A is the total observations of Hs= 1.5 m and is equal to 22575 observations.

$$P(A \cap B) = \frac{\text{Favorable outcome}}{\text{Possible outcomes}} = \frac{22331.1}{100000} = 0.22331$$

$$P(A) = \frac{\text{Favorable outcome}}{\text{Possible outcomes}} = \frac{22575}{100000} = 0.22575$$

This gives

$$P(B|A) = \frac{0.22331}{0.22575} = 0.989 \sim 99 \%$$

Meaning that there is a 99 percent chance of a Tz value in the range from 5.5 to 10 s given that the significant wave height is 1.5 meter. For the two remaining significant wave heights chosen, the same procedure is followed given the result of a 97.5% percent chance of a Tz value in the range of 6.5-11.5 seconds when the significant wave height is 3.5 meters, and a 96% chance of a Tz value in the range of 7.5 – 12.5 seconds given a Hs of 6.5 meters.

The sea states chosen are therefore:

- Hs = 1.5 m , Tz [5.5, 7.5]
- Hs = 3.5 m, Tz [6.5, 8.5]
- Hs = 6.5 m, Tz [7.5, 9.5]

### 3.5.3 Wind

There are several wind types and theories which can be chosen in Orcaflex[38]. The different types consist of:

**Constant**

By choosing constant wind type the allowable parameters to adjust are the wind speed and wind direction which remains constant during the whole simulation[41].

**NPD spectrum[40], API spectrum, ESDU spectrum**

The theories of these wind spectrums are described in chapter 2.2.5 and these are spectrums in which the wind speed varies randomly over time[41]. In all of these cases the wind direction remains constant over time, and the spectrums are defined by the reference mean speed, meaning the 1-hour mean speed at an elevation of 10 meters above the mean water level, and the elevation above the mean water level at which the wind speed is to be calculated.

The wind speed is in these cases modelled to be ramped from mean wind speed to the dynamic wind speed during a build-up period.

**User defined spectrum**

In the user defined spectrum, the user enters the mean wind speed directly rather than being calculated according to the above theories which use the reference mean speed and elevation.

**Time history (Speed)**

The wind speed variation is determined by the user by setting up a time history with the desired wind speeds. The mean speed and direction must be entered for the statics calculations, and the wind direction remains constant over time.

**Time history (Speed and direction)**

The wind speed and direction variation are determined by the user by setting up a time history in which the speed and direction of the wind is applied for given times and intervals. The mean wind speed and direction must be entered for statics calculations.

Since this is the only wind type which allows change in direction over time, this is the one chosen for the simulations. As the goal is to implement a yaw controller and find torque on the universal joint due to yawing operations in different sea states, it is reasonable to choose a wind type which allows for wind direction change over time. The turbine shall then start to yaw when the wind starts to change direction.

**3.5.4 Currents**

Orcaflex[38] allows the user to implement current by entering the current speed and direction. These parameters can be applied to different profiles in which the user can adjust the depth and rotation of

the profiles. In this research, the currents have been neglected.

### 3.6 Simulation setup

The setup of the simulation is based on the information given on environment and turbine structure, in addition to shown calculations in the paper. The yaw rate interval selected in the research is 0.1 degrees per second, 0.3 degrees per second, and 0.5 degrees per second.

0.5 degrees per second is considered the general yaw rate[26], while 0.3 degrees per second is the default value of Hywind Tampen's 8 MW wind turbines[52]. 0.1 degrees per second is a chosen value because the yaw rate of 0.3 and 0.5 might be too high based on the writer's assumption, due to the usage of universal joint where forces from yawing could be translated to this single point.

The yaw controller will react as soon as it notices offset wind, and the rate of change of wind direction will be adjusted to the relevant yaw rate.

The mean and dynamic wind speed is set to 11 m/s for all simulations because the 10 MW turbine used is optimized for 10 MW at 11 m/s by a previous study[59].

There are a total of 57 simulations in which the results are based on. These include the yaw rates chosen and the significant wave heights and the corresponding zero-crossing periods calculated in 4.6.2. Below is an overview.

Table 9: List of simulations

<b>Simulations</b>		
<b>Yaw rate [deg/s]</b>	<b>Significant wave height [m]</b>	<b>Zero-crossing period [s]</b>
0.1	-	-
0.3	-	-
0.5	-	-
0.1	1.5	[5.5, 6.5, 7.5, 8.5, 9.5, 10.5]
0.1	3.5	[6.5, 7.5, 8.5, 9.5, 10.5, 11.5]
0.1	6.5	[7.5, 8.5, 9.5, 10.5, 11.5, 12.5]
0.3	1.5	[5.5, 6.5, 7.5, 8.5, 9.5, 10.5]

<i>0.3</i>	<i>3.5</i>	<i>[6.5, 7.5, 8.5, 9.5, 10.5, 11.5]</i>
<i>0.3</i>	<i>6.5</i>	<i>[7.5, 8.5, 9.5, 10.5, 11.5, 12.5]</i>
<i>0.5</i>	<i>1.5</i>	<i>[5.5, 6.5, 7.5, 8.5, 9.5, 10.5]</i>
<i>0.5</i>	<i>3.5</i>	<i>[6.5, 7.5, 8.5, 9.5, 10.5, 11.5]</i>
<i>0.5</i>	<i>6.5</i>	<i>[7.5, 8.5, 9.5, 10.5, 11.5, 12.5]</i>

## 4. Results and discussions

This chapter contains the results from the simulations with a main focus on the torque applied to the universal joint. The chapter also includes the turbine efficiency during different sea states and with regards to yaw alignment error. The subchapters 5.2 and 5.4 provides a summary of the results of torque applied to the universal joint and the turbine efficiency, respectively. To start off, some selected figures and global results from simulations are shown.



*Figure 33: Turbine before and after yawing[38]*

The figures above show the modeled structure in Orcaflex[38], in a sea state with a significant wave height of 6.5 meters, a zero-crossing period of 11.5 seconds. The turbine yaw rate is 0.5 degrees per second towards a 50-degree offset wind. The figure to the left shows the structure before the nacelle rotates towards the wind, and the figure to the right shows when the nacelle has turned 50 degrees. The figure to the right also shows the maximum inclination of the structure in this sea state, with a maximum declination angle reaching approximately 2.7 degrees. The graph below shows the inclination of the structure over the simulation time.

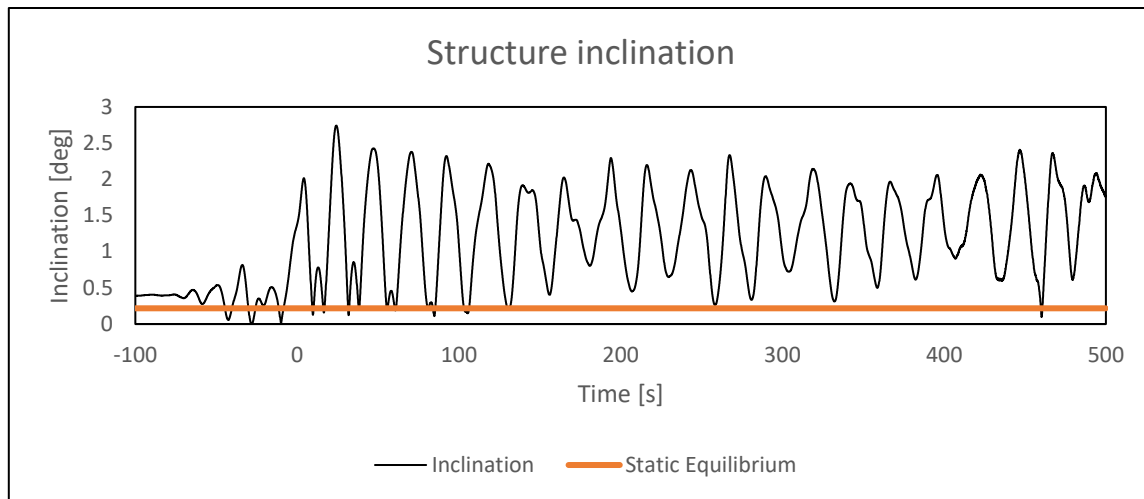


Figure 34: Structure inclination over time

As seen in the graph above, the structure does not oscillate constantly about the equilibrium as in Bar Avi and Benaroya's research of the two DOF articulated tower[23]. Instead, the declination is mostly kept at a positive value during the simulation, due to constant wind force on the structure. Excluding the constant wind, the structure will oscillate more about the static equilibrium while the total inclination is reduced, as seen in the figure below.

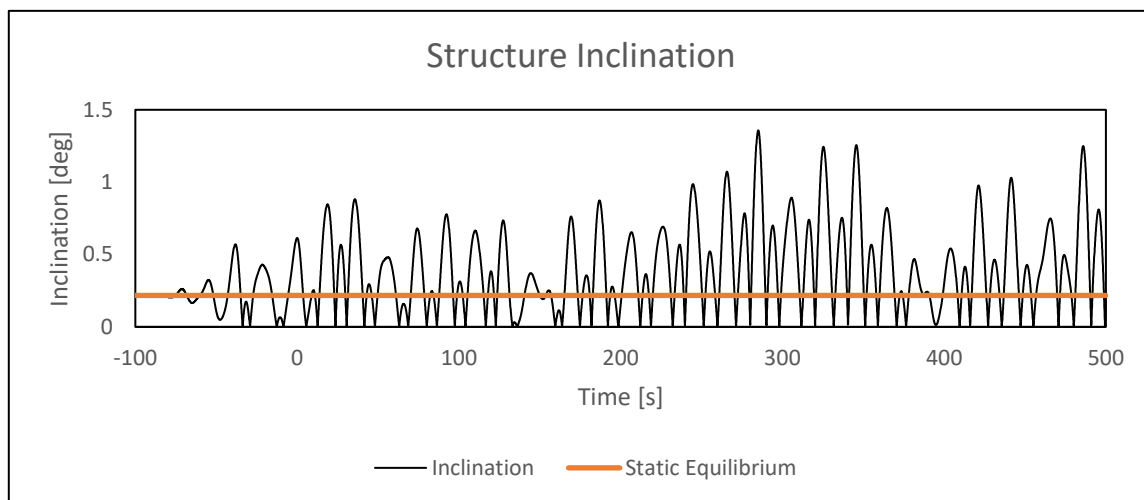


Figure 35: Structure inclination excluding wind force

## 4.1 Applied torque on universal joint

### 4.1.1 Wind loads only

In the first simulation, only wind is applied with a constant speed of 11 m/s. This wind changes direction to suit the yaw rate selected for the simulations. The goal is to see the torque caused by only the yaw operation regardless of any waves, and to see the relationship between the yaw movement and the torque.



Table 10: Torque values when only wind is applied

Torque overview			
Yaw rate [deg/s]	Max torque [kN*m]	Avg. Torque [kN*m]	Max torque cause
0.1	4728	1888	Yaw stop
0.3	8847	2167	Yaw stop
0.5	11246	2485	Yaw stop

The higher yaw rate, the higher torque peaks from findings. The highest measured torque was 11246 kN in the trial with yaw rate at 0.5 degrees per second, while the lowest of the torque peaks and the average torque was when the yaw rate was set to 0.1 degrees per second. For all sequences, the high torque cause was the yaw start and stop operation (excluding turbine start-up phase) as seen in the graph below for yaw rate 0.1 deg/s.

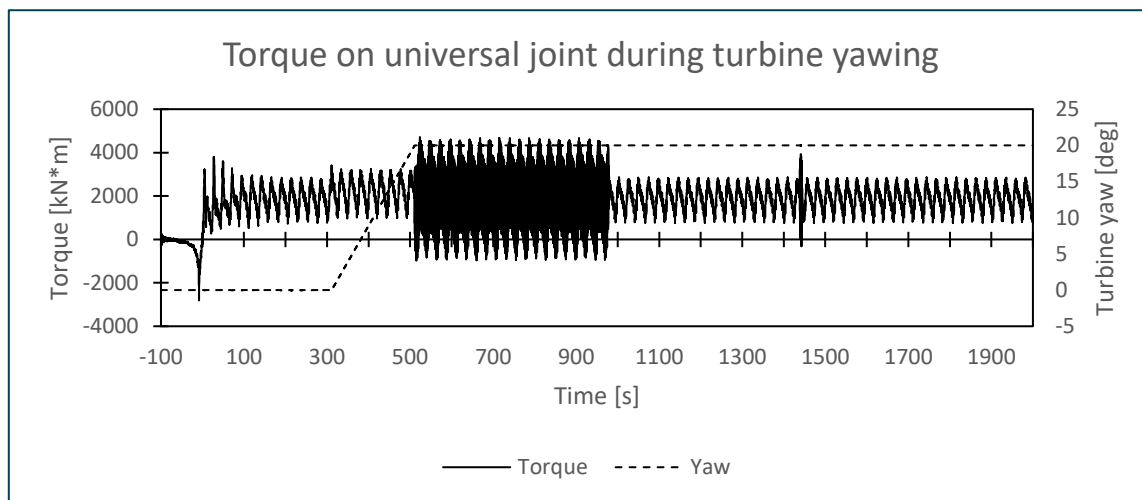


Figure 36: Torque on universal joint at yaw rate 0.1

In the sequence from 100 to 0, the turbine blade rotation starts up, and the first peak at approximately 0 second is caused by the turbine starting to capture all of the wind projected towards the blades which causes the turbine to incline.

The torque on the universal joint constantly varies between 900-2600 kN\*m in the period from 0-300 seconds. The wind changes direction at 300 seconds, and thereby the yaw controller reacts and starts heading towards the wind direction. The short peak at 300 seconds is caused by the yaw torque needed to overcome the turbine's inertia in order to start the yawing operation. This torque is then translated to the universal joint as seen in the graph at 300 seconds.

During the yawing of the turbine (300-500 seconds) the torque is slightly higher than before the yawing started, but the behavior of the torque on the universal joint is similar, and consistent.

The highest torque peak and frequency can be spotted from 500 seconds, in which the yaw stops as it has reached the angle of the wind change. The deceleration of the turbine causes large forces and disturbance of the turbine movement which can be seen in the figure below.

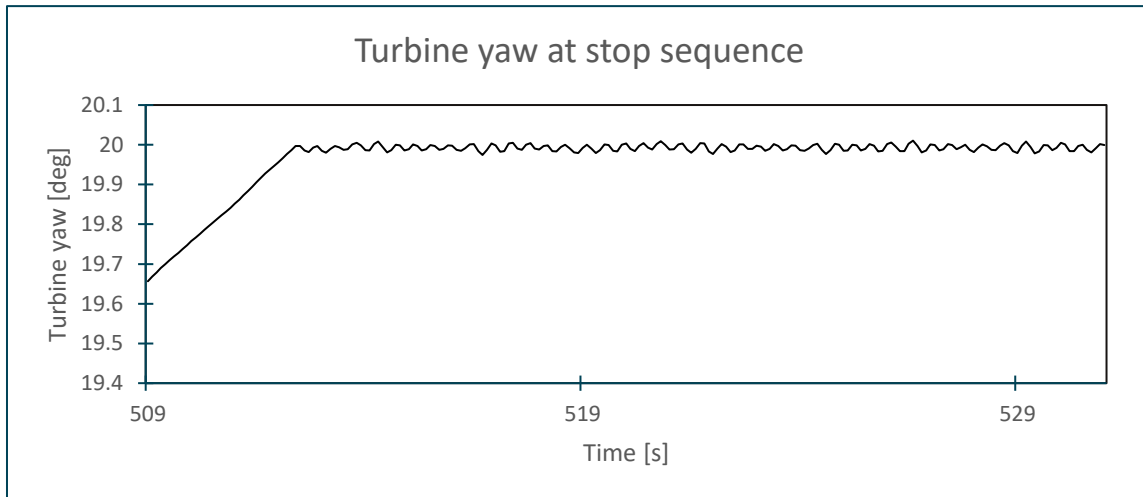


Figure 37: Turbine yawing behaviour

The rotational motion of the turbine is relatively smooth during the yawing, but when the rotation suddenly stops, the deceleration affects the turbine, which causes the large torque on the universal joint from 500 seconds to approximately 980 seconds. The torque then decreases and stabilizes. The yaw trend from this sequence can be seen in the figure below.

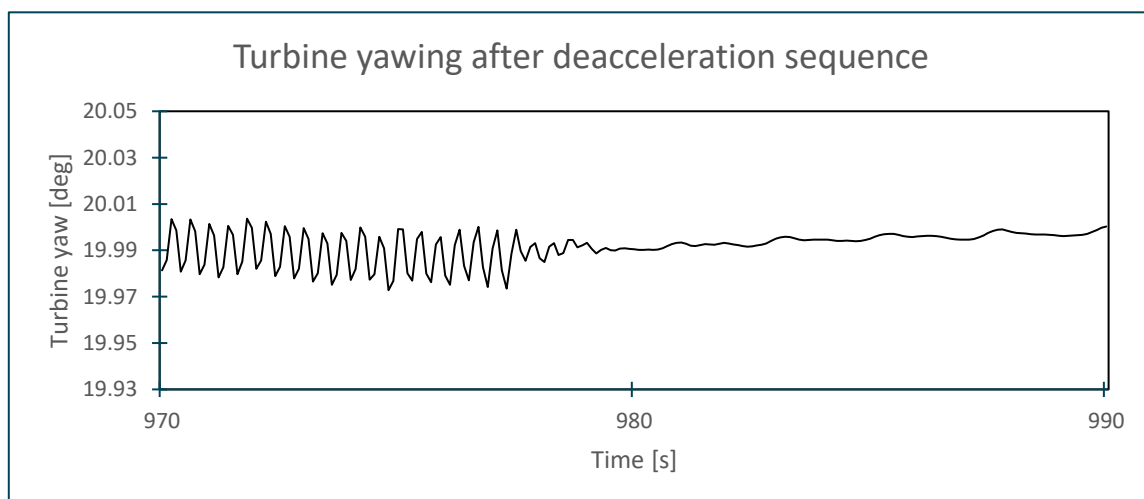


Figure 38: Turbine behavior after deceleration

#### 4.1.2 $H_s = 1.5$ m

The results of torque on the universal joint in a sea state with  $H_s = 1.5$  m are based on a zero -crossing

period from 5.5 to 10.5 seconds, which was determined based on the calculations in 3.5.2. The results can be seen in the tables below where average torque and max torque is shown for the different configurations of Tz and yaw rate over a time period of 600 seconds. Green and red marking represents the lowest and the highest torque on the universal joint respectively.

Table 11:  $H_s=1.5$ , Average torque on universal joint

Tz [s]	5.5	6.5	7.5	8.5	9.5	10.5
Yaw rate [deg/s]						
0.1	1728	1733	1734	1731	1732	1728
0.3	2051	2061	2068	2050	2030	2021
0.5	2552	2561	2563	2553	2503	2442

The lowest average torque on universal joint for a sea state of significant wave height of 1.5 meters occurred at a yaw rate of 0.1 degrees per second and a zero-crossing period, Tz, of 5.5 and 10.5 seconds, with a value of 1728 kN\*m. The highest torque was measured at 2563 kN\*m and occurred at a yaw rate of 0.5 degrees per second in waves with a zero-crossing period of 7.5 seconds. This results in a 912 kN\*m difference.

Table 12:  $H_s=1.5$ , Max torque on universal joint

Tz [s]	5.5	6.5	7.5	8.5	9.5	10.5
Yaw rate [deg/s]						
0.1	4488	4870	4597	4986	4925	4681
0.3	8547	8376	8674	8529	8515	9251
0.5	12642	12448	12522	12346	12815	12472

For the maximum torque, there is a significant difference between the lowest and highest occurrence of the torque applied to the universal joint. The lowest value is 4488 kN\*m at a yaw rate of 0.1 deg/s and zero-crossing period of 5.5 s, while the highest torque value of 12815 occurred with a yaw rate of 0.5 deg/s and a zero-crossing period of 9.5 s. This results in an 8327 kN\*m difference.

#### 4.1.3 $H_s = 3.5$ m

The results of torque on the universal joint in a sea state with  $H_s = 3.5$  m are based on a zero-crossing period from 6.5 to 11.5 seconds, which was determined based on the calculations in 3.5.2. The results can be seen in the tables below where average torque and max torque is shown for the different configurations of  $T_z$  and yaw rate over a period of 600 seconds. Green and red marking represents the lowest and the highest torque on the universal joint respectively.

Table 13:  $H_s=3.5$ , Average torque on universal joint

<b>Tz [s]</b>	<b>6.5</b>	<b>7.5</b>	<b>8.5</b>	<b>9.5</b>	<b>10.5</b>	<b>11.5</b>
<b>Yaw rate [deg/s]</b>						
<b>0.1</b>	1733	1737	1737	1735	1724	1743
<b>0.3</b>	2046	2054	2028	2042	2034	2044
<b>0.5</b>	2552	2561	2563	2553	2503	2442

The lowest average torque on universal joint for a sea state of significant wave height of 3.5 meters occurred at a yaw rate of 0.1 degrees per second and a zero-crossing period,  $T_z$ , of 10.5 seconds, with a value of 1724 kN\*m. The highest torque was measured to 2563 kN\*m and occurred at a yaw rate of 0.5 degrees per second in waves with a zero-crossing period of 8.5 seconds. This results in an 839 kN\*m difference.

Table 14:  $H_s=3.5$ , Max torque on universal joint

<b>Tz [s]</b>	<b>6.5</b>	<b>7.5</b>	<b>8.5</b>	<b>9.5</b>	<b>10.5</b>	<b>11.5</b>
<b>Yaw rate [deg/s]</b>						
<b>0.1</b>	4932	5200	5220	4933	5271	5598
<b>0.3</b>	9127	9649	8804	9548	9560	9798
<b>0.5</b>	13431	14206	14080	13924	14442	13948

For the maximum torque, there is a significant difference between the lowest and highest occurrence of the torque applied to the universal joint. The lowest value is 4932 kN\*m at a yaw rate of 0.1 deg/s and zero-crossing period of 6.5 s, while the highest torque value of 14442 occurred with a yaw rate of 0.5 deg/s and a zero-crossing period of 10.5 s. This results in a 9510 kN\*m difference.

#### 4.1.4 $H_s = 6.5$

The results of torque on the universal joint in a sea state with  $H_s = 6.5$  m are based on a zero-crossing period from 7.5 to 12.5 seconds, which was determined based on the calculations in 3.5.2. The results can be seen in the tables below where average torque and max torque is shown for the different configurations of  $T_z$  and yaw rate over a period of 600 seconds. Green and red marking represents the lowest and the highest torque on the universal joint respectively.

Table 15:  $H_s=6.5$ , Average torque on universal joint

<b>Tz [s]</b>	<b>7.5</b>	<b>8.5</b>	<b>9.5</b>	<b>10.5</b>	<b>11.5</b>	<b>12.5</b>
<b>Yaw rate [deg/s]</b>						
<b>0.1</b>	1748	1745	1777	1748	1768	1752
<b>0.3</b>	2046	2037	2051	2064	2069	2049
<b>0.5</b>	2493	2485	2511	2531	2532	2497

The lowest average torque on universal joint for a sea state of significant wave height of 6.5 meters occurred at a yaw rate of 0.1 degrees per second and a zero-crossing period,  $T_z$ , of 8.5 seconds, with a value of 1745 kN\*m. The highest torque was measured to 2532 kN\*m and occurred at a yaw rate of 0.5 degrees per second in waves with a zero-crossing period of 11.5 seconds. This results in a 786 kN\*m difference.

Table 16:  $H_s=6.5$  Max torque on universal joint

<b>Tz [s]</b>	<b>7.5</b>	<b>8.5</b>	<b>9.5</b>	<b>10.5</b>	<b>11.5</b>	<b>12.5</b>
<b>Yaw rate [deg/s]</b>						
<b>0.1</b>	4955	6061	5362	6112	6337	5899
<b>0.3</b>	10455	9511	10287	11007	11314	10861
<b>0.5</b>	14013	14590	14725	14905	16522	15862

For the maximum torque, there is again a significant difference between the lowest and highest occurrence of the torque applied to the universal joint. The lowest value is 4955 kN\*m at a yaw rate of 0.1 deg/s and zero-crossing period of 7.5 s, while the highest torque value of 16522 occurred with a yaw

rate of 0.5 deg/s and a zero-crossing period of 11.5 s. This results in a 9510 kN\*m difference.

**4.2 Applied torque summary**

*4.2.1 Increase in torque on universal joint due to increase in yaw rate*

An increase in yaw rate has shown a significant increase in torque on the universal joint, and from the first trial of only wind, the difference between the lowest maximum torque value, at yaw rate of 0.1 deg/s and the highest maximum torque value, at yaw rate of 0.5 deg/s is 6518 kN\*m. Below are graphs which shows these time series of only wind applied.

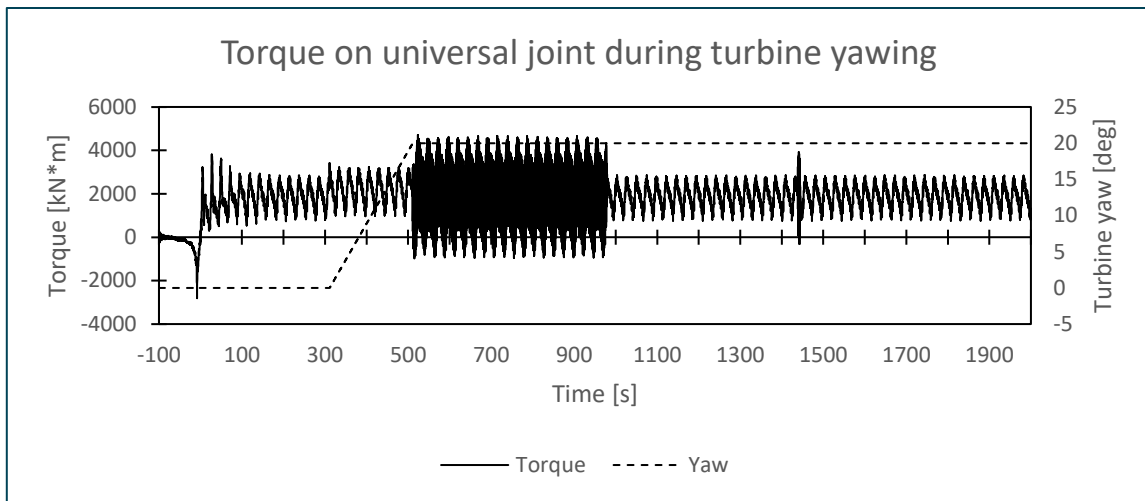


Figure 39: Torque on universal joint, only wind, Yaw rate = 0.1

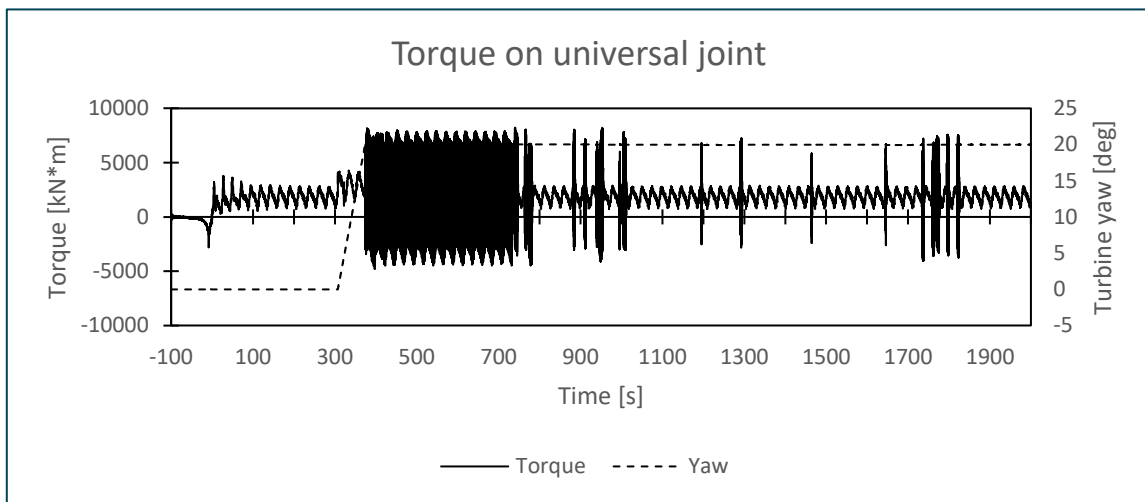


Figure 40: Torque on universal joint, only wind, Yaw rate = 0.3

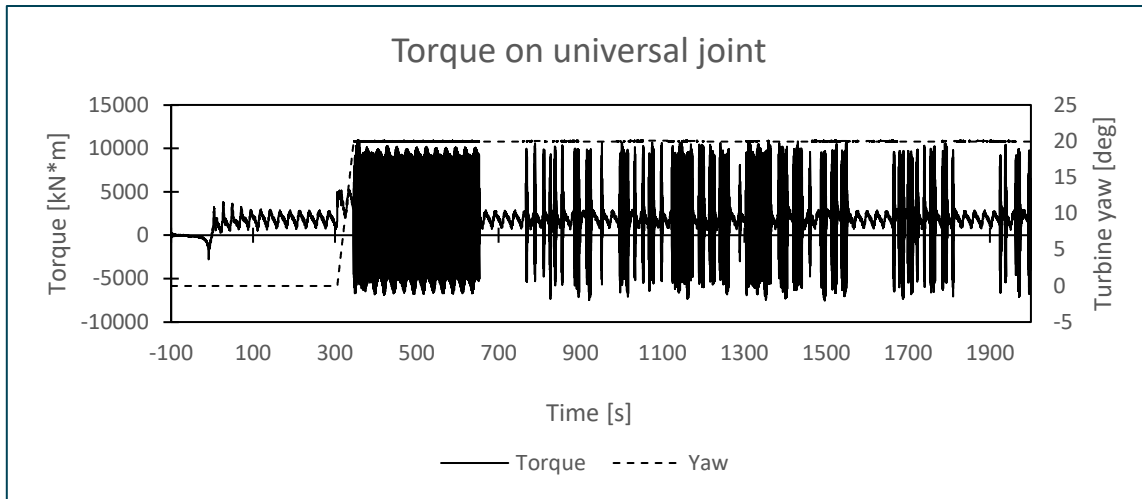


Figure 41: Torque on universal joint, only wind, Yaw rate = 0.5

The results from the three simulations of the different yaw rates are equal until the yawing operation starts. For all three simulations there is a small peak at the moment when the turbine starts to yaw, due to the torque needed to overcome the inertia of the generator, blades, etc. The next peak is a high frequency torque peak which occurs in the yaw-deacceleration phase. This high frequency torque sequence lasts the longest for the trial of yaw rate 0.1 degree per second, but the peaks are much smaller than for the trial of a yaw rate of 0.5 degree per second. The torque applied to the universal joint then decreases and stabilizes for the trial of yaw rate of 0.1 degree per second, while for the two other trials, the universal joint is exposed to further torque peaks in the aftermath of the deaccelerations as seen in the figures. from time 700.

The most significant difference in these three trials is the torque applied to the universal joint when the yawing stops, and this is due to the deacceleration since the deacceleration of a rate of 0.5 deg/s is much higher than a deacceleration of a rate of 0.1 deg/s. The difference in angular deacceleration during yaw stop sequence can be seen in the figure below.

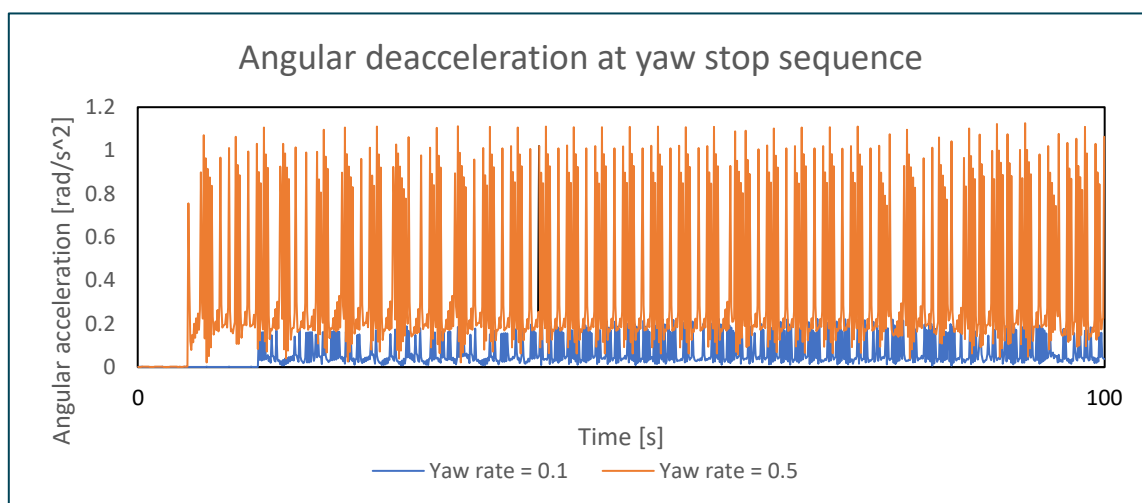


Figure 42: Angular deacceleration at Yaw rate 0.1 and 0.5

The graph shows that the angular deacceleration of a yaw rate of 0.5 degrees per second is five times the deacceleration for the simulation with a yaw rate of 0.1 degrees per second. The deacceleration period can then be seen as the critical period of high torque values.

When only considering the wind loads, the increase in average torque on the universal joint due to increase in yaw rate can be shown as:

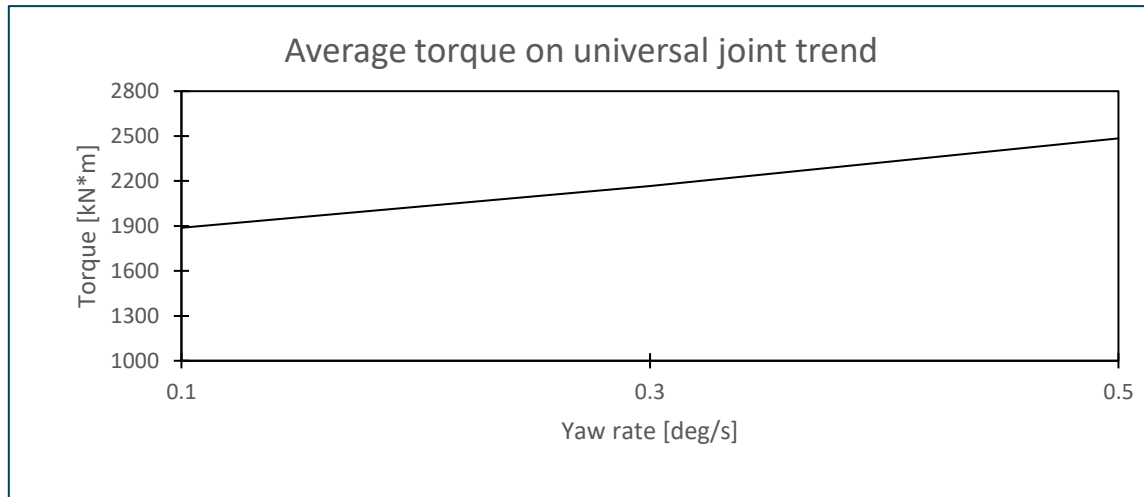


Figure 43: Average torque from increasing yaw rate

The average torque seems to increase linearly with the yaw rate, but the maximum values will increase more drastically as seen in the graph for maximum torque trend below.

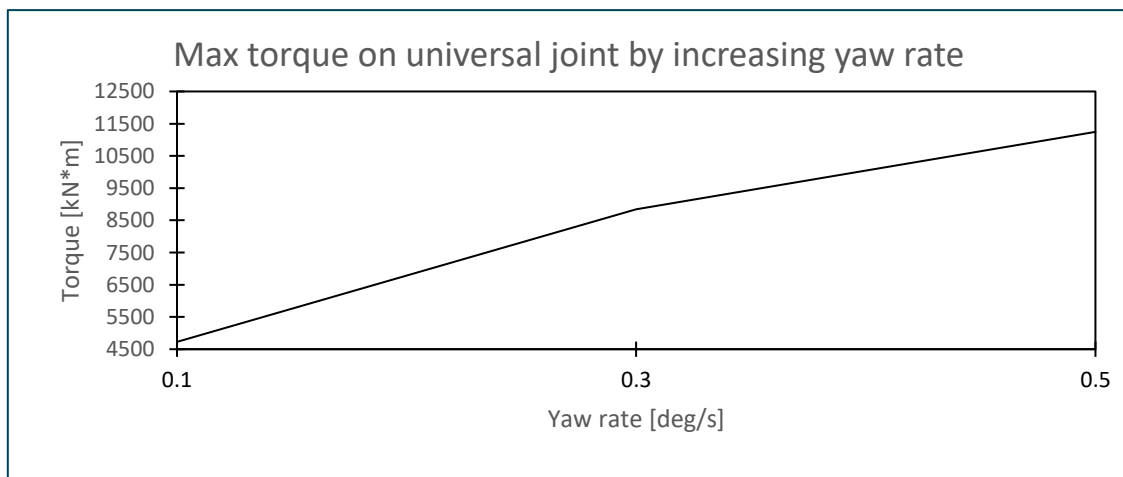


Figure 44: Max torque from increasing yaw rate

There is a max torque value of 6518 kN\*m difference between a yaw rate of 0.1 deg/s and 0.5 deg/s.

#### 4.2.2 Increase in torque on universal joint due to increase in $H_s$

For the simulations including waves, there was expected to be an increase in the torque applied to the universal joint due to an increase of the significant wave height. The graph below shows the trend of the average torque applied to the universal joint without turbine yawing, and by increasing the significant



wave height.

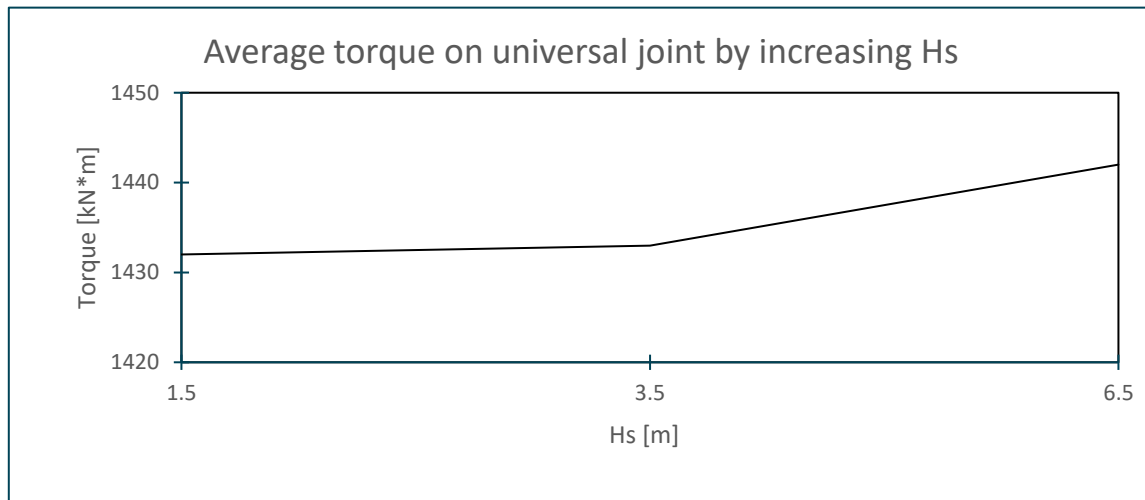


Figure 45: Increase in torque from increasing Hs

The result shows that during non-yawing operation, the torque increases by approximately 10 kN\*m from a sea state with significant wave height 1.5 m to 6.5 m.

The highest torque value from findings was 16522 kN\*m and occurred in a sea state with a significant wave height of 6.5 meters, a zero-crossing period of 11.5 seconds and a yaw rate of 0.5 degrees per second. This max peak occurred during the deceleration of the turbine when the turbine stopped the yaw motion. The simulation can be seen in the figure below.

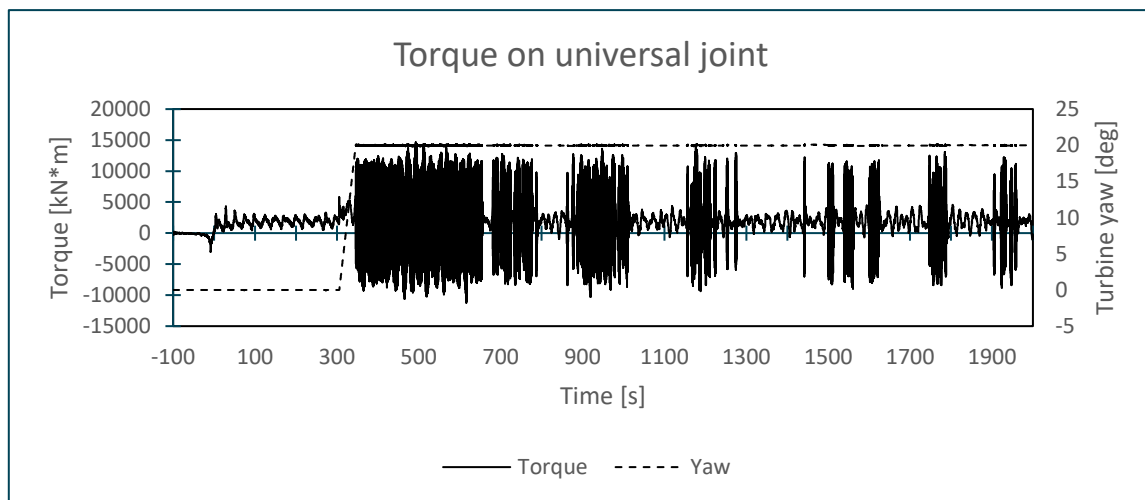


Figure 46: Highest torque simulation

### 4.3 Turbine efficiency

This result part looks at the efficiency of the turbine during environmental conditions including wind loads, and in sea states with significant wave height of 1.5, 3.5, and 6.5 meters. The turbine also starts to yaw when the wind is gradually changing direction to 20 degrees, and the yaw rate considered is 0.1 degrees/second.

#### 4.3.1 Wind loads only

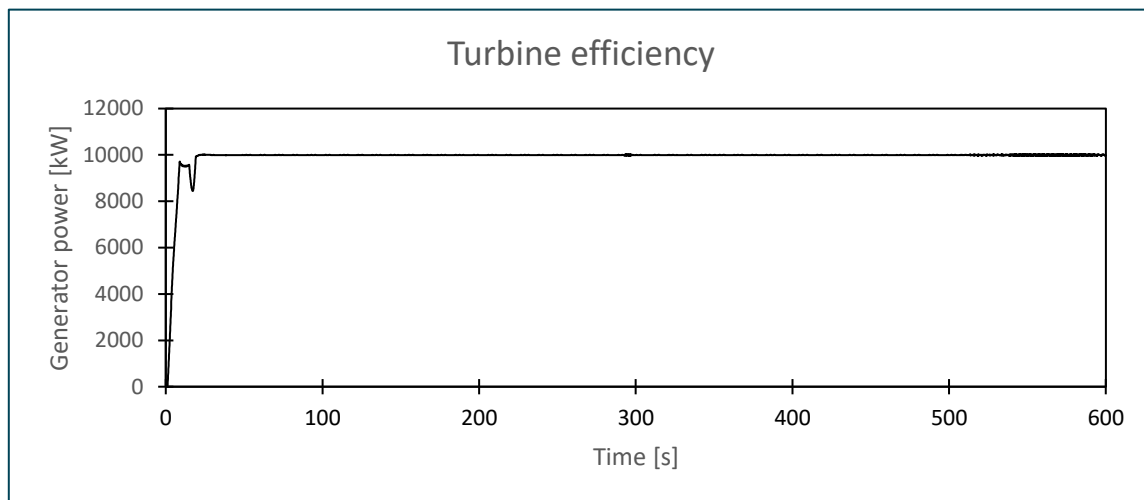


Figure 47: Turbine efficiency over time

The graph above shows the generator power in kilowatts over time. Only wind is applied in this simulation, and as the wind load is applied at 0 seconds, the graph shows that after the turbine starts to produce power, it stabilizes at 10 000 kW's, or 10 MW, as is intended for the turbine at a wind speed of 11 m/s. The average generator power is found to be 9921 including the build-up phase.

#### 4.3.2 $H_s = 1.5 m$

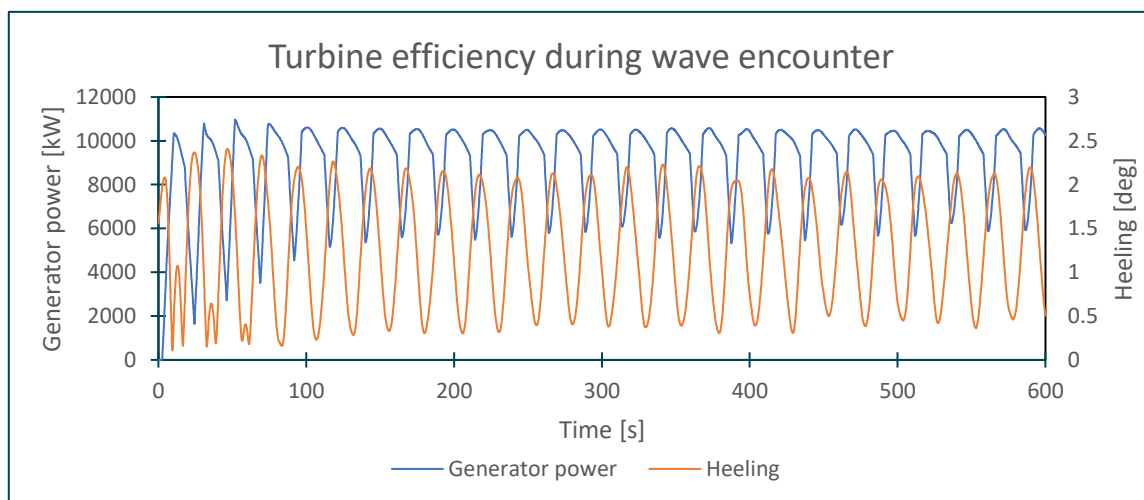


Figure 48: Turbine efficiency,  $H_s = 1.5 m$

The turbine efficiency when applying waves is reduced, and the average generator power is reduced to 9016, meaning that in the average generator power potential loss is 905 kW in the time period of 600 seconds, or 10 minutes. The main reason for this loss has a connection with the heeling of the structure in waves. The swept area of the blades towards the wind is reduced and the turbine efficiency varies in the heeling sequence, as can be seen in the graph below, showing a closer look at the times of heeling for the structure.

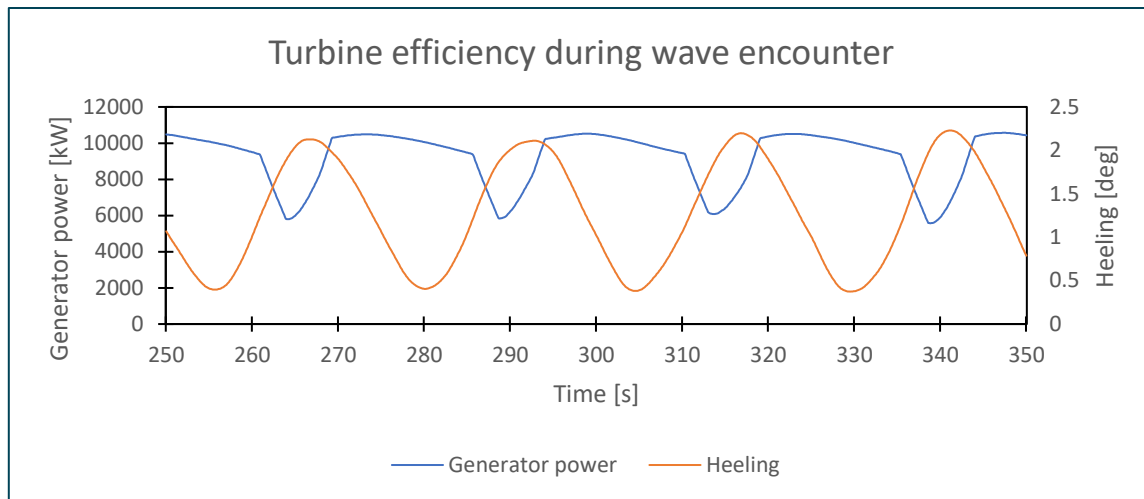


Figure 49: Turbine efficiency during heeling trend

The trend of the graph above shows that the generator power peaks occur in the sequence where the heeling of the structure is at a minimum.

#### 4.3.3 $H_s = 3.5$ m

The results for a sea state with a significant wave height of 3.5 meters shows the same trend as the previous with a significant wave height of 1.5 meters. The increase in significant wave height does reduce the turbine efficiency dramatically. The turbine efficiency trend in a sea state with a  $H_s$  of 3.5 m can be seen in the figure below.

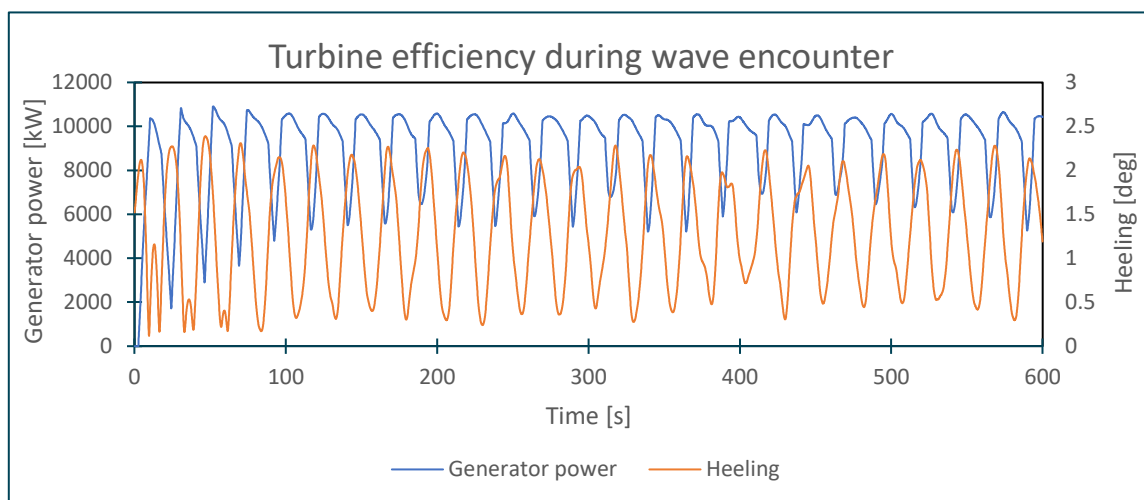


Figure 50: Turbine efficiency,  $H_s = 3.5$  m

By looking at the graph below, it shows the same behavior as for the simulation with a significant wave height of 1.5 meters.

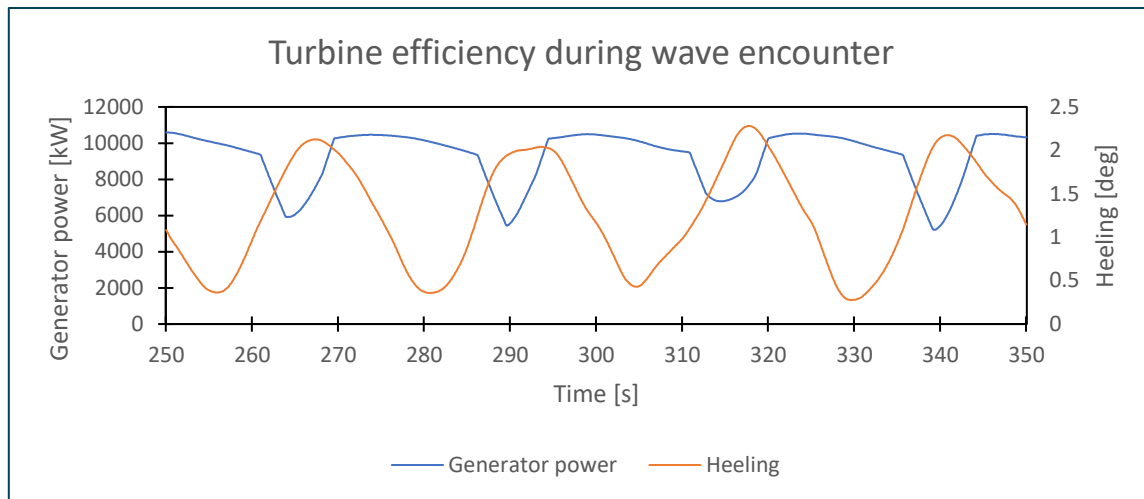


Figure 51: Turbine efficiency during heeling trend

#### 4.3.4 $H_s = 6.5$ m

Again, the same trend follows for a sea state with significant wave height of 6.5 meters. The average heeling does not dramatically increase but the peaks are somewhat higher reaching just above 2.5 degrees.

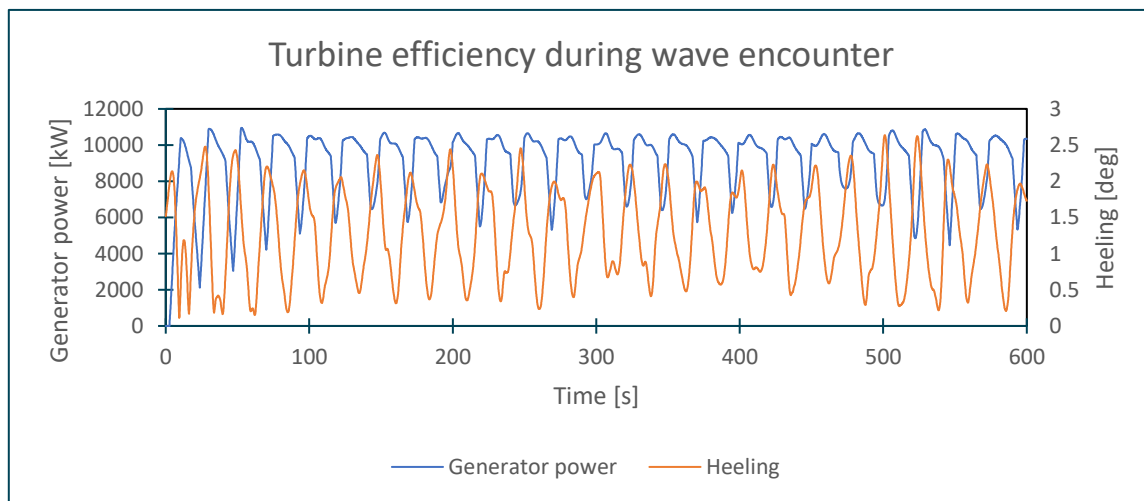


Figure 52: Turbine efficiency,  $H_s = 6.5$  m

The generated power is approximately the same as for the sea states with a significant wave height of 1.5 m and 3.5 m. Taking a closer look at the relationship between the generator power and the heeling, there are some differences to spot compared to the two previous sea states, especially at about 310 seconds.

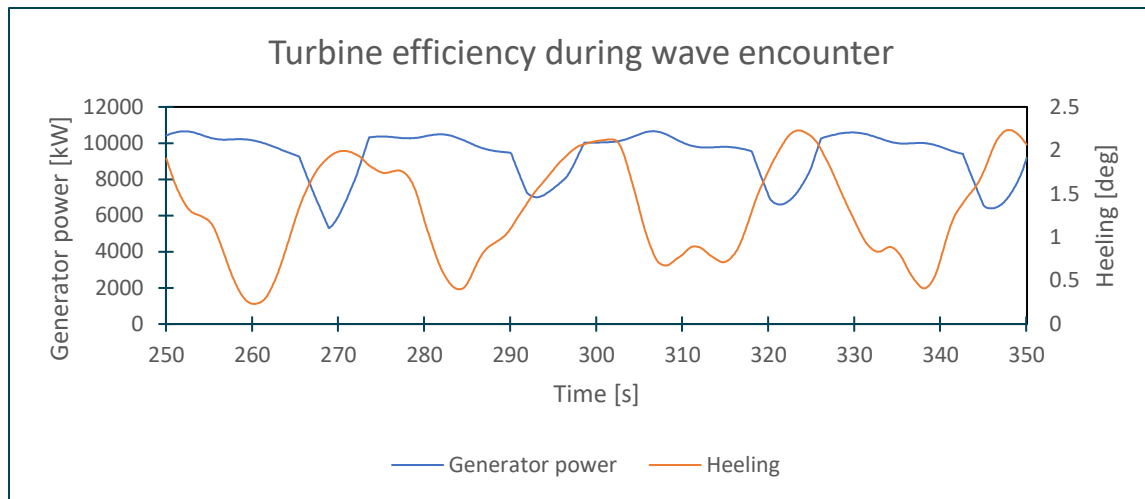


Figure 53: Turbine efficiency during heeling trend

The reason for this behavior is that the turbine starts to yaw and looks to have a greater effect for this sea state than the two previous. Below is the same graph including display of turbine yawing.

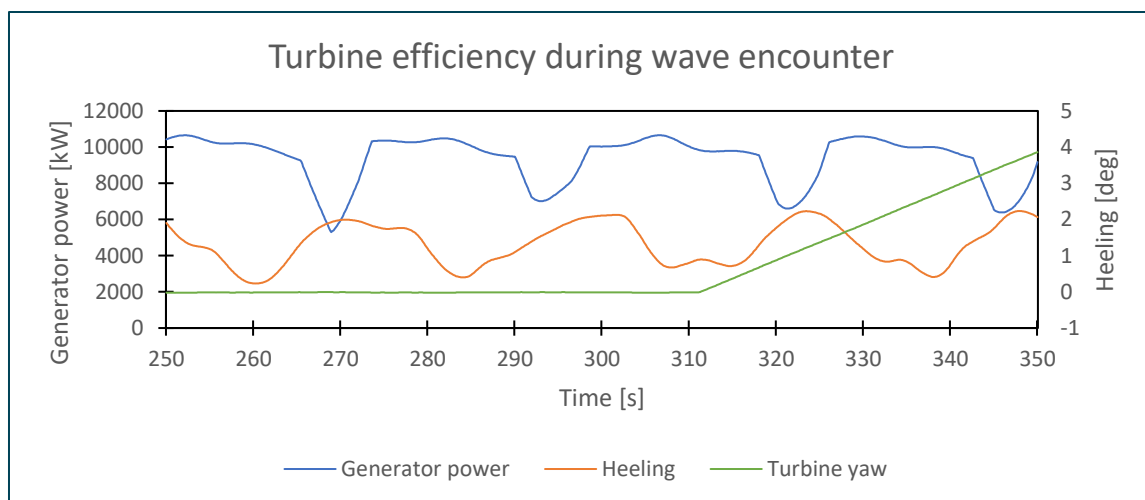


Figure 54: Generator power influence by turbine yawing

As seen in the graph above, the irregularity of the structure heeling at 310 seconds can be explained by the start of turbine yawing.

#### 4.3.5 Yaw error

This result section looks at the turbine potential production loss due to yaw misalignment error. Three misalignment errors are looked at, and these are 4 degrees, 8 degrees, and 20 degrees. To see the effect of production loss due to turbine misalignment to the wind, only wind is applied in the simulations.

The following graphs shows the generator power over time for 4 degrees, 8 degrees, and 20 degrees

misalignment, respectively.

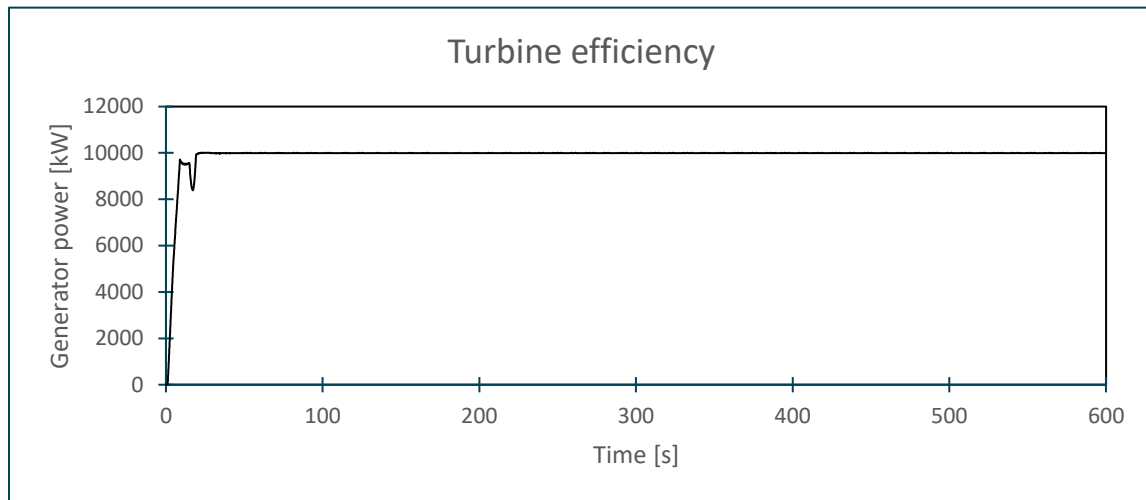


*Figure 55: Turbine efficiency, yaw misalignment = 4 degrees*

The result for a yaw misalignment of four degrees shows a constant generator power over time close to 10 MW as the turbine is optimized for.

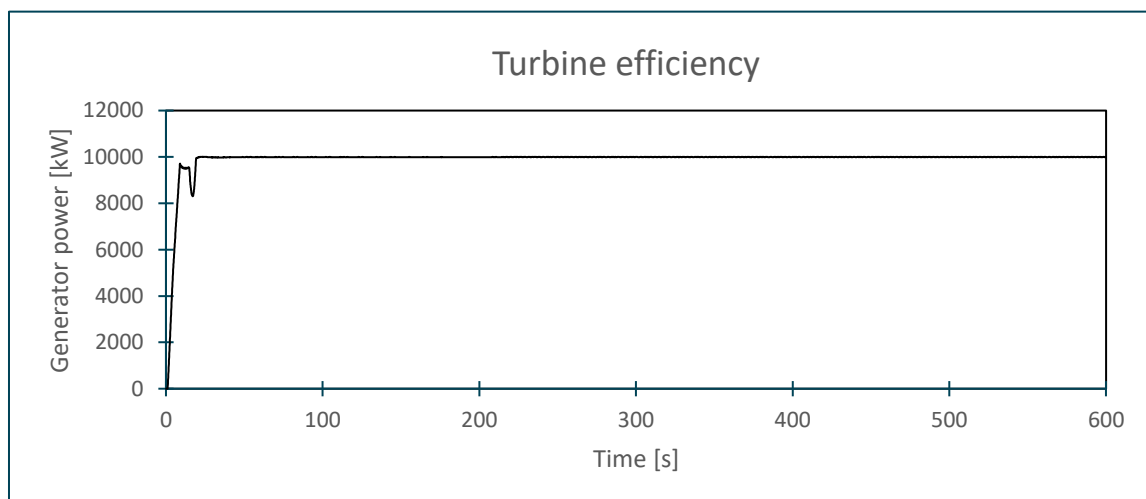


*Figure 56: Turbine efficiency, yaw misalignment = 8 degrees*

An eight degrees turbine misalignment does not significantly decrease the generator power, and as for

the results of four degrees misalignment, the generator power is constant over time.

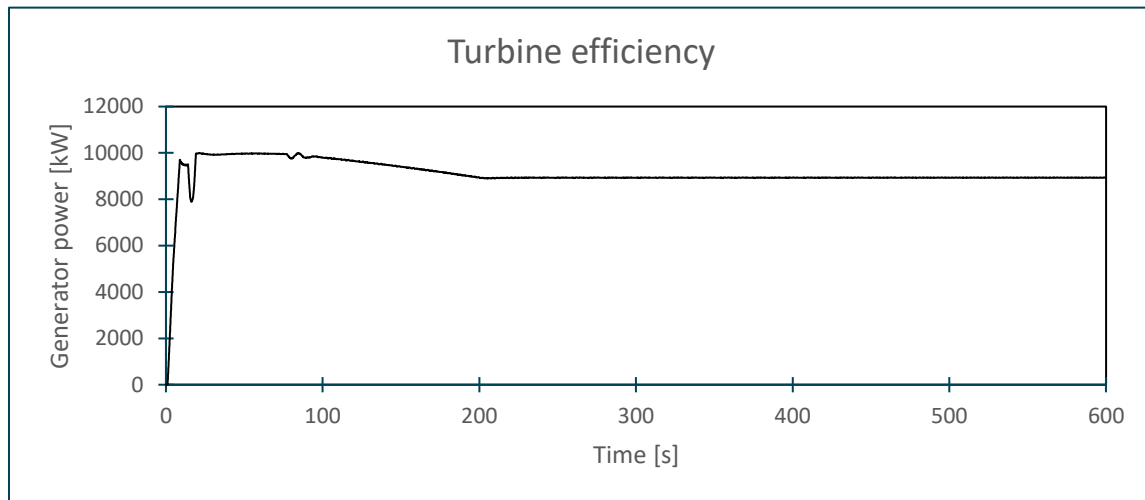


Figure 57: Turbine efficiency, yaw misalignment = 20 degrees

The final simulation shows the turbine efficiency when the turbine is 20 degrees misaligned to the wind, and the result shows a decrease in generator power which stabilizes around 8.9 MW's, which is 1.1 MW less than for the optimized scenario of zero degrees misalignment. Over time a 1.1 MW difference in generator power will lead to significant loss of production.

#### 4.4 Turbine efficiency summary

The results show that the turbine efficiency is significantly reduced when waves are present, causing heeling of the structure, which causes the turbine blades to be misaligned to the wind. The increase in significant wave height did not impact the heeling nor the turbine efficiency in great measures. Below is a trend of the average generator power at significant wave heights of 0, 1.5, 3.5, and 6.5.

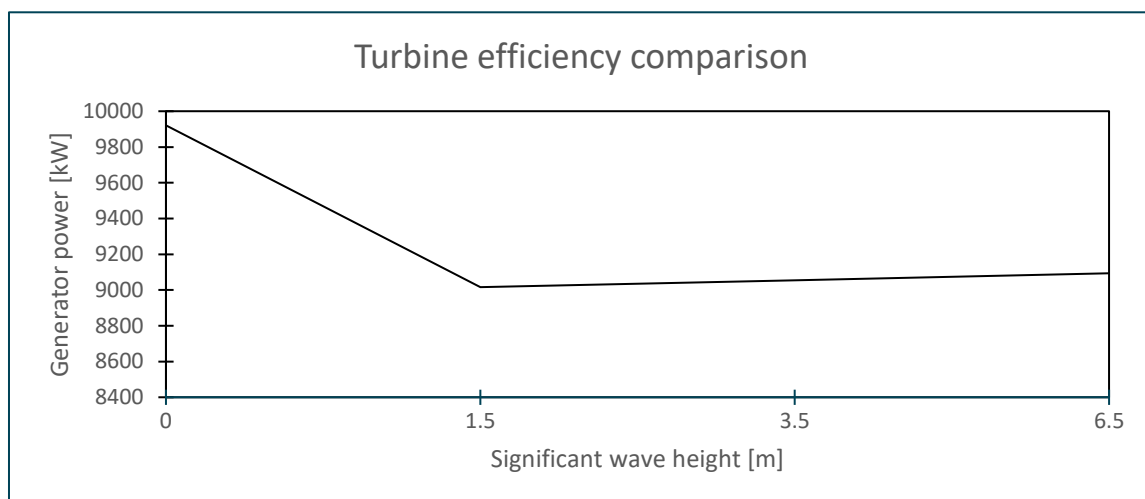


Figure 58: Turbine efficiency trend

As seen in the graph, the major drop in generator power happens when waves are applied, and an increase in further wave height does not impact the generator power significantly.

As the yaw misalignment error increased, it is found that the generator power decreased. The decrease from 4 to 8 degrees misalignment is minimal, while the decrease is more significant at 20 degrees misalignment as seen in the figure below.

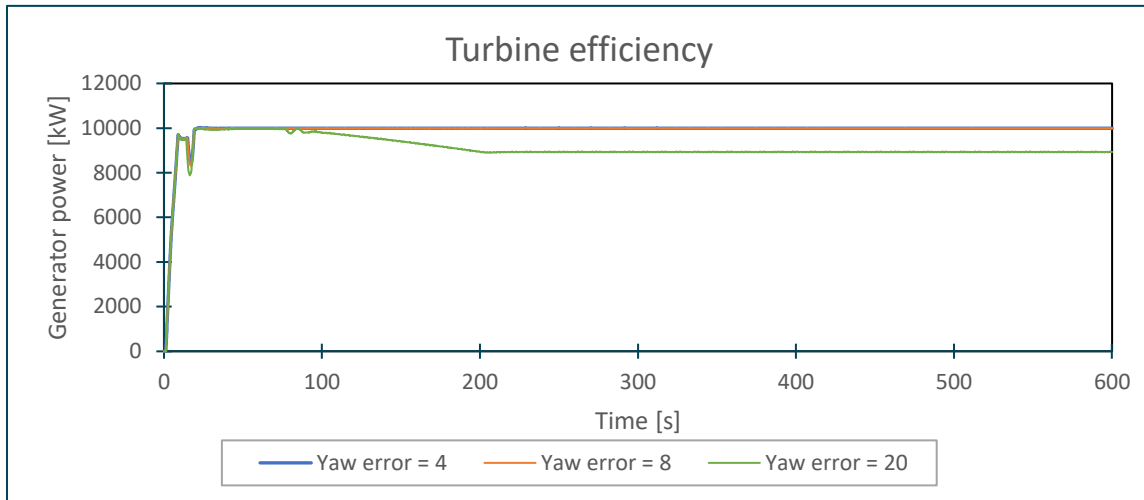


Figure 59: Turbine efficiency at yaw misalignments

The average generator power for the yaw misalignments can be seen in the figure below.

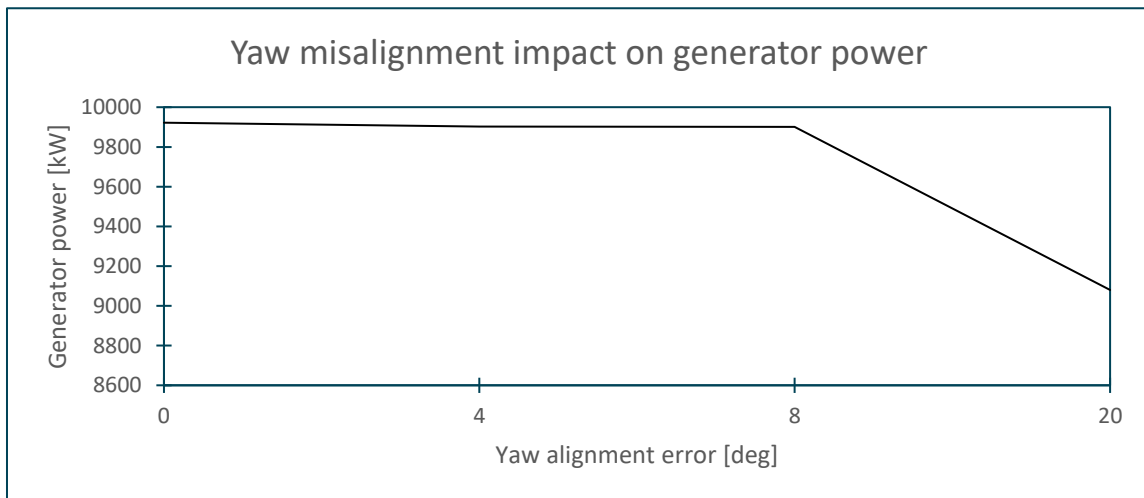


Figure 60: Generator efficiency trend by increasing yaw misalignment

The turbine efficiency is reduced when the yaw misalignment increases but the results show that a four- or eight-degree misalignment does not influence the efficiency significantly. However, 20 degrees turbine misalignment will lead to great loss of generator power over time.



## 5. Conclusion

This research has shown that the Hybrid Wind Turbine concept of Offshore Kinetics could be suitable for a 10 MW wind turbine on a depth of 170 meters. 15661 tonnes (14800 tonnes including turbine, blades, etc.) of ballast is needed to keep a downwards positive force due to the significant lift force from the Hydrogen in the stabilization tank and the buoyancy force from the displaced volume. The stability properties of the structure are desirable with just over 2.7 degrees inclination of structure in a sea state with a significant wave height of 6.5 meters.

In regard to the torque applied to the universal joint, the turbine yaw stop-sequence was the main factor for the high torque values. The turbine yaw start-sequence contributes to an applied torque on the universal joint in a short period of time but contributed to much less extent than the stop sequence. As it was the yaw stop sequence which contributed to the significant torque on the universal joint, the increase in yaw rate significantly increased the torque due to an increase in deceleration needed.

The highest average torque measured was 2532 kN which is lower than the calculated max design torque on the universal joint for Northeast Frigg[18] of 5886 kN. The highest max torque values was however almost three times the max design torque on the universal joint for Northeast Frigg[18].

The increase in significant wave height did not contribute to a significant increase in torque applied to the universal joint alone but the largest value of significant wave height (6.5 m) combined with the fastest yaw rate of 0.5 degrees per second gave the highest torque value in the simulations. The results did not show a clear pattern of torque values in regard to the zero-crossing period,  $T_z$ .

The turbine efficiency was found to be approximately optimal when only applying wind, while the efficiency was reduced when including waves due to the heeling of the structure reducing the blades' swept area during heeling. As an increase in the significant wave height did not greatly impact the inclination of the structure, it did not impact the turbine efficiency either.

Yaw misalignment of four and eight degrees did not affect the efficiency of the turbine in great measures over the simulated time but in a long-term period, these misalignments could contribute to a significant production loss. A yaw misalignment of 20 degrees showed a great reduction in generator power in the simulation. A constant misalignment over a longer period could then make the turbine inefficient.

The conclusion can then be summarized to:

- The general stability properties of the structure are sufficient regarding inclination for the simulated sea states, just above 2.7 degrees, and in terms of GM-value.
- 15661 tonnes of ballast needed to ensure net downwards force due to buoyancy force from

displaced volume and the lift force from Hydrogen in stabilization tank

- The torque applied to the universal joint increases significantly with the increase of yaw rate
- The yaw stopping sequence gives the maximum values of torque applied to the universal joint
- Yaw stopping sequence produces significant torque values over a 500 second time period
- Turbine efficiency is reduced when the structure encounters waves
- Turbine efficiency is not much reduced by further increasing the significant wave height due to very small increase in inclination/heeling of structure
- Yaw misalignment of four and eight degrees does not significantly reduce the turbine efficiency in the short-term
- A yaw misalignment of 20 degrees reduces the turbine efficiency in the short-term and could make the turbine inefficient in a long-term period

## 6. Further work

For further work there are several aspects that would be interesting to look at. Further work on yaw controller configuration by including yaw brakes and optimize these breaks such that the torque peaks at turbine yaw stopping sequence are reduced. This could be done by modifying yaw controller script so that the brakes are applied when the turbine is close to facing the wind direction.

Research on vertical placement of the universal joint to reduce the torque could be considered and could include an optimization part of balancing the vertical placement while also satisfy buoyancy properties. As an option, double hinged articulated tower design as presented in[24], could be considered.

As described in the conclusion, a fatigue study must be executed on the universal joint for the Hybrid Wind Turbine, as it might be the most significant issue next to the peak loads.

For the buoyancy and ballast tanks, an optimization study regarding the relationship between these properties giving net force upwards or downwards would be helpful for identifying in which configurations gives the least torque to the universal joint.

A failure mode study could identify the forces applied to the structure in different cases which could include:

- Sudden yaw control failure (fails to start or fails to stop rotation)
- Blade pitch control failure/misalignment (more drag than lift on blades)
- Blade rotation failure (sudden stop or brake failure)

Extreme conditions should be further assessed in terms of 50 and 100-year winds and waves.

## 7. References

- [1] N. Government, "Ambitious offshore wind initiative," in *Press release*, R. Holmsen, Ed., No:83/22 ed. <https://www.regjeringen.no/en/aktuelt/ambitious-offshore-wind-power-initiative/id2912297/>: Norwegian Government, 2022.
- [2] Miljødirektoratet, "Equinor søker om å inkludere kraftforsyning fra Hywind Tampen i tillatelsen til Gullfaks og Snorre," Miljødirektoratet, Ed., ed. <https://www.miljodirektoratet.no/hoeringer/2022/januar-2022/equinor-soker-om-a-inkludere-kraftforsyning-fra-hywind-tampen-i-tillatelsen-til-gullfaks-og-snorre/>: Miljødirektoratet, 2022.
- [3] Equinor. "Hywind Tampen." Equinor. (accessed 10.04.2022, 2022).
- [4] O. Kinetics, "OKW Ireland," 2018.
- [5] F. Bu, W. Huang, Y. Hu, Y. Xu, K. Shi, and Q. Wang, *Study and implementation of a control algorithm for wind turbine yaw control system* (2009 World Non-Grid-Connected Wind Power and Energy Conference). IEEE, 2009, pp. 1-5.
- [6] F. Watanabe, T. Takahashi, H. Tokuyama, Y. Nishizawa, and I. Ushiyama, "Modelling passive yawing motion of horizontal axis small wind turbine: derivation of new simplified equation for maximum yaw rate," *Wind Engineering*, vol. 36, no. 4, pp. 433-441, 2012.
- [7] B. Snyder and M. J. Kaiser, "Ecological and economic cost-benefit analysis of offshore wind energy," *Renewable Energy*, vol. 34, no. 6, pp. 1567-1578, 2009.
- [8] W. Europe, "Offshore Wind In Europe," *windeurope.org*, 2021.
- [9] A. M. Kaynia, "Seismic considerations in design of offshore wind turbines," *Soil Dynamics and Earthquake Engineering*, vol. 124, pp. 399-407, 2019.
- [10] K. T. Hood, S. M. Torres, and R. D. Palmer, "P10. 1 AUTOMATIC DETECTION OF WIND TURBINE CLUTTER USING DOPPLER SPECTRAL FEATURES."
- [11] E. Al-Ahmar, M. Benbouzid, Y. Amirat, and S. B. Elghali, "DFIG-based wind turbine fault diagnosis using a specific discrete wavelet transform," in *2008 18th International Conference on Electrical Machines*, 2008: IEEE, pp. 1-6.
- [12] L. Saidi, J. B. Ali, E. Bechhoefer, and M. Benbouzid, "Wind turbine high-speed shaft bearings health prognosis through a spectral Kurtosis-derived indices and SVR," *Applied Acoustics*, vol. 120, pp. 1-8, 2017.
- [13] W. E. T. Office. "How A Wind Turbine Works." Office of Efficiency & Renewable Energy. (accessed 03.05.2022, 2022).
- [14] P. Uys, J. Farkas, K. Jarmai, and F. Van Tonder, "Optimisation of a steel tower for a wind turbine structure," *Engineering structures*, vol. 29, no. 7, pp. 1337-1342, 2007.
- [15] H. A. Effat and A. M. El-Zeiny, "Geospatial modeling for selection of optimum sites for hybrid solar-wind energy in Assiut Governorate, Egypt," *The Egyptian Journal of Remote Sensing and Space Science*, 2022.
- [16] Z. Jiang, "Installation of offshore wind turbines: A technical review," *Renewable and Sustainable Energy Reviews*, vol. 139, p. 110576, 2021.

- [17] K. Andersen *et al.*, "Suction anchors for deepwater applications," in *Proceedings of the 1st International Symposium on Frontiers in Offshore Geotechnics, ISFOG, Perth, 2005*, pp. 3-30.
- [18] L. Habardsholm, "Environmental impact from removal of offshore installations: the North East Frigg field case," in *SPE Health, Safety and Environment in Oil and Gas Exploration and Production Conference, 1994*: OnePetro.
- [19] M. Murtedjo, E. B. Djatmiko, H. Sudjianto, and I. Campus–Sukolilo, "The influence of buoyancy parameters on the dynamic behavior of articulated tower," *Jurnal Mekanikal*, no. 19, pp. 32-47, 2005.
- [20] S. Chandrasekaran and A. Jain, *Ocean structures: Construction, materials, and operations*. Crc Press, 2017.
- [21] T. Beinset, "Master Thesis 2022 " in *MMO*, P. A. Aga, Ed., ed: Western Norway University of Applied Sciences, 2022.
- [22] O. Kinetics, "OK-Wind Turbine Concept," 2019.
- [23] P. Bar-Avi and H. Benaroya, "Stochastic response of a two DOF articulated tower," *International journal of non-linear mechanics*, vol. 32, no. 4, pp. 639-655, 1997.
- [24] M. M. Zaheer and N. Islam, "Dynamic response of articulated towers under correlated wind and waves," *Ocean Engineering*, vol. 132, pp. 114-125, 2017.
- [25] P. Zhang *et al.*, "Dynamic Response of Articulated Offshore Wind Turbines under Different Water Depths," *Energies*, vol. 13, no. 11, p. 2784, 2020.
- [26] M. Kim and P. Dalhoff, "Yaw Systems for wind turbines—Overview of concepts, current challenges and design methods," in *Journal of Physics: Conference Series*, 2014, vol. 524, no. 1: IOP Publishing, p. 012086.
- [27] P. Zhang, Y. Li, J. Gu, T. Yin, Z. Hu, and Y. Tang, "Dynamic Response of a Conceptual Designed Articulated Offshore Wind Turbine," *Journal of Offshore Mechanics and Arctic Engineering*, vol. 143, no. 2, 2021.
- [28] N. MOHD NOR, "INVESTIGATION OF GUYED TOWER AND ARTICULATED TOWER AS A DEEPWATER PLATFORM," 2007.
- [29] K. Sadeghi and A. H. Bichi, "Offshore tower platforms: an overview of design, analysis, construction and installation," *Academic Research International*, vol. 9, no. 1, pp. 62-68, 2018.
- [30] Q. Bai and Y. Bai, *Subsea pipeline design, analysis, and installation*. Gulf Professional Publishing, 2014.
- [31] B. Pettersen, *Hydrodynamikk 3 (Marin Teknikk 3)*. 2018.
- [32] D. W. I. Association. "Wind Turbine Towers." (accessed 19.03.2022, 2022).
- [33] J.-M. Franssen and P. V. Real, *Fire Design of Steel Structures: Eurocode 1: Actions on structures; Part 1-2: General actions--Actions on structures exposed to fire; Eurocode 3: Design of steel structures; Part 1-2: General rules--Structural fire design*. John Wiley & Sons, 2012.

- [34] T. Benson. "Aerodynamic Forces." (accessed 03.05.2022, 2022).
- [35] S. C. Misra, *Design principles of ships and marine structures*. CRC Press, 2015.
- [36] R. H. Stewart, *Introduction to physical oceanography*. Robert H. Stewart, 2008.
- [37] A. F. Molland, *The maritime engineering reference book: a guide to ship design, construction and operation*. Elsevier, 2011.
- [38] Orcina. "Orcaflex." Orcina. (accessed 14.04.2022, 2022).
- [39] G. Dnv, "DNV GL-ST-0119 Floating wind turbine structures," *DNV GL*, 2018.
- [40] K. E. Kaasen, "Time domain model representations of standard wind gust spectra," in *The Ninth International Offshore and Polar Engineering Conference*, 1999: OnePetro.
- [41] *Environment: Wind data*. (2022). Orcina,  
<https://www.orcina.com/webhelp/OrcaFlex/Content/html/Environment,Winddata.htm>.  
Accessed: 04.04.2022.
- [42] M. Bächer, E. Whiting, B. Bickel, and O. Sorkine-Hornung, "Spin-it: Optimizing moment of inertia for spinnable objects," *ACM Transactions on Graphics (TOG)*, vol. 33, no. 4, pp. 1-10, 2014.
- [43] R. Nave, "Mechanics," in *Hyperphysics*, ed. <http://hyperphysics.phy-astr.gsu.edu/hbase/mi.html>: Hyperphysics, 2000.
- [44] K. Academy. (2022) Torque, moments, and angular momentum. *Khan Academy*.
- [45] A. Menon. "Ship Motions - The Ultimate Guide." *Marine Insight*. (accessed 14.04.2022, 2022).
- [46] R. Kyle, Y. C. Lee, and W.-G. Früh, "Propeller and vortex ring state for floating offshore wind turbines during surge," *Renewable Energy*, vol. 155, pp. 645-657, 2020.
- [47] L. Dostal, E. Kreuzer, and N. Sri Namachchivaya, "Non-standard stochastic averaging of large-amplitude ship rolling in random seas," *Proceedings of the Royal Society A: Mathematical, Physical and Engineering Sciences*, vol. 468, no. 2148, pp. 4146-4173, 2012.
- [48] Y. Liu, S. Liu, L. Zhang, F. Cao, and L. Wang, "Optimization of the yaw control error of wind turbine," *Frontiers in Energy Research*, vol. 9, p. 5, 2021.
- [49] J. Yang *et al.*, "Review of control strategy of large horizontal-axis wind turbines yaw system," *Wind Energy*, vol. 24, no. 2, pp. 97-115, 2021.
- [50] W. Liu, B. Tang, and Y. Jiang, "Status and problems of wind turbine structural health monitoring techniques in China," *Renewable Energy*, vol. 35, no. 7, pp. 1414-1418, 2010.
- [51] J. Dai, T. He, M. Li, and X. Long, "Performance study of multi-source driving yaw system for aiding yaw control of wind turbines," *Renewable Energy*, vol. 163, pp. 154-171, 2021.
- [52] S. Gamesa, "Yaw rate specification," ed, 2022.
- [53] E. Marin and H. Pedersen, "Pointing to the right direction," *EWEA, Malmo, Sweden*, 2014.
- [54] E. G. M. Henrik S. Pedersen "Yaw Misalignment and Power Curve Analysis," presented at the

- EWEA Analysis of Operating Wind Farms, Bilbao, 14-15 April, 2016.
- [55] *Inventor*. (2022). <https://www.autodesk.com/products/inventor/features>.
- [56] *Excel*. (2022). <https://www.microsoft.com/en-ww/microsoft-365/excel>.
- [57] Orcina, "Renewables: K02 10MW fixed-bottom OWT."
- [58] Python. "Python." (accessed 23.04.2022, 2022).
- [59] P. Bortolotti *et al.*, "IEA Wind TCP Task 37: Systems engineering in wind energy-WP2. 1 Reference wind turbines," National Renewable Energy Lab.(NREL), Golden, CO (United States), 2019.
- [60] *Environment: Seabed data*. (2022). Orcina, <https://www.orcina.com/webhelp/OrcaFlex/Default.htm>.
- [61] *Wave load*, G. Dnv, <https://rules.dnv.com/docs/pdf/DNV/CG/2018-01/DNVGL-CG-0130.pdf>, 2018.

## Appendix 1 – Torque results $H_s = 1.5$

Yaw rate = 0.1

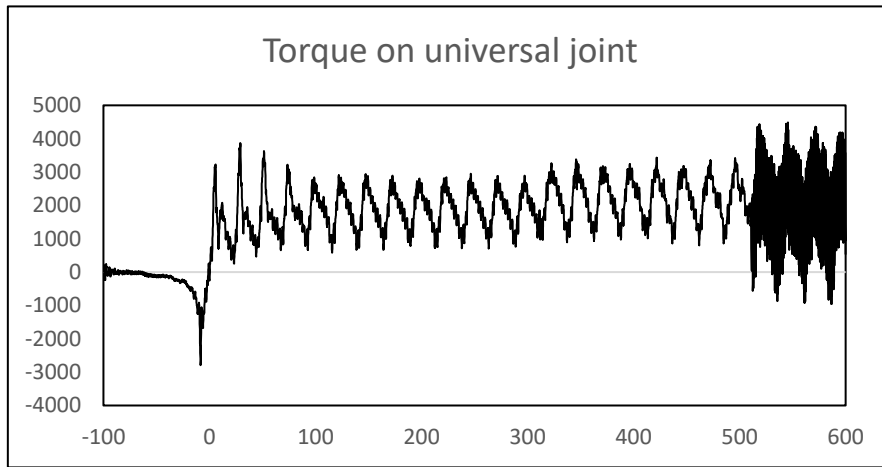


Figure 61:  $T_z = 5.5$

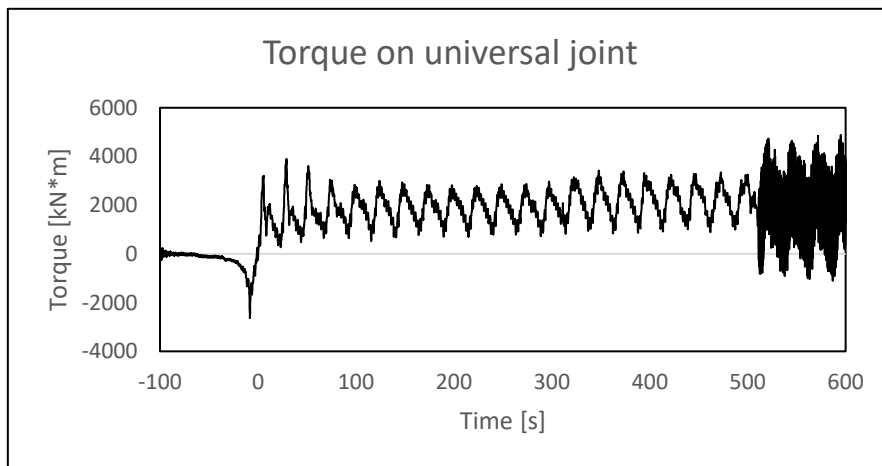


Figure 62:  $T_z = 6.5$

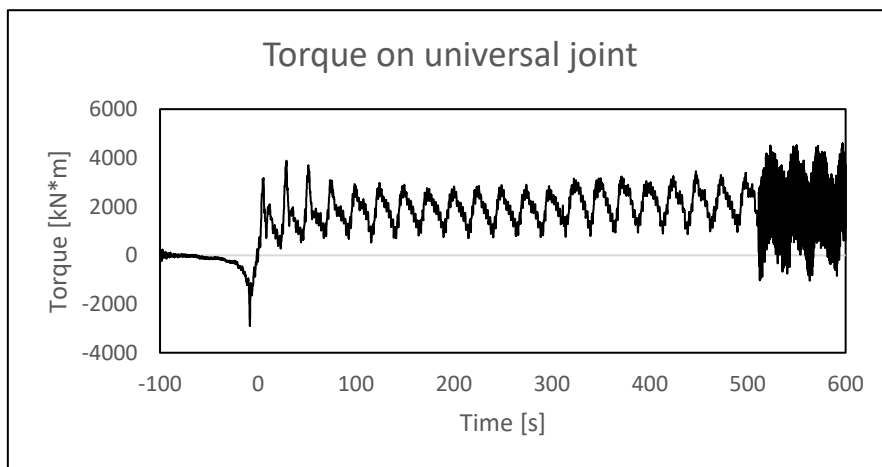
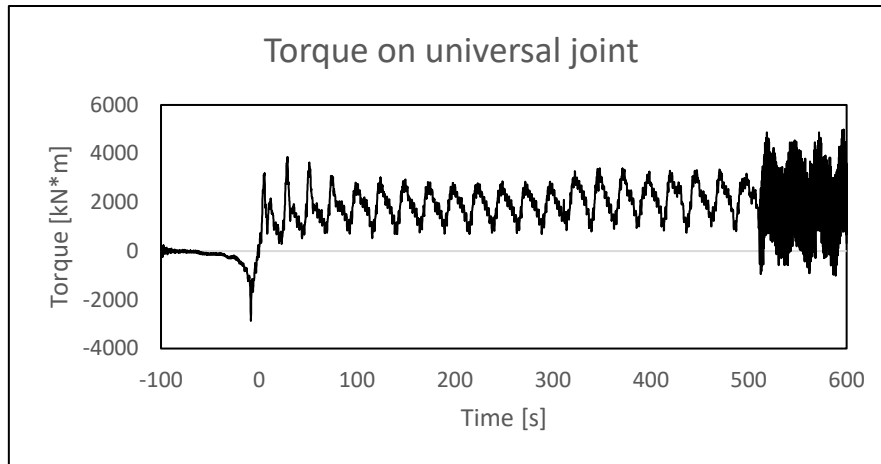
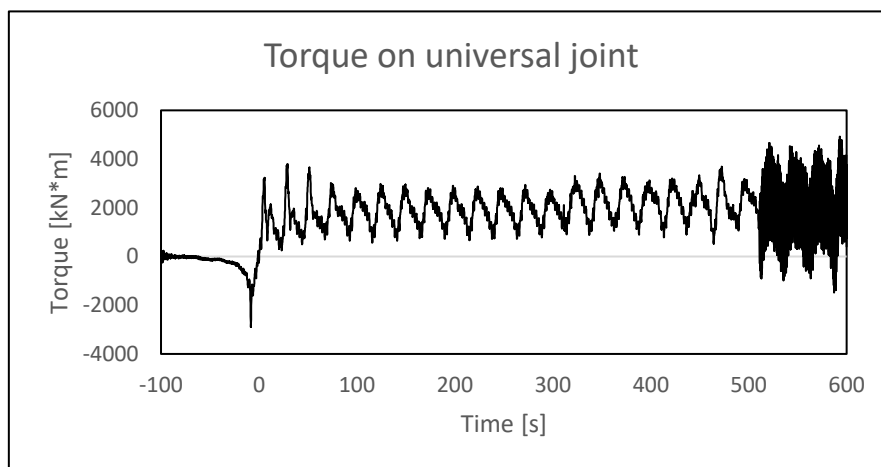
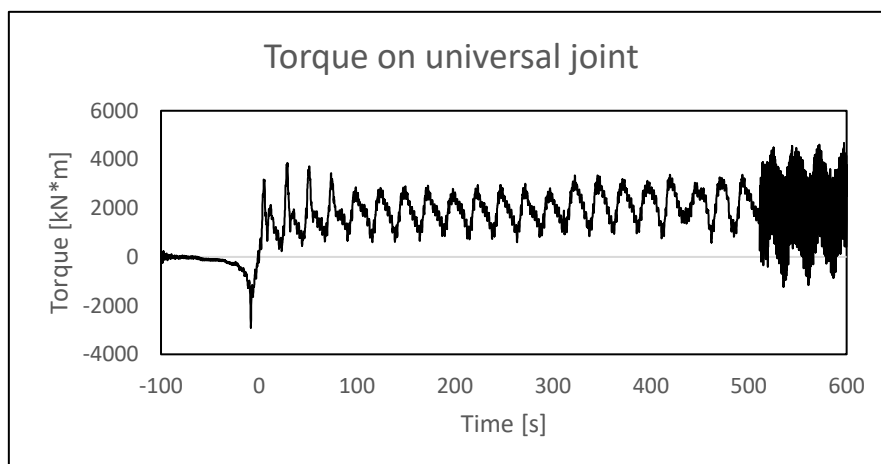


Figure 63:  $T_z = 7.5$



*Figure 64:  $T_z = 8.5$* *Figure 65:  $T_z = 9.5$* *Figure 66:  $T_z = 10.5$* 

**Yaw rate = 0.3**

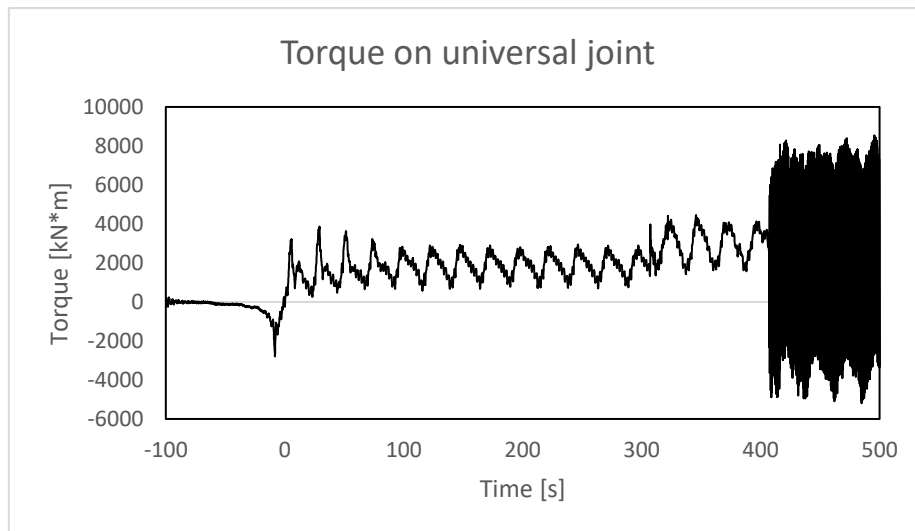


Figure 67:  $T_z = 5.5$

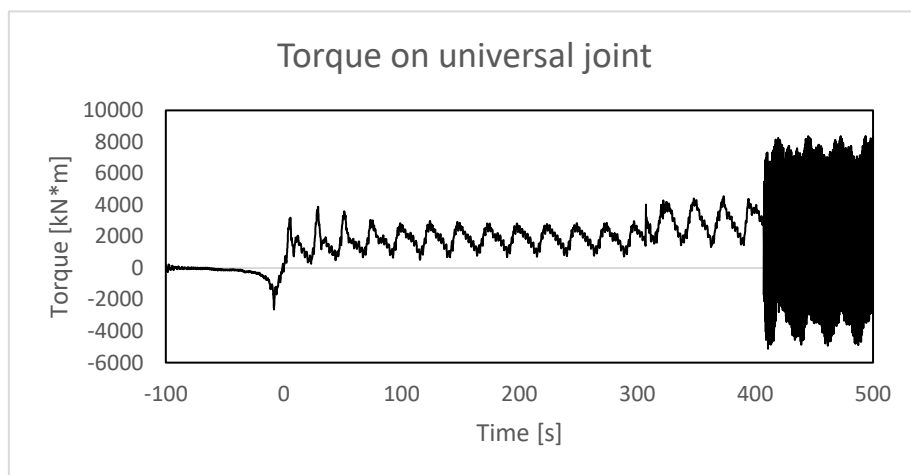


Figure 68:  $T_z = 6.5$

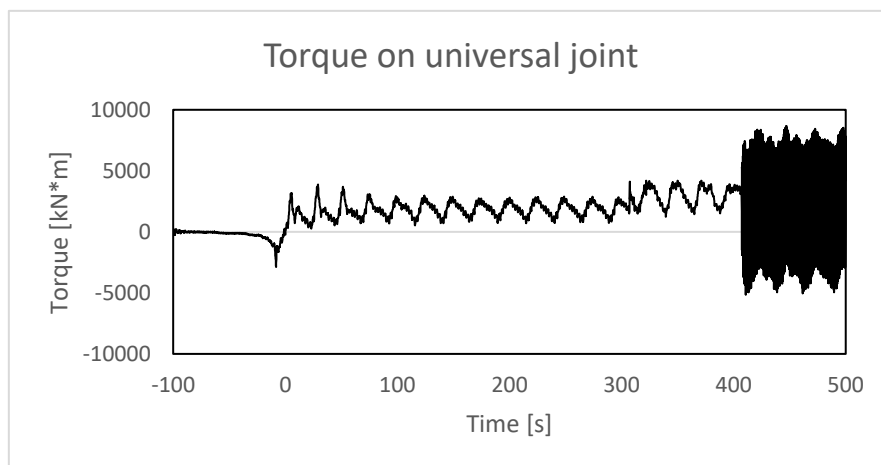
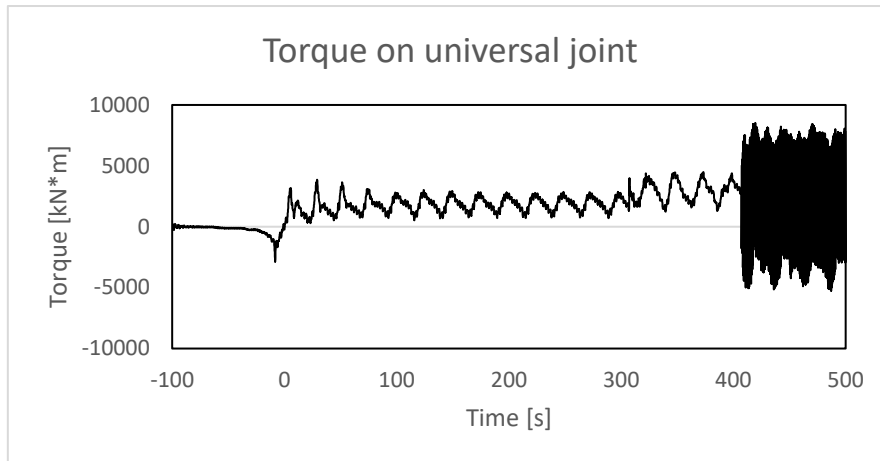
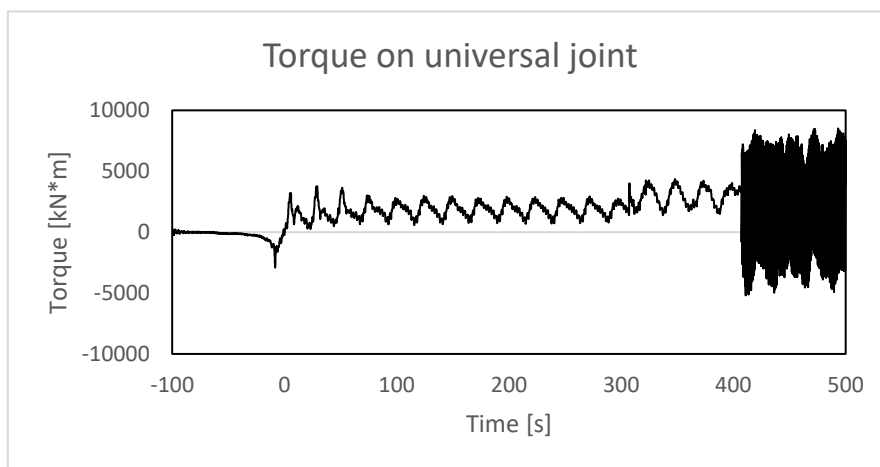
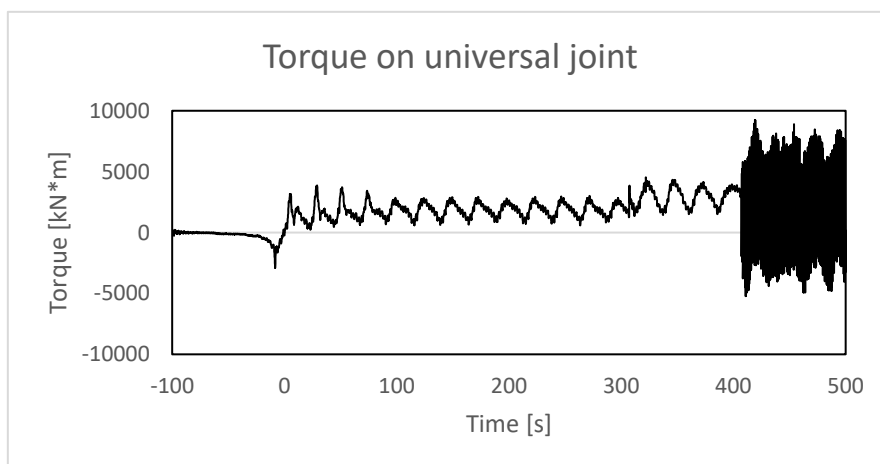
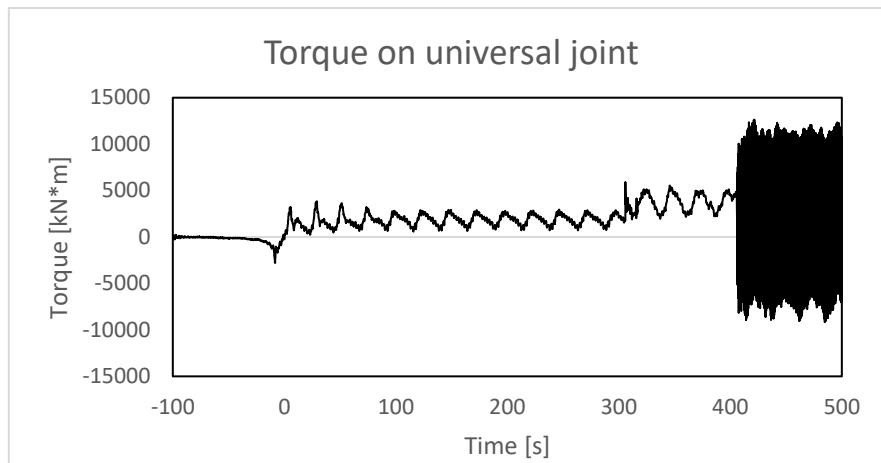
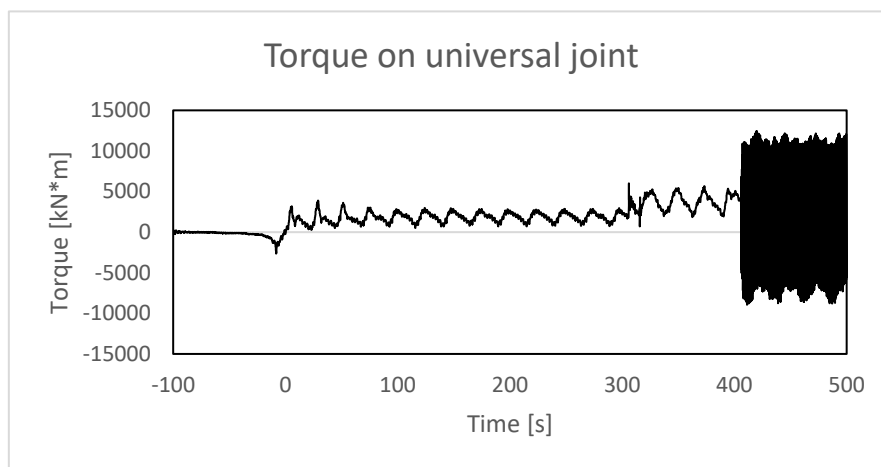
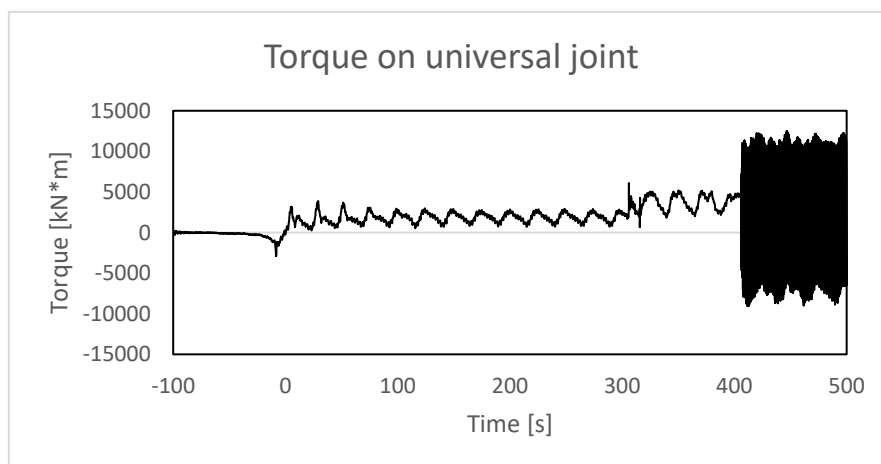
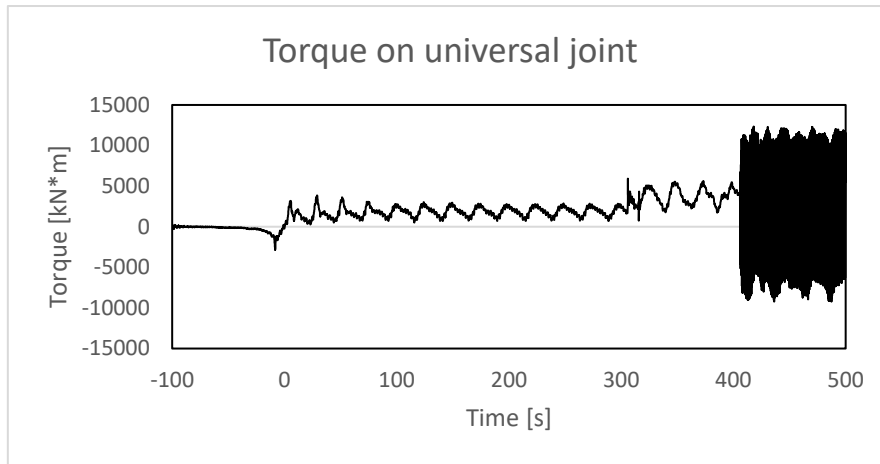
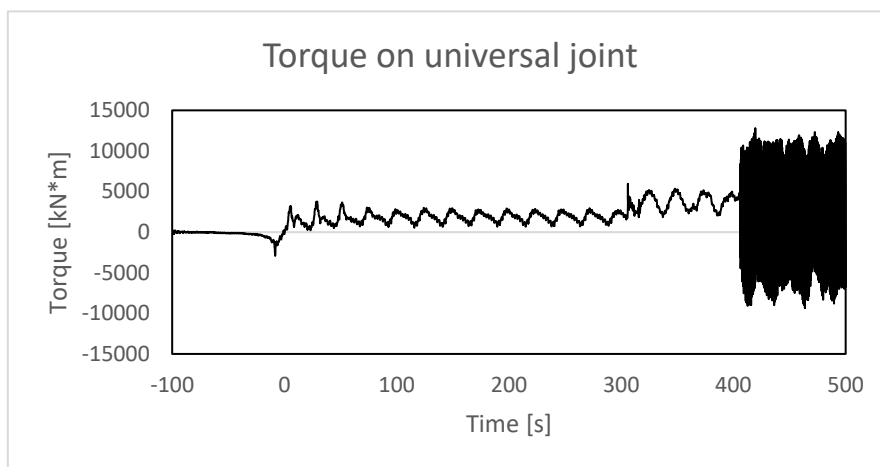
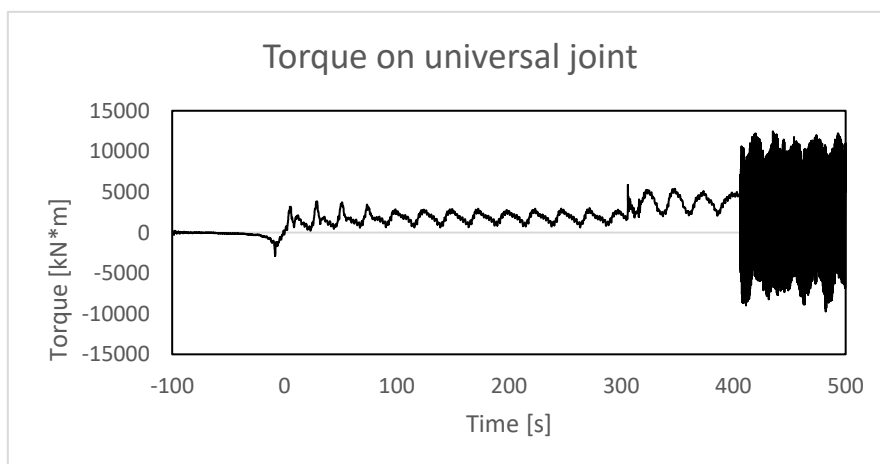


Figure 69:  $T_z = 7.5$

*Figure 70:  $T_z = 8.5$* *Figure 71:  $T_z = 9.5$* *Figure 72:  $T_z = 10.5$* 

**Yaw rate = 0.5**

*Figure 73:  $T_z = 5.5$* *Figure 74:  $T_z = 6.5$* *Figure 75:  $T_z = 7.5$*

*Figure 76:  $T_z = 8.5$* *Figure 77:  $T_z = 9.5$* *Figure 78:  $T_z = 10.5$*

## Appendix 2 – Torque results $H_s = 3.5$

Yaw rate = 0.1

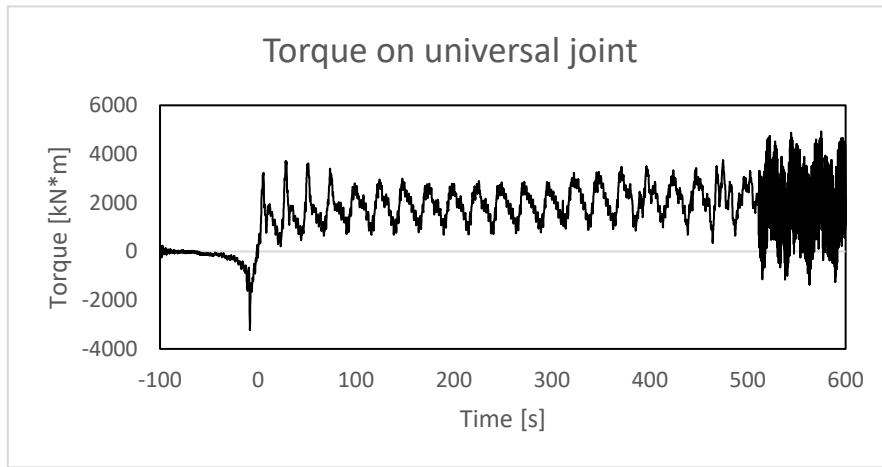


Figure 79:  $T_z = 6.5$

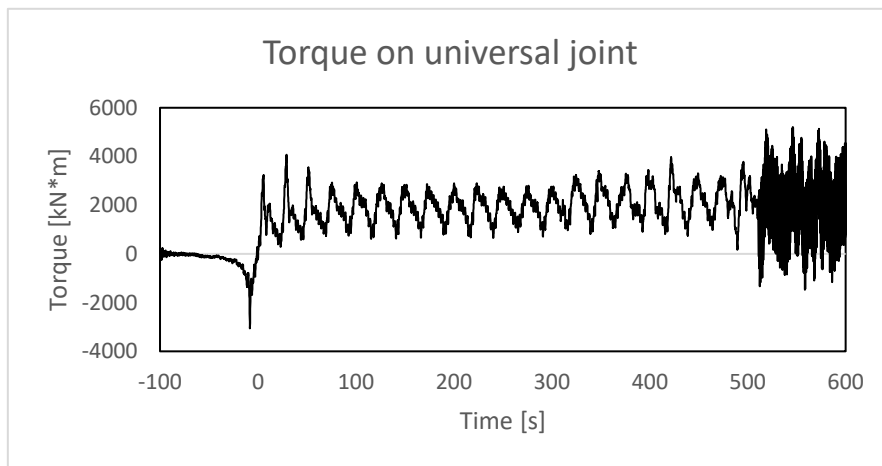


Figure 80:  $T_z = 7.5$

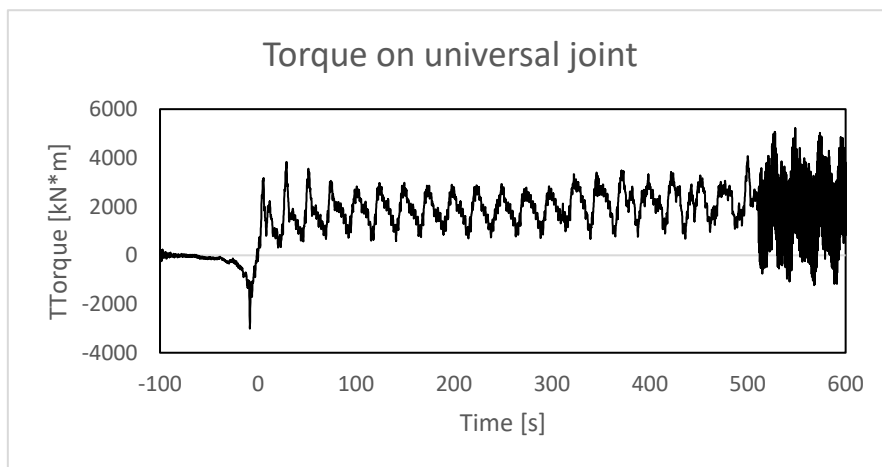
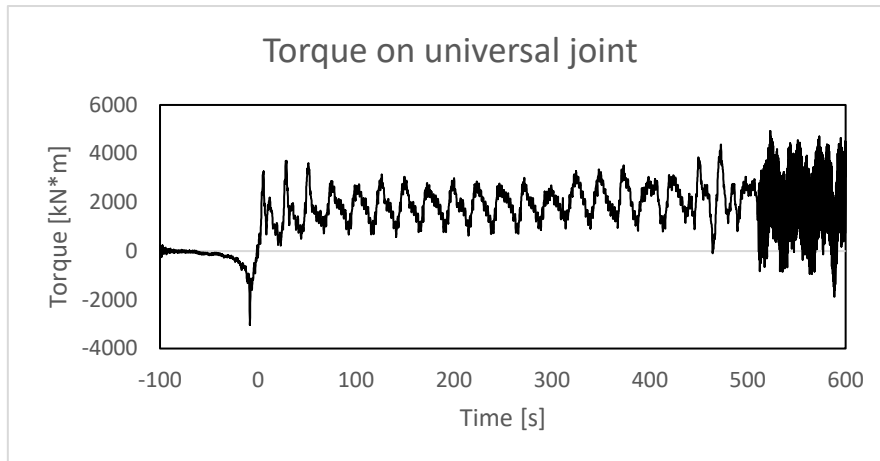
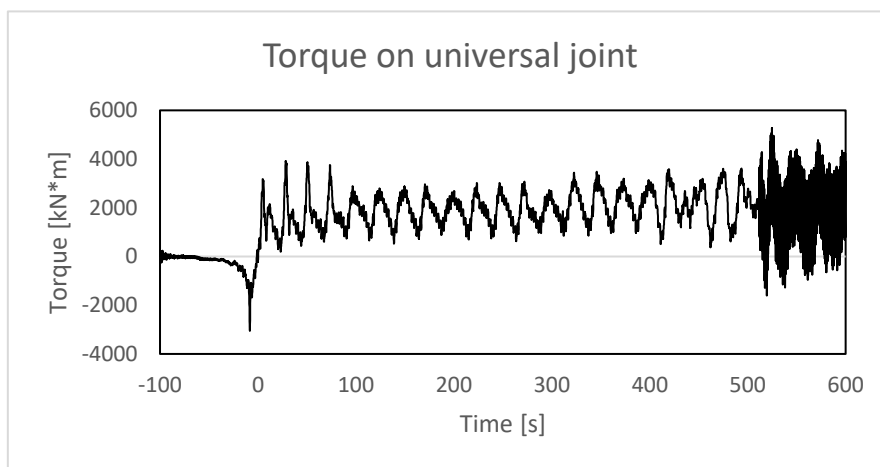
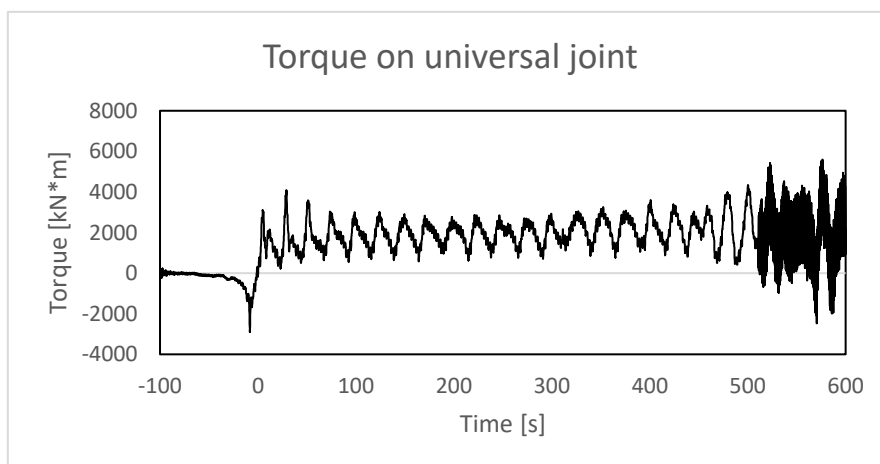


Figure 81:  $T_z = 8.5$

*Figure 82:  $T_z = 9.5$* *Figure 83:  $T_z = 10.5$* *Figure 84:  $T_z = 11.5$*

**Yaw rate = 0.3**

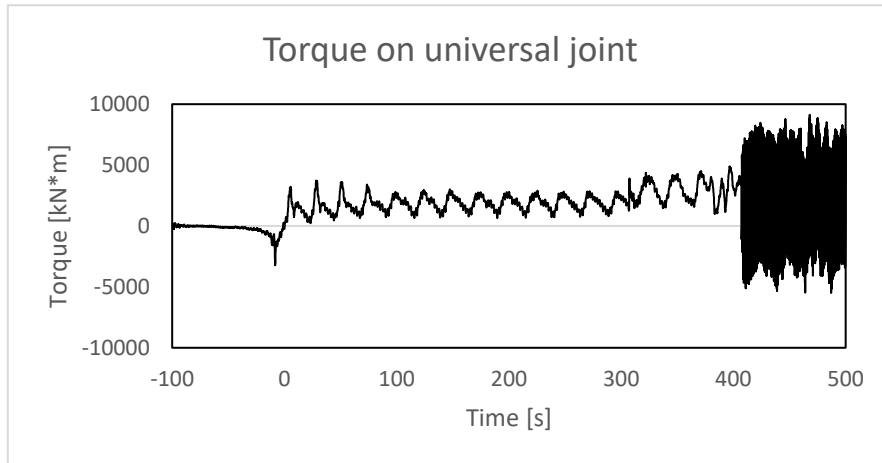


Figure 85:  $T_z = 6.5$

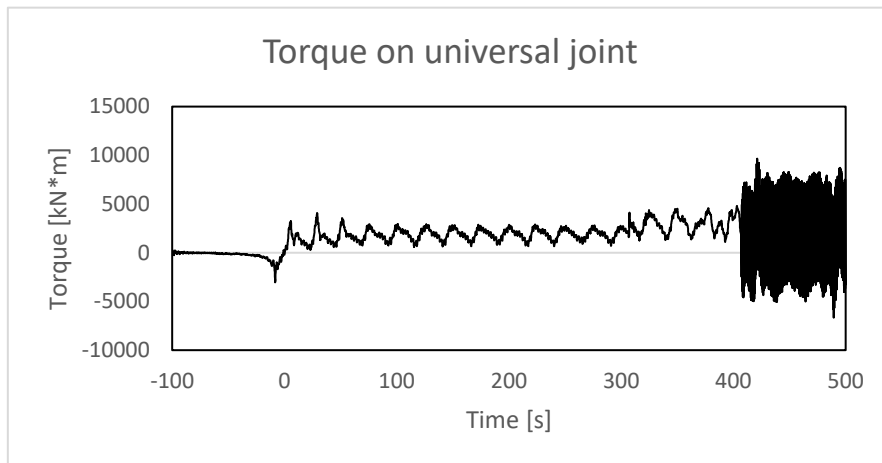


Figure 86:  $T_z = 7.5$

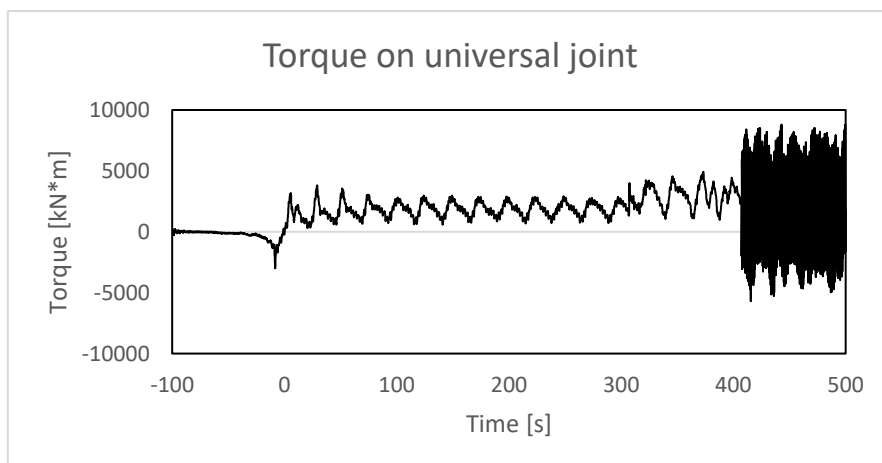
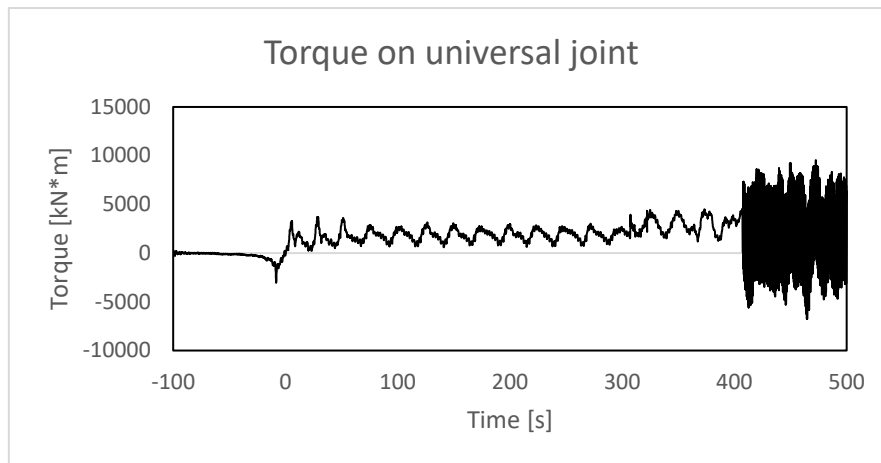
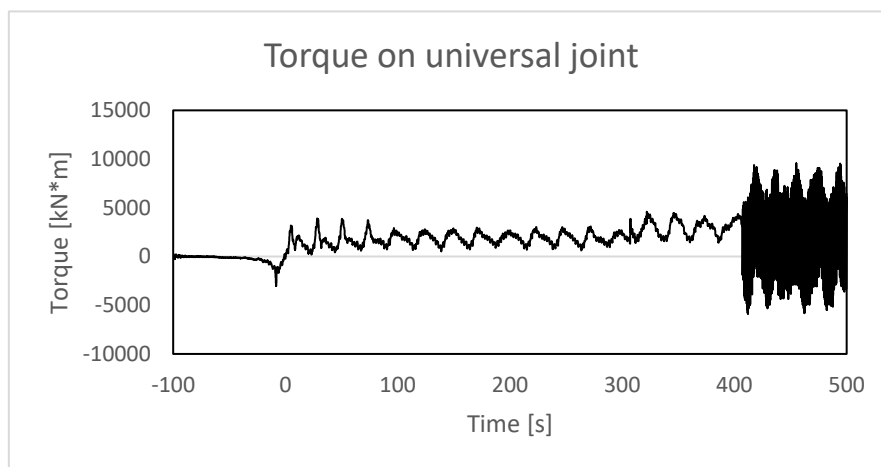
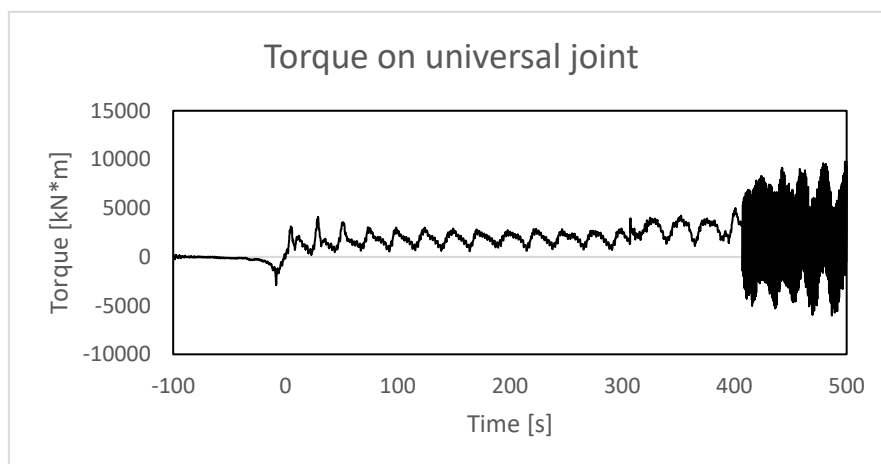


Figure 87:  $T_z = 8.5$



*Figure 88:  $T_z = 9.5$* *Figure 89:  $T_z = 10.5$* *Figure 90:  $T_z = 11.5$*

**Yaw rate = 0.5**

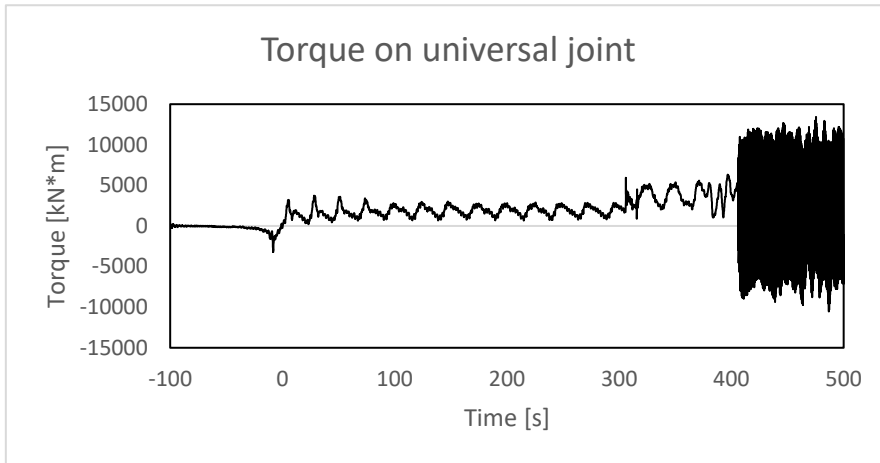


Figure 91:  $T_z = 6.5$

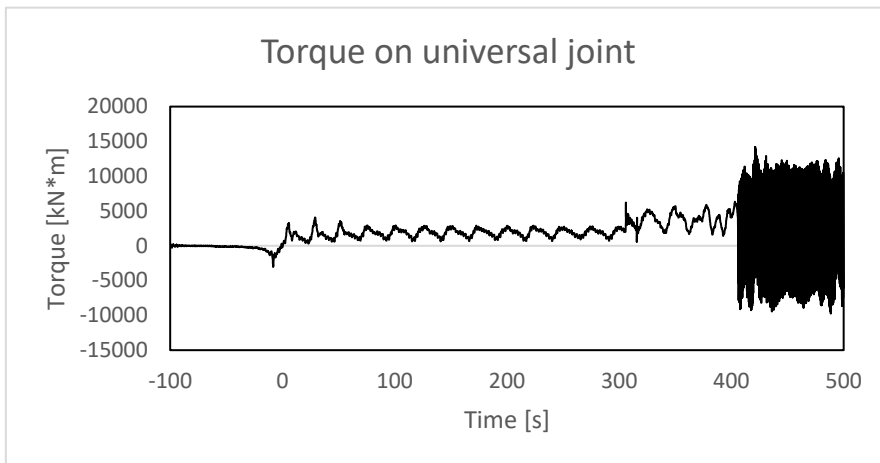


Figure 92:  $T_z = 7.5$

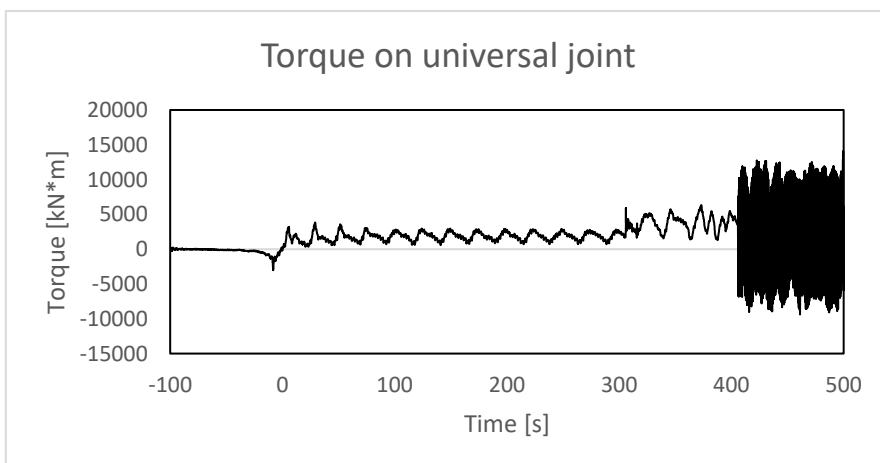
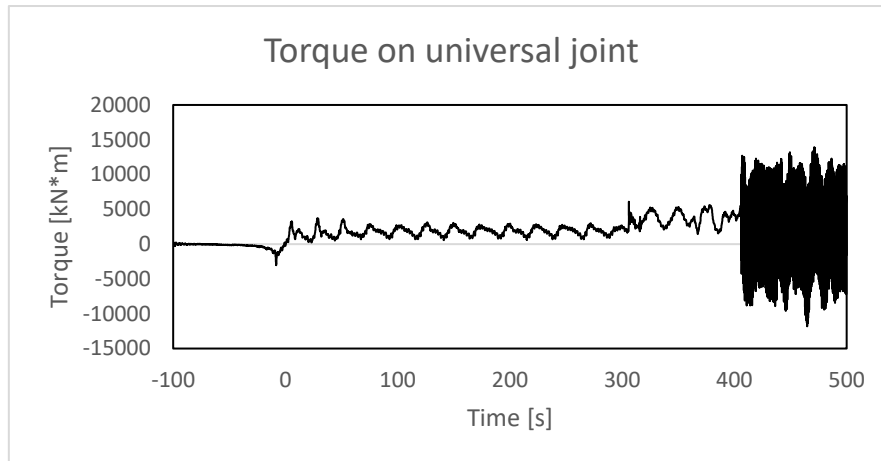
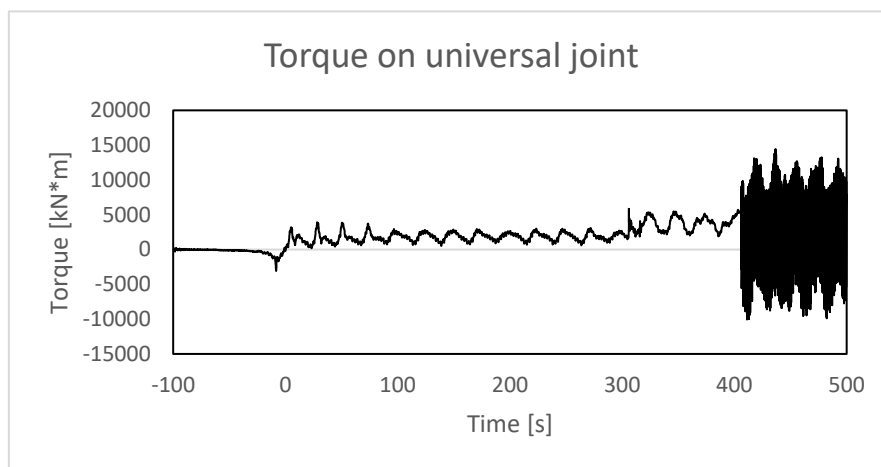
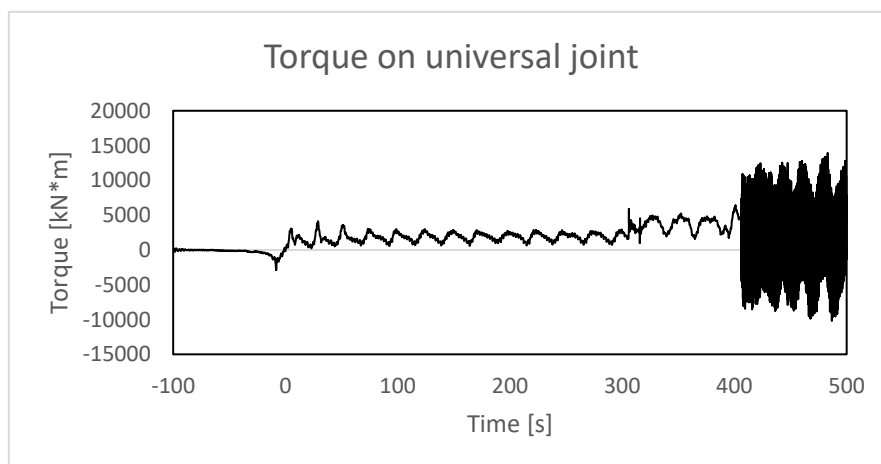


Figure 93:  $T_z = 8.5$

*Figure 94:  $T_z = 9.5$* *Figure 95:  $T_z = 10.5$* *Figure 96:  $T_z = 11.5$*

## Appendix 3 – Torque results $H_s = 6.5$

Yaw rate = 0.1

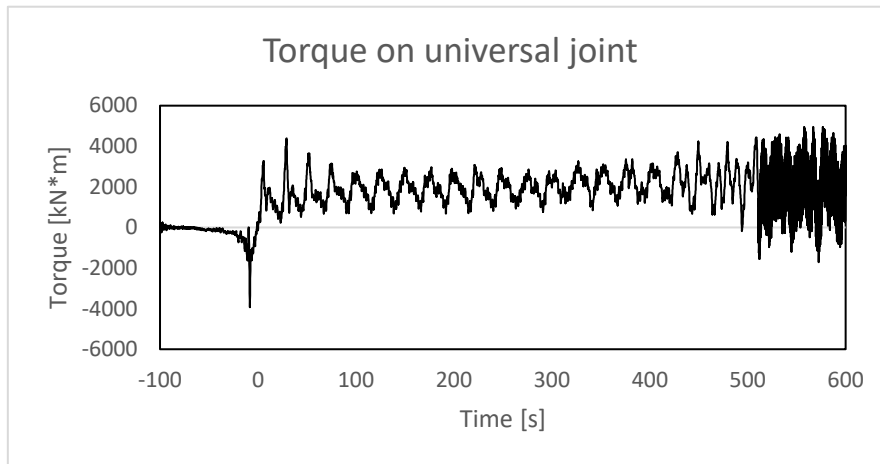


Figure 97:  $T_z = 7.5$

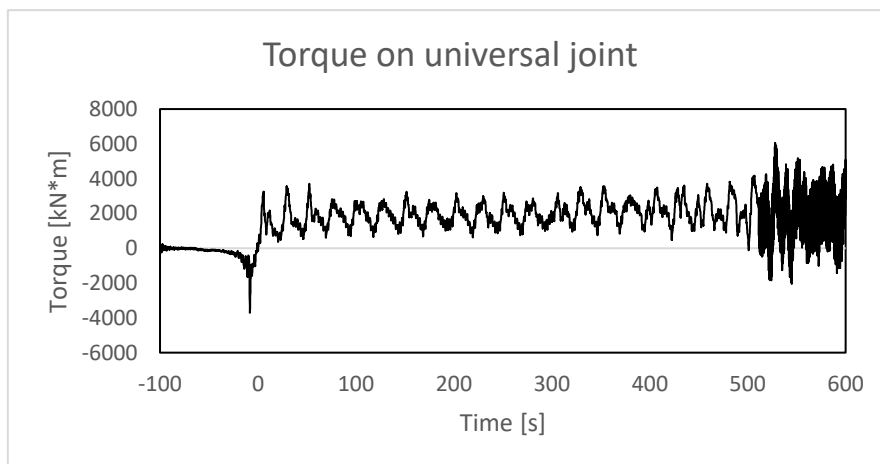


Figure 98:  $T_z = 8.5$

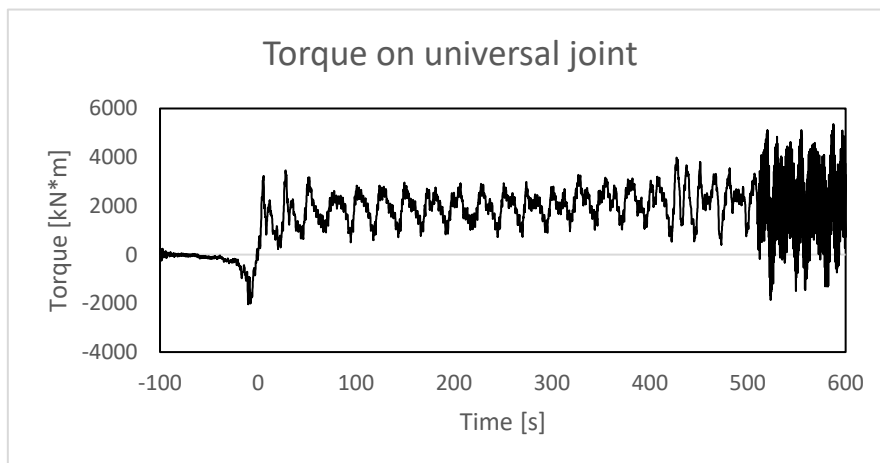


Figure 99:  $T_z = 9.5$

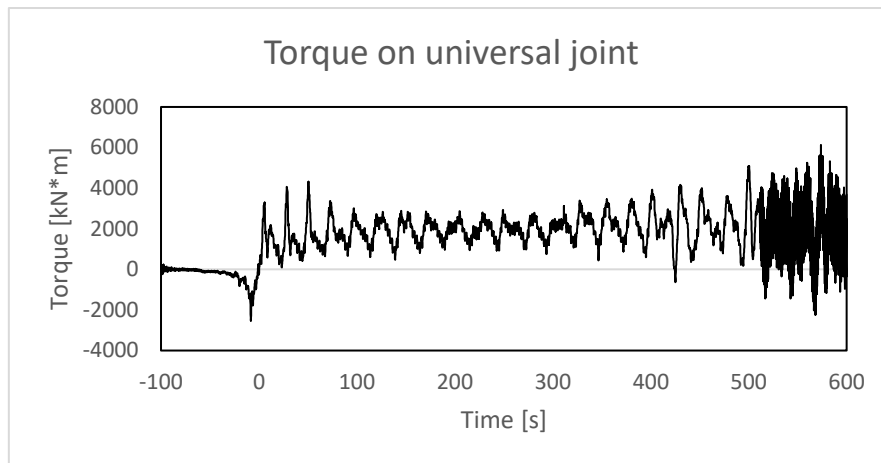


Figure 100:  $T_z = 10.5$

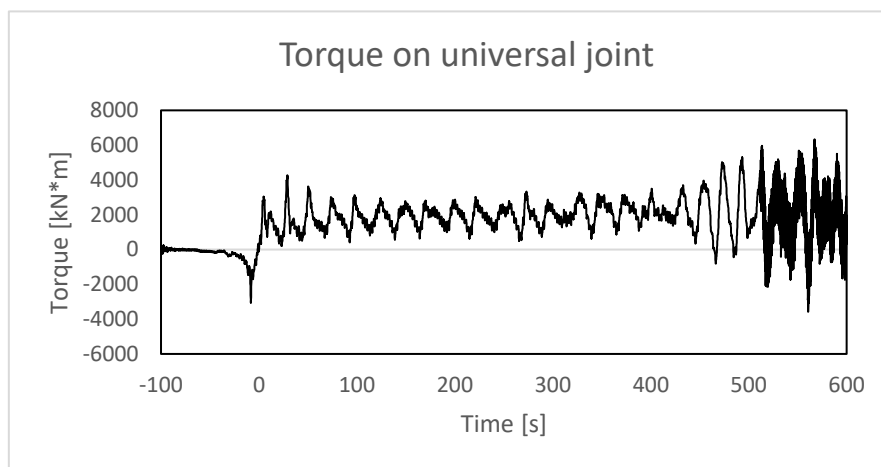


Figure 101:  $T_z = 11.5$

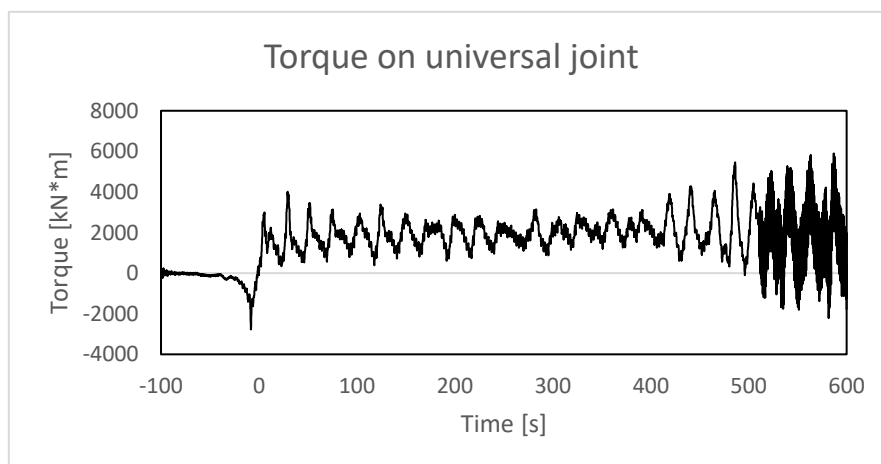
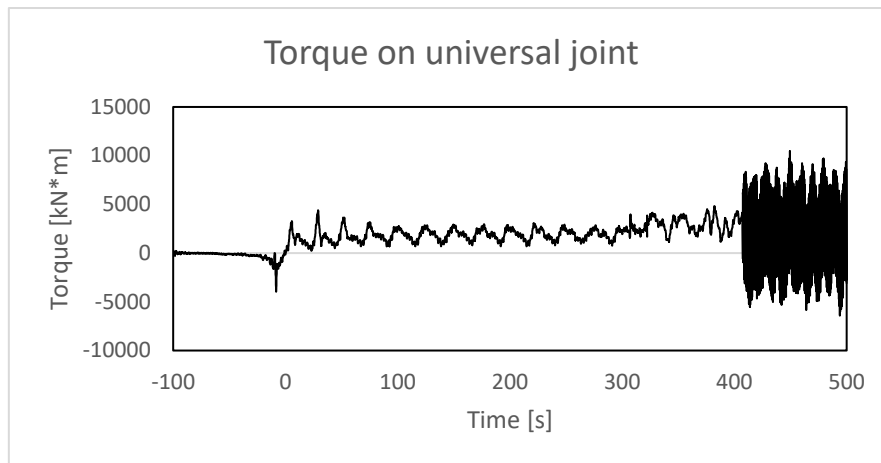
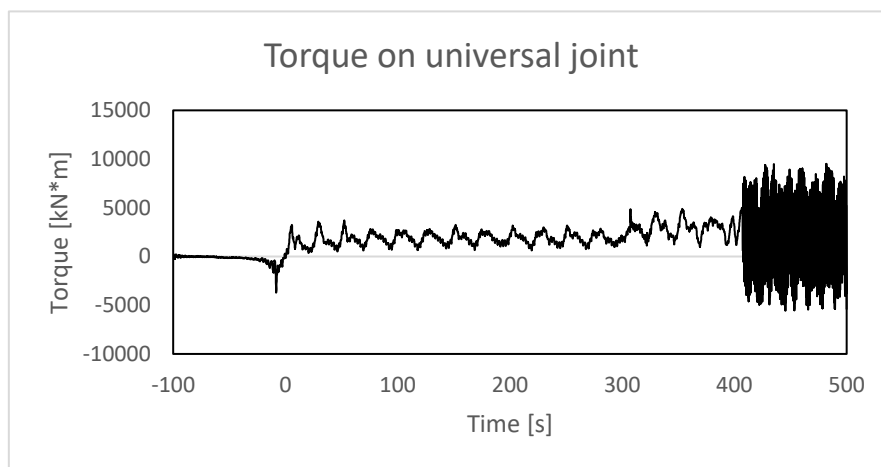
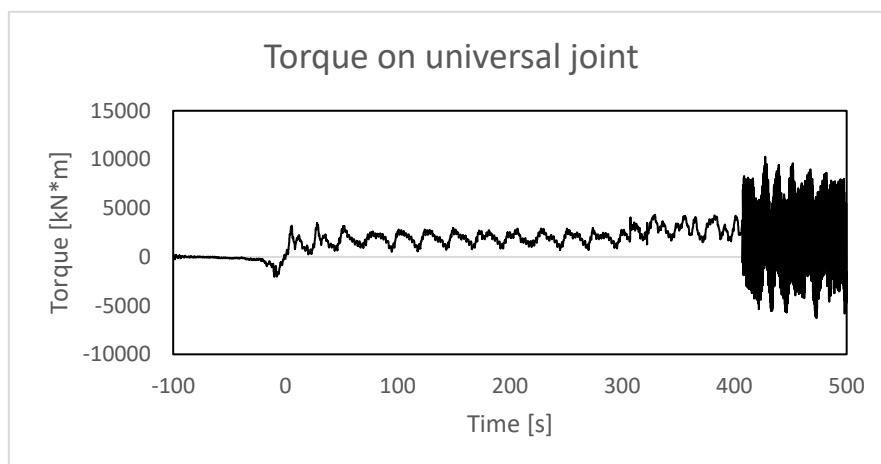


Figure 102:  $T_z = 12.5$

**Yaw rate = 0.3**

*Figure 103:  $T_z = 7.5$* *Figure 104:  $T_z = 8.5$* *Figure 105:  $T_z = 9.5$*

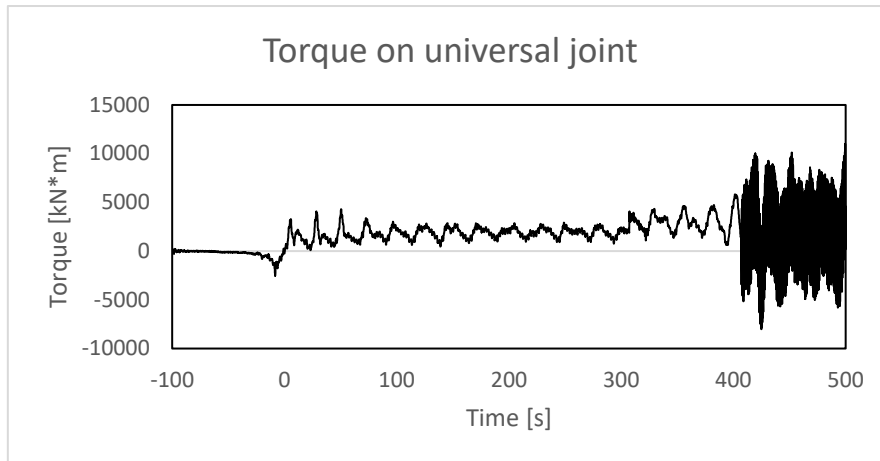


Figure 106:  $T_z = 10.5$

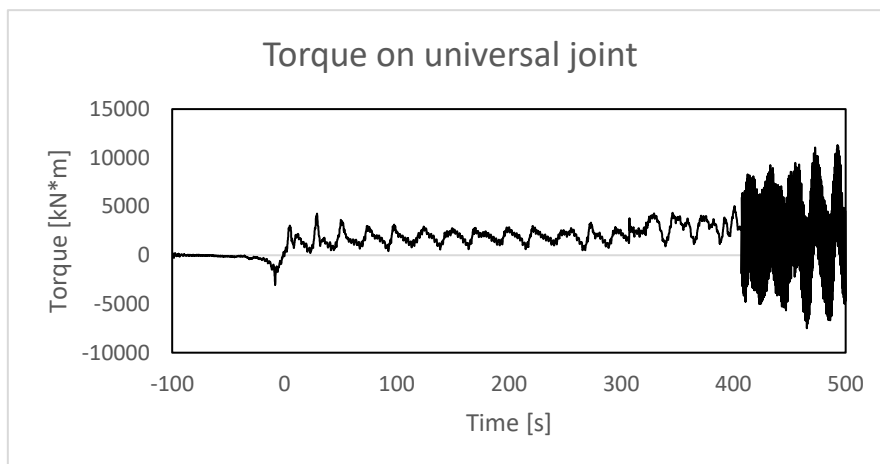


Figure 107:  $T_z = 11.5$

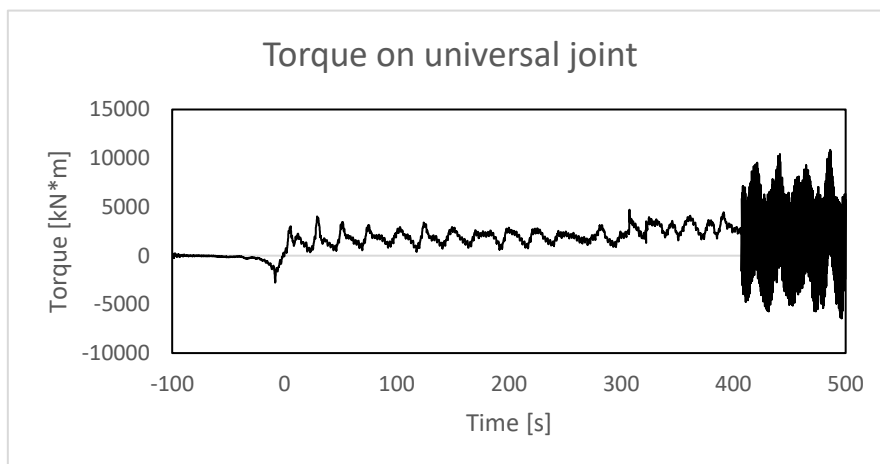
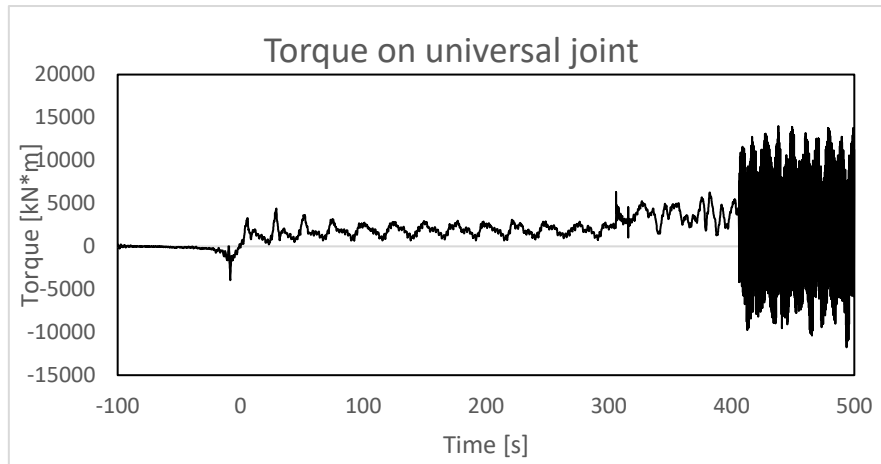
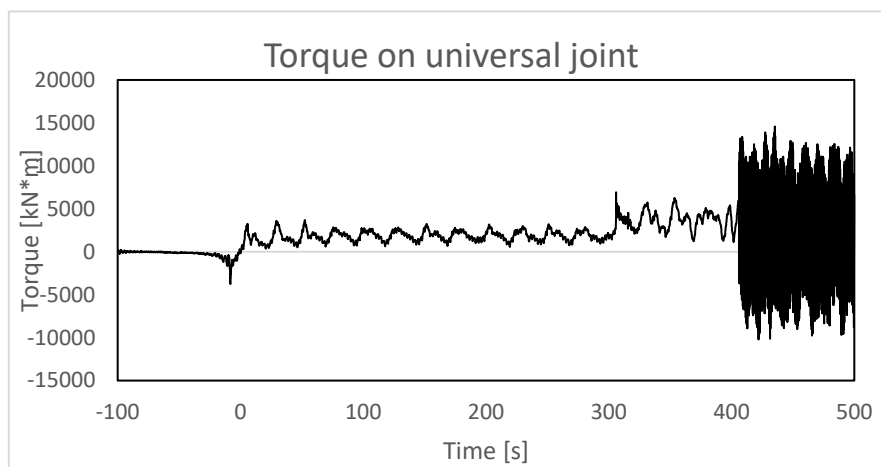
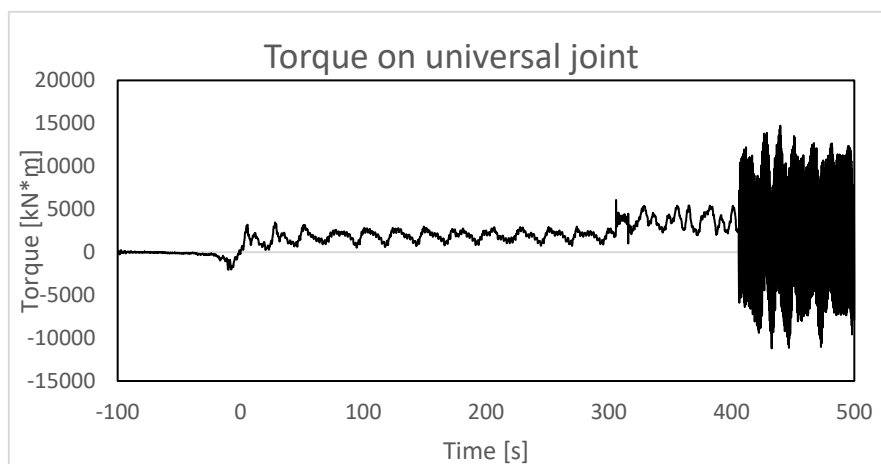
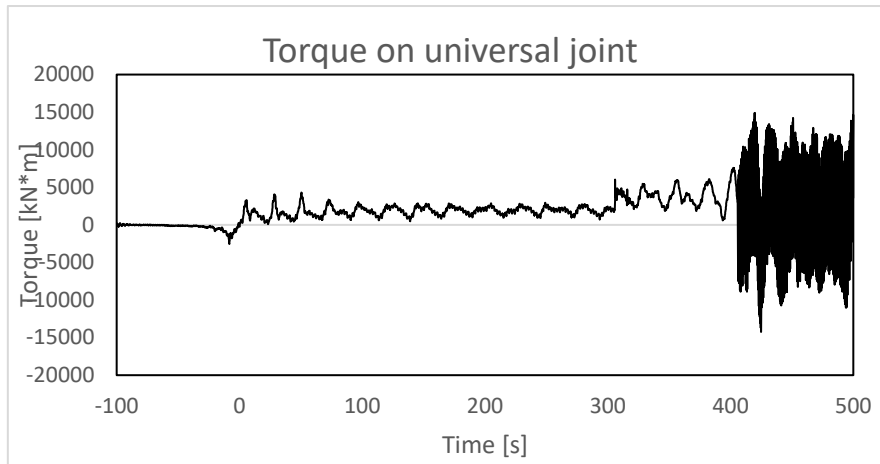
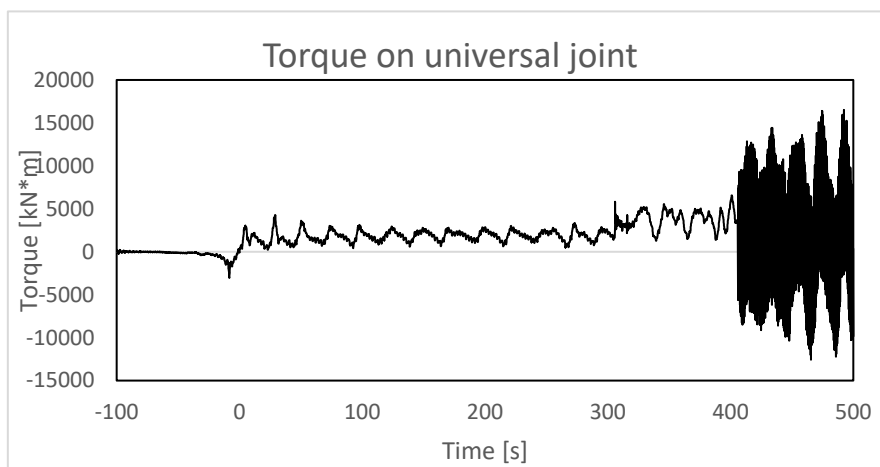
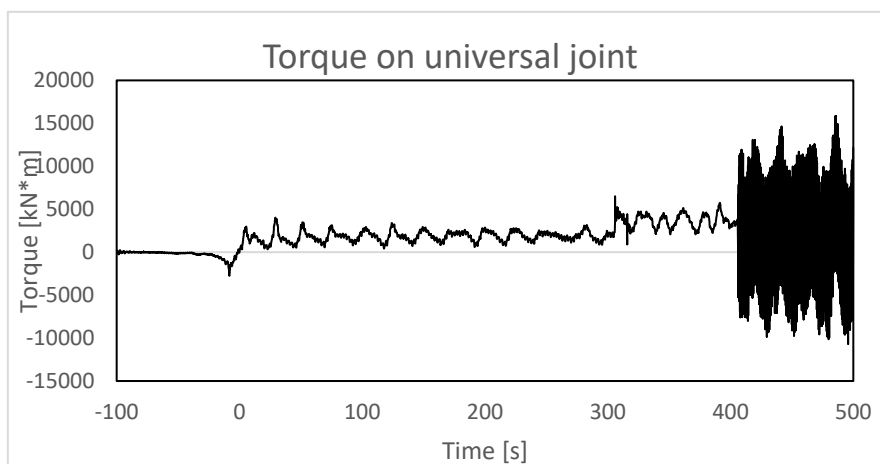


Figure 108:  $T_z = 12.5$

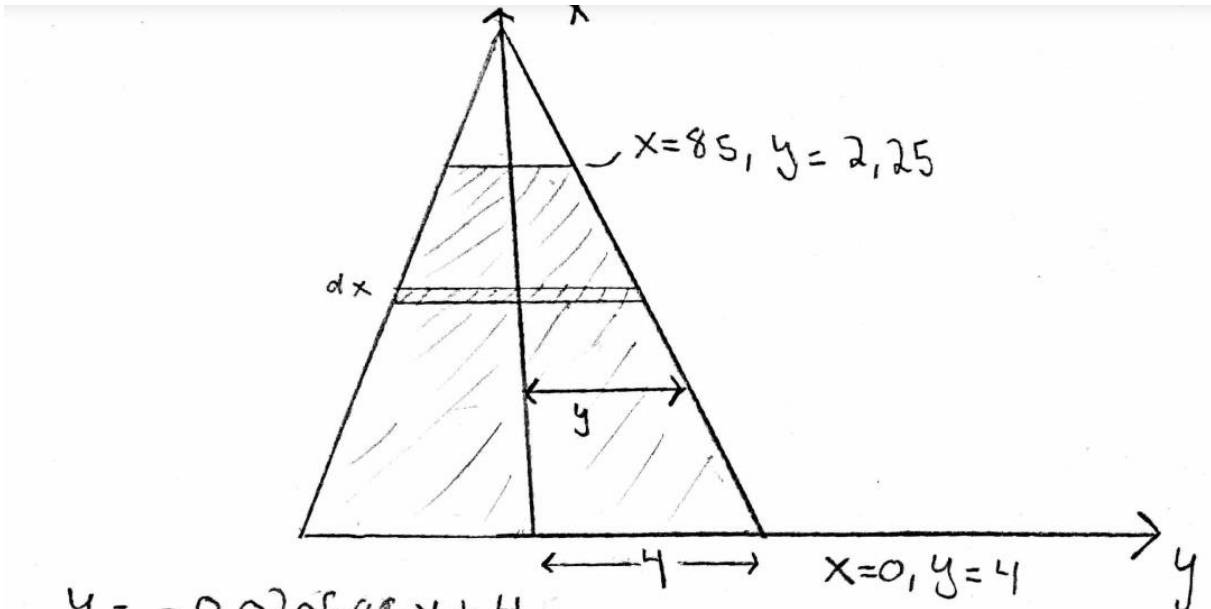
**Yaw rate = 0.5**

*Figure 109:  $T_z = 7.5$* *Figure 110:  $T_z = 8.5$* *Figure 111:  $T_z = 9.5$*



*Figure 112:  $T_z = 10.5$* *Figure 113:  $T_z = 11.5$* *Figure 114:  $T_z = 12.5$*

## Appendix 4 – Calculation of Moment of inertia, $I_z$ , for tower section



$$y = -0,020588 \cdot x + 4,5$$

$$dV = \pi y^2 \cdot dx$$

$$dm = \rho dV = \rho \cdot \pi y^2 dx$$

$$dI = \frac{1}{2} dm \cdot y^2$$

$$= \frac{1}{2} \rho \pi y^2 \cdot y^2 dx$$

$$= \frac{1}{2} \rho \pi \cdot y^4 dx$$

$$\bar{I} = \frac{1}{2} \rho \pi \int_0^{85} (-0,020588x + 4,5)^4 dx$$

$$y^4 = (-0,020588x + 4)^4$$

$$(a+b)^n = \sum_{i=0}^n \binom{n}{i} \cdot a^{(n-i)} \cdot b^i$$

$$a = -0,020588x, \quad b = 4$$

$$\Rightarrow \sum_{i=0}^4 \binom{4}{i} (-0,020588x)^{(4-i)} \cdot 4^i$$

$$= \frac{4!}{0! (4-0)!} (-0,020588x)^4 \cdot 4^0 + \frac{4!}{1! (4-1)!} (-0,020588x)^3 \cdot 4^1$$

$$+ \frac{4!}{2! (4-2)!} (-0,020588x)^2 \cdot 4^2 + \frac{4!}{3! (4-3)!} (-0,020588x)^1 \cdot 4^3$$

$$+ \frac{4!}{4! (4-4)!} (-0,020588x)^0 \cdot 4^4$$

$$= -1,79662 \cdot 10^{-7} x^4 - 0,00013962 x^3 + \frac{0,08138x^2}{2}$$

$$- 5,270528x + 256$$

$$\Rightarrow \int_0^{85} (-0,020588x + 4)^4 dx$$

$$= \left[ \frac{1}{5} \cdot 1,79662 \cdot 10^{-7} x^5 - \frac{1}{4} \cdot 0,00013962 \cdot x^4 + \frac{1}{3} \cdot 0,08138 x^3 - 5,270528 \cdot x^2 + 256x \right]_0^{85}$$

$$= 159,413 - 1822 + 8329,582 - 19039,78 + 21760$$

$$= \underline{9387,232 \text{ m}^5}$$

Same Method for 3,98m

$$\Rightarrow \int_0^{85} (-0,020588x + 3,98)^4 dx$$

$$= \left[ \frac{1}{5} \cdot 1,97383 \cdot 10^{-7} x^5 - \frac{1}{4} \cdot 0,00013 x^4 + \frac{1}{3} \frac{0,08050 x^3}{2} - \frac{1}{2} \cdot 5,18984 x^2 + 250,918x \right]_0^{85}$$

$$= \underline{9165,32 \text{ m}^5}$$

$$\Rightarrow I_z = \frac{1}{2} g \pi \cdot (9387,232 - 9165,32) \text{ m}^5$$

$$= \frac{\pi}{2} \frac{7850 \text{ kg}}{\text{m}^3} \cdot 221,8 \text{ m}^5$$

$$I_z = \underline{\underline{2735104 \text{ kg} \cdot \text{m}^2}}$$

General Summary Project Status Custom Save Physical

Solids  
 The Part

Material  
 Steel

Density 7.850 g/cm<sup>3</sup> Requested Accuracy Low

General Properties

Mass	261189.971 kg (Relative)	<input type="checkbox"/>	X	-0.000 mm (Relative E)
Area	3.328748761647E+09		Y	38520.599 mm (Relative E)
Volume	3.3272607794169E+1	<input type="checkbox"/>	Z	-0.000 mm (Relative E)

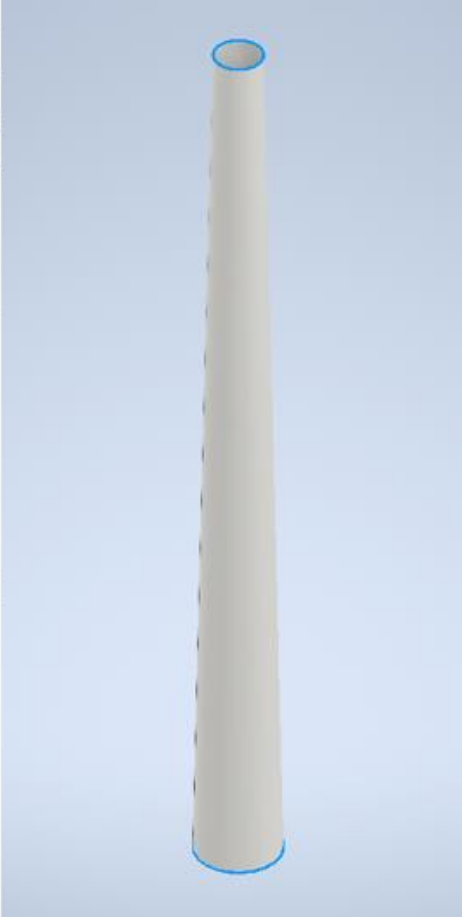
Inertial Properties

Principal Moments

I1	1.54489213030	I2	2.73438474882	I3	1.54489213030
----	---------------	----	---------------	----	---------------

Rotation to Principal

Rx	0.00 deg (Relative)	Ry	45.00 deg (Relative)	Rz	0.00 deg (Relative)
----	---------------------	----	----------------------	----	---------------------



## Appendix 5 – Excel calculation sheet

	A	B	C	D	E	F	G	H
1								
2	<b>Description</b>		<b>symbol</b>		<b>value</b>		<b>unit</b>	<b>comments</b>
3		<u>Lower section</u>						
4								
5	Length		Ls		128		m	
6	Diameter outside		Odsb		8		m	
7	Diameter inside		Idsub		7.96		m	
8	Displaced volume		Nabla1		6433.981755		m <sup>3</sup>	
9	Inside volume		Vi		6369.802787		m <sup>3</sup>	
10	Material density		Rhos		7.85		T/m <sup>3</sup>	
11	Weight section		Ws		503.8048988		T	
12	Weight per meter		Tm		3.935975772		T/m	
13	Center of gravity		COG		64		m	
14	Inertia x		Ix		691871.9592		T*m <sup>2</sup>	
15	Inertia y		Iy		691871.9592		T*m <sup>2</sup>	
16	Inertia z		Iz		8020.67475		T*m <sup>2</sup>	
17	Area cross section		As		0.501398188		m <sup>2</sup>	
18	Radii of gyration		Rgs		3.990012531		m <sup>2</sup>	
19								
20	Mass ballast		Mba		0		T	
21	Center of gravity ballast		COGba		0		m	
22	Inertia ballast							
23	Force ballast						kN	
24								
25	<b>Buoyancy tank</b>							
26	Length buoyancy tank		Lb		22		m	
27	Length inside		Li		21.92		m	
28	Diameter outside		Db		17		m	
29	Diameter inside		db		16.96		m	
30	Displaced volume		Nablab		4993.561523		m <sup>3</sup>	
31	Inside volume		Vib		4970.090056		m <sup>3</sup>	
32	Material density		Rhob		7.85		T/m <sup>3</sup>	
33	Weight section		Wb		184.2510162		T	
34	Weight per meter		Tmb		8.375046191		T/m	
35	Center of gravity b		COGb		139		m	
36	Inertia x		Ix		14071.8827			
37	Inerti Y		Iy		14071.8827			
38	Ineria Z		Iz		13280.8501		T*m <sup>2</sup>	
39	Area cross section		Ab					
40	Radii of gyration		Rgb		8.490005889		m <sup>2</sup>	
41								
42	<b>From buoyancy tank to sea surface</b>							
43	Length		Ls		20		m	
44	Diameter outside		Ds		8		m	
45	Diameter inside		ds		7.96		m	
46	Displaced volume		Nabla1		1005.309649		m <sup>3</sup>	
47	Inside volume		Vi		995.2816854		m <sup>3</sup>	
48	Material density		Rhos		7.85		T/m <sup>3</sup>	
49	Weight section		Ws		78.71951544		T	
50	Weight per meter		Tm		3.935975772		T/m	
51	Center of gravity		COG		160		m	
52	Inertia x		Ix		3250.599063		T*m <sup>2</sup>	
53	Inertia y		Iy		3250.599063		T*m <sup>2</sup>	
54	Inertia z		Iz		1253.23043		T*m <sup>2</sup>	

58	<u>Topside section</u>			
59				
60	Length topside section	Lt	115	m
61	Length const Dia	Lt1	30	m
62	Diameter	Dt	8	m
63	Diameter inside	Dti	7.96	
64	Outside Vol const dia		1507.964474	m <sup>3</sup>
65	Inside Vol const dia		1492.922528	m <sup>3</sup>
66	Mass const dia		118.0792732	T
67	Mass per meter	m/m	3.935975772	T/m
68	Center of gravity		185	m
69	Inertia x		9795.868309	T*m <sup>2</sup>
70	Inertia Y		9795.868309	T*m <sup>2</sup>
71	Inertia Z	I const	1879.845645	T*m <sup>2</sup>
72	Radii of gyration	Rg	3.990012531	m <sup>2</sup>
73				
74	<u>Coned section from 30 m - 115 m</u>			
75	Length section	L cone	85	m
76	Function of radius	r(z)	0.020588x+4	
77	Diameter at 30m	D30	8	m
78	Diameter at 115m	D115	4.5	m
79	Inside dia @ 30m	d30	7.96	m
80	Inside dia @115m	d115	4.46	m
81				m <sup>3</sup>
82	Volume integrated	Vcone	33.27593	m <sup>3</sup>
83	Mat density	Rhot	7.85	T/m <sup>3</sup>
84	Center of gravity	COGt	228.3333333	m
85	Mass	Mcone	261.2160505	T
86	Mass per meter	M/m cone	3.073130006	T/m
87	Inertia x	Ix	154489.213	
88	Inertia Y	Iy	154489.213	
89	Inertia Z	Iz_cone	2734.405	T*m <sup>2</sup>
90	Radii of gyration	Rg cone	3.235426143	m <sup>2</sup>

<u>Environmental inputs</u>				
Wave height	H		TBD	m
Wave period	Tp		TBD	s
Wind speed	Vwind		TBD	m/s
Water depth	h		170	m
Density water	Rhow		1.025	T/m <sup>3</sup>
Density air	Rhoa		0.001225	T/m <sup>3</sup>
Density hydrogen	Rhoh		0.00008375	T/m <sup>3</sup>
Gravitational acceleration	g		9.80565	m/s <sup>2</sup>
<u>Properties substructure</u>				
Total volume steel			145.9962744	
Total mass	mtot		1146.070754	T
Total inertia x	Ix_tot		6560792.62	T*m <sup>2</sup>
Total inertia y	Iy_tot		6560792.618	T*m <sup>2</sup>
Total inertia z	Iz_tot		27169.01	T*m <sup>2</sup>
Total radii of gyration	rtot		19.70545709	m <sup>2</sup>
Center of mass	zG		132.9164058	m
Center of buoyancy	zB		96.77319588	m
Gravitational force	Fg		11237.96869	kN
Buoyancy force hydrogen	Fbh		49949.25609	kN
Buoyancy force from nabla	Fbnabla		114855.852	kN
Buoyancy force total	Fbtot		164805.1081	kN
<b>NetForce</b>	<b>F</b>		<b>-153567.1394</b>	<b>kN</b>
<b>Net force (abs)</b>	<b>Fnet</b>		<b>153567.1394</b>	

## Appendix 6 – Excel Solver

The initial calculated net force was 153567.14 kN upwards. Need ballast to ensure net force downwards or equal to zero.

	R	S	T	U	V	W
30	NetForce	F		-153567.1394		kN

Initial ballast mass is zero.

	A	B	C	D	E	F	G
20	Mass ballast		Mba		0		T

Using Excel solver to set the objective «NetForce» to zero by changing the variable «Mass ballast».

Solver Parameters

Set Objective:

To:  Max  Min  Value Of:

By Changing Variable Cells:

Subject to the Constraints:

Make Unconstrained Variables Non-Negative

Select a Solving Method:

Solving Method  
Select the GRG Nonlinear engine for Solver Problems that are smooth nonlinear. Select the LP Simplex engine for linear Solver Problems, and select the Evolutionary engine for Solver problems that are non-smooth.

	R	S	T	U	V	W
30	NetForce	F		-3.7736E-07		kN



The net force is approximately zero when the mass of the ballast is 15661.08 for the substructure.

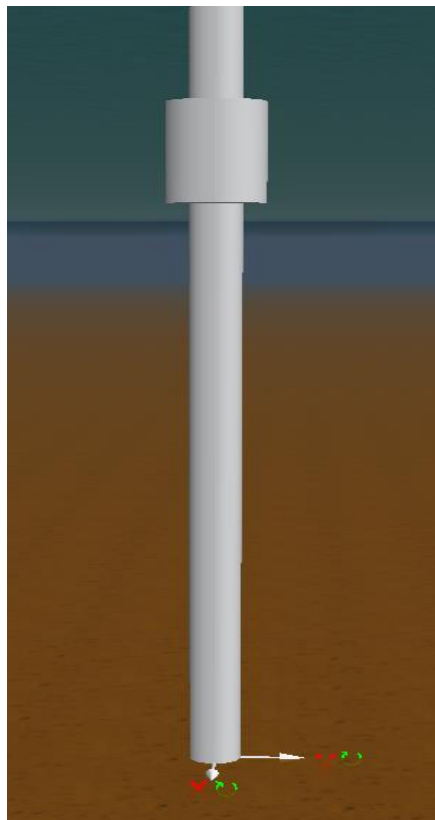
	A	B	C	D	E	F	G
20	Mass ballast		Mba		15661.08717		T

## Appendix 7 – Building the model in Orcaflex

1. A constraint is used to improvise the universal joint and allows two degrees of freedom: Rx and Ry.



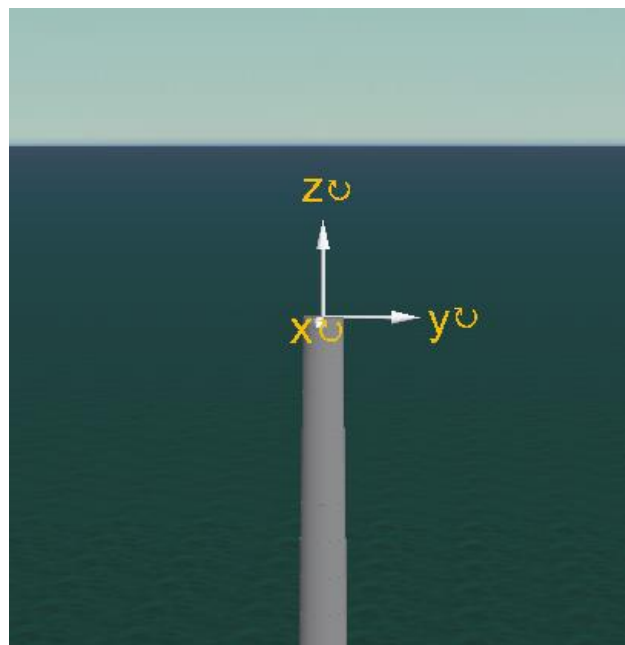
2. A 6D buoy is then modelled according to drawings from Offshore Kinetics and connected to the constraint.



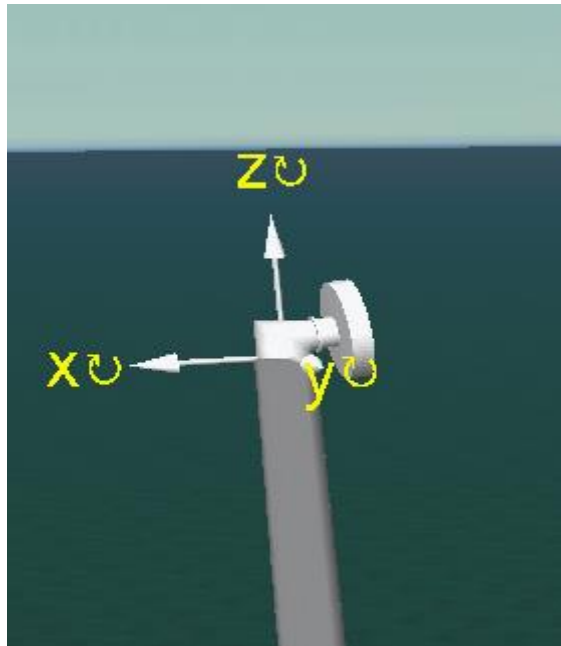
3. The tower is then connected to the 6D buoy.



4. A second constraint which is used as the yaw controller is then connected to the tower.



5. The nacelle is then connected to the constraint



6. The blade assembly is connected to the nacelle



7. Finally, the hub is connected to the blade assembly

